MECHANICAL AND SURFACE PROPERTIES OF TECHNICAL AND SINGLE FLAX FIBER IN MICRO AND NANO SCALE

A Thesis
Submitted to the Graduate Faculty
of the
North Dakota State University
of Agriculture and Applied Science

By

Shabbir Ahmed

In Partial Fulfillment of the Requirements
for the Degree of
MASTER OF SCIENCE

Major Department:
Mechanical Engineering

June 2017

Fargo, North Dakota

North Dakota State University
Graduate School

Title

Mechanical and Surface Properties of Technical and Single Flax Fiber in Micro and Nano Scale

By

Shabbir Ahmed

The Supervisory Committee certifies that this ***disquisition*** complies with North Dakota State University's regulations and meets the accepted standards for the degree of

MASTER OF SCIENCE

SUPERVISORY COMMITTEE:

Dr. Chad Ulven
Chair

Dr. Scott Pryor

Dr. Xinnan Wang

Dr. Long Jiang

Approved:

6/29/17
Date

Dr. Alan R. Kallmeyer
Department Chair

ABSTRACT

The continued search for sustainable and eco-friendly materials led to the integration of bio-fibers as the reinforcement in composite materials. However, a wide variation in their mechanical properties poses a considerable challenge for their incorporation in load bearing and structural bio-composite materials. In this thesis, a rigorous experimental investigation is performed for quantifying this variation in mechanical properties of flax fiber such as ultimate strength, ultimate strain, and elastic modulus. The effect of stalk diameter and variety on strength and strain was investigated on a statistical basis. Probability distribution models were proposed for predicting the probability of failure on a given strength. A dynamic in-situ failure analysis was performed on technical flax fibers with the help of scanning electron microscopy (SEM) to investigate the micro and nanoscale failure behavior. A reliable measurement method of surface energy of a single flax fiber was proposed and performed by atomic force microscopy (AFM).

ACKNOWLEDGMENTS

At the outset, I would like to thank my advisor, Professor Dr. Chad A. Ulven , for his all-out support and guidance during my sojourn at NDSU. I have been fortunate enough to have an advisor who provided me the freedom to explore on my own. I strongly believe, my experience at composites group in NDSU would be an asset for the next step of my life, as I have decided to follow in his footsteps to become a teacher and researcher.

I would like to thank Dr. Long Jiang and Dr. Scott Pryor, my thesis committee members, for their constructive review and insightful comments on my thesis.

I would like to gratefully acknowledge the financial and technical support provided by Composite Innovation Center (CIC), Winnipeg, Canada. Special thanks to Mercedes, Shawna, and Lin Ping for helping me with the tensile testing data for comparison purposes and always keeping me updated with newer results. I also would like to acknowledge the equipment support provided by the Electron Microscopy (EM) Center, NDSU. The lab supervisors, Scott Payne and Jayma Moore, have always been helpful with the sample preparation and experimental setup.

Special thanks to Professor Dr. Xinnan Wang for helping me with the Atomic Force Microscopy (AFM) and Nano-indentations. His door was always open for me and he took special care of my academic success.

Thanks to all of my colleagues for their support and help. Special thanks to undergrad researchers: Noah, Joe, Geneva, Carrera and Samantha. They never hesitated to help me with the experiments when I needed, even outside their scheduled hours. Thanks is due to Krystal who helped me with the ChemDraw.

TABLE OF CONTENTS

LIST OF TABLES

LIST OF FIGURES

LIST OF ABBREVIATIONS

CMF .....Cellulose microfibrils

HC .....Hemicellulose

HG.....Homogalactururonan

GALPA ..... Galactopyranosyluronic acid

SEM .....Scanning electron microscopy

TEM .....Transmission electron microscopy

AFM..... Atomic force microscopy

AE .....Acoustic emission

SASX .....Small angle x-ray diffraction

FTIR.....Fourier transform infrared spectroscopy

TGA .....Thermogravimetric analysis

ANOVA .....Analysis of varience

EDTA.....Ethylenediaminetatra acetic acid

FESEM.....Field emission scanning electron microscopy

LIST OF SYMBOLS

σ .....Stress

E .....Young's modulus

G .....Shear modulus

r_0 .....Interatomic distance

e .....Electron charge

γ .....Surface energy

γ_p .....Polar component of surface energy

γ_d .....Dispersive component of surface energy

S .....Spreading co-efficient

γ_L .....Surface energy of liquid

γ_S .....Surface energy of solid

γ_{SL} .....Surface energy of solid liquid interface

σ_c .....Critical stress of crack propagation

μ .....Population mean

$\bar{x}$ .....Sample mean

s .....Sample standard deviation

W_a .....Work of adhesion

LIST OF APPENDIX FIGURES

CHAPTER 1. INTRODUCTION

1.1. Background

Composite materials have emerged as the materials of choice for engineers and material scientists in the 21st century. They offer superior mechanical and thermal properties over traditional monolithic materials such as iron, aluminum, and steel in terms of weight, thermal expansion, stiffness, strength, fatigue resistance, flexibility in design, and ease of fabrication. To be considered a composite material, there should at least be two distinct phases. One as a continuous phase usually referred to as the matrix and the other is a discontinuous phase usually known as the reinforcement. The matrix phase may be polymer, metal or ceramic. The reinforcing element may be continuous fibers, short fibers, particulates, whiskers, flakes etc. The most commonly used fibers are glass fiber, boron fiber, graphite fiber and aramid fiber. The most important class of composite materials is the continuous fiber reinforced polymer matrix composites. The matrix serves as a binder and holder of the fiber that is embedded in the matrix, protects the fiber from the environment, and transfers load to the fiber, thus allowing the composite to achieve very high strength. Statistics published by the Society of the Plastics Industry (SPI) Composites Institute reveals that the quantities of composites manufactured and used in United States has steadily increased since 1978 until now. In the period of only 10 years, from 1978 to 1988, the consumption of composites increased around 270 million pounds [1]. At present, composite materials are being extensively used in every sector. For maintaining a clean environment, it is required that every material should be ecofriendly and environment friendly.

Very recently, concern has been expressed regarding the disposal of composite materials after they have surpassed their useful life. This is because most composite materials are manufactured from petroleum based polymer resins, such as epoxy, polyurethane, etc. combined

with mineral and synthetic fibers such as glass and carbon fibers, respectively. These types of composite materials are not bio-degradable and difficult to recycle or reuse. Even if the recycling is possible, it is typically very expensive. As a result, these composite materials ultimately end up in landfills. However, the number of landfills are decreasing drastically and incineration of these materials contribute to environmental pollution. In United States, the amount of landfills decreased from 8000 to 2314 between 1988 and 1998 [2-4]. Hence, it is a major concern for scientists and engineers as well as legislative bodies of the state for proper disposal of these materials.

The term bio-composite is of recent origin, and this type of composite material is capable of addressing the above mentioned environmental issues[5]. In bio-composites, natural fibers such as flax, hemp, ramie, etc. are used as reinforcing element and bio-polymers derived from cellulose, starch, lactic acid etc. are used as the matrix element [6]. In addition to recyclability, bio-composites offers some other benefits too. They are light weight, nontoxic and nonabrasive. The property of being lighter weight comes from the hollow nature of natural fibers. Due to the presence of a lumen (central hollow cavity in the fiber structure), the density of natural fibers ($1.5\ g/cm^3$) are much lesser than the glass fibers ($2.5\ g/cm^3$).

European auto industries have paid much attention for the utilization of natural fibers and bio-composites into the car body. An industrial report states that on an average each and every manufactured car incorporates 5-10 kg of natural fibers [5]. This trend is more pronounced in German and Austrian car industries. They have used 8.5 to 9 kilo-tons of flax fiber in 2001 [7]. BMW 3, 5, and 7 series have incorporated bio-composites in door panels, headliner panels, foot lining, and seat back. The incorporation of bio-composites into these parts have resulted in a 20-30% weight reduction [8], which also enabled them to achieve better fuel efficiency, and in turn

significantly lower CO_2 emission. It is estimated that if the lifetime of a car is 175,000 km, one kilogram of weight saving can result in a fuel savings of 5.95- 8.4 liter of gasoline [9]. This fuel saving would result in a corresponding avoidance of emissions and burnt out gases. When glass fiber reinforced composites are fractured due to collision or accidents, they generate very sharp fractured surface. However, the fractured surface of bio-composites are usually blunt and nonabrasive, which also increases the safety of the passengers.

Bio-composites have better sound and vibration absorption properties as well [10]. Because fibrous materials can absorb sound over a broader frequency range than other materials [11-13]. With this in mind, they are increasingly finding applications in diverse fields such as in the field of energy and impact absorption [14]. They are being used as floor coverings, bicycle helmets, security helmets for construction areas, and monitor housing for computers. Another use of bio-composites are for various furniture elements such as deck surface boards, picnic tables etc [15].

However, before being able to use bio-composites in structural and load bearing applications, rigorous investigation is required with the mechanical and surface properties of natural fibers alone. This thesis aims to study the mechanical and surface properties of technical as well as single flax fibers.

1.2. Objectives

The main objective of this thesis is to assess the viability of flax fiber as a reinforcing agent in composite materials for load bearing applications.

To achieve this goal, first tensile testing was performed and mechanical properties such as the strength, failure strain, and Young's modulus were determined for different variety of flax fibers in order to assess the effect of variety and stalk diameter. Then a dynamic in-situ failure

analysis was performed with the help of SEM. Finally, to assess the surface characteristics of flax fiber, surface energy of a single flax fiber was determined with the help of atomic force microscopy.

Once the above mentioned tasks were complete, the specific objectives of the research are summarized as follows:

1. To determine the distribution of strength, failure strain, Young's modulus, failure time and diameter of each of the six varieties of flax fiber studied in this thesis.
2. To investigate the statistical significance of mean of the large diameter sample and the small diameter sample by hypothesis testing and ANOVA analysis.
3. To assess the degree of fit of different probability distribution and find their associated parameters.
4. To propose a probability distribution model for the strength distribution of flax fibers based on the highest degree of fit.
5. To investigate the micro-scale and nano-scale failure mechanism of single as well as technical flax fiber and explain them with respect to the failure of flax fiber reinforced composite materials.
6. To investigate the internal structure of flax fiber and their contribution in energy absorbing mechanism
7. To investigate the wetting characteristics such as adhesion and contact angle and surface energy of flax fibers.

1.3. Literature review

Natural fibers are an attractive choice for the utilization in advanced polymer matrix composite materials as reinforcing agents due to their lighter weight and lesser dermal abrasion

characteristics, reduced energy requirement during processing, better vibration dampening characteristics, better insulation, and sound absorption capabilities [16]. In addition, the increasingly stringent laws on pollution and the environment have facilitated the need for increased manufacturing of bio-based composite materials. In this respect, flax fibers, a bast natural fiber, have found a growing interest and acceptability in the manufacturing of bio-based composite materials as reinforcing agents. Although natural fibers lack many of the impressive properties of synthetic fibers such as higher uniformity, higher strength and corrosion resistance, thermal stability and non-flammability, their characteristic biodegradability, moderate mechanical properties, and non-toxic nature have outweighed these shortcomings[17].

Flax fiber bundles are located at the exterior part of the flax stem and reside in between the cortex and the phloem tissue. Each stem contains approximately 20-51 fiber bundles or fascicles and each bundle is comprised of around 10-30 elementary fibers [18-20]. Though the stem length varies from 20 to 150 cm, the length of elementary flax fibers is typically between 20-30 mm and can extend up to 120 mm [18]. The typical diameter of an elementary fiber varies from 5-15 μm and a few elementary fibers are grouped together to form a technical fiber[21]. Typically, the diameter of technical fibers vary between 35-150 μm (Figure 1)[22].

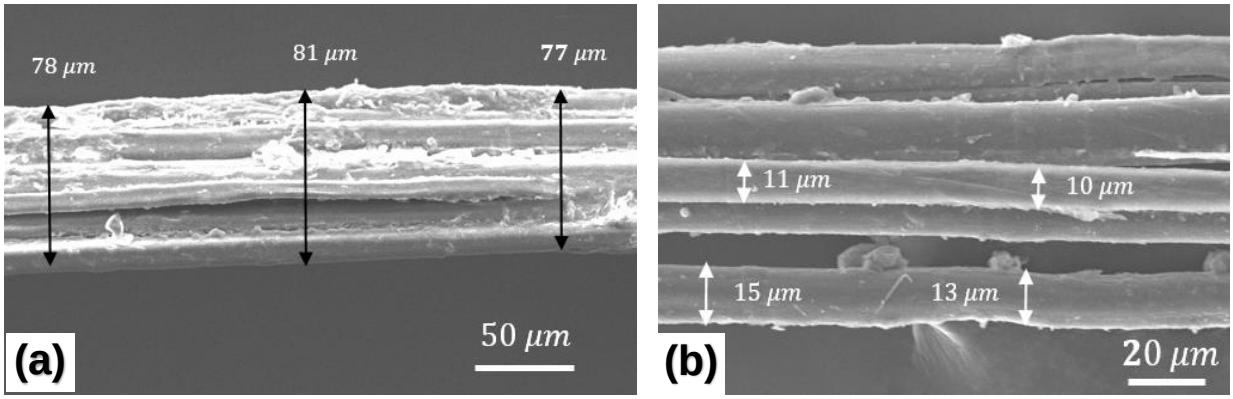

Figure 1.1: (a) Technical fiber: several individual cells bonded together by pectin (b) single fiber: individual sclerenchyma cells, diameter varies between 15-20 micrometer

Elementary fibers are essentially multinucleate single elongated sclerenchyma cells [23]. These elementary fibers are not uniform monofilaments like glass or carbon fibers, rather they are layered structure and a composite in itself. Flax fibers also have a hollow interior, which is called lumen. However, in mature flax the lumen tends to be very small [24]. Being a flowery plant, flax fiber cell walls fall into the category of type I walls. A flax fiber cell wall is comprised of two individual walls: the primary wall and the secondary wall. The primary wall is a single layer with a thickness of around 0.2 μm and it consists mainly of cellulose, hemicellulose (xyloglucan and/or glucomannan, or arabinoxylan) and pectic polysaccharides [25, 26]. Type II walls are present in rice and barley and rich in arabinoxylan. But they contain less than 10% pectin. Lignin is the characteristic element of secondary wall and it is deposited on the preexisting polysaccharide matrix of cellulose and hemicellulose [27]. In addition to these primary components, there may be trace amounts of wax, proteins (structural glycoproteins, arabinogalactan proteins), enzymes and minerals (Ca, K, Na, Fe, Mg, Si, Zn, and B together can add up to 5% of the dry weight of the cell wall).

Previously it was proposed that the cell wall polymers (xyloglucan, pectin and glycoprotein) are covalently linked to one another [28]. However, the lack of compelling evidence has motivated researchers to abort this hypothesis. The most recent models propose that a non-covalent interaction exists between wall polymers [29-31]. It is stipulated that two completely different but mutually interacting networks form the backbone of the cell wall. One network is composed of pectic polysaccharides (homogalacturonan, rhamnogalacturonans, rhamnogalacturonan II) and the other one is composed of cellulose and xyloglucan. According to this model, cellulose xyloglucan network is believed to be the major load bearing element in the cell wall while the pectin network rather act as scaffolding element and controls wall porosity.

They are not usually associated with load bearing functions. This pectin network may also function as sites for binding positively charged molecules such as enzymes and trigger specific catalytic activities. In this way, they may function as a sensor of mechanical stress or elastic strain in the cell wall, thereby controlling the rate at which wall polysaccharides are synthesized. Usually the strength of flax fibers depends on the amount of cellulose in the cell wall. It is reported that the cellulose content of flax fiber varies between 71-81% depending on the growing conditions, variety and location [32, 33]. Hemicellulose, lignin, pectin, and wax content varies between 18.6-20.6 %, 2.2-3 %, 2.3-4 %, and 1.7 % respectively [34-37]. The presence of wax can be removed by organic solvent extraction process. Waxes can also affect the surface properties of flax fiber such as adhesion and wetting.

Cellulose is a very large polymeric chain having the repeat unit of $\beta - D -$ glucopyranose ring (Figure 1.2). This ring has six carbon atoms and five –OH groups. After the formation of $\beta - 1 - 4$ glycosidic linkage through condensation reaction, each repeat units are left with three –OH groups. A typical ramie, cotton, and flax contains around 6500, 7000, and 8000 repeat units respectively. Due to the presence of a large number of –OH groups in cellulose polymeric chains, they are hydrophilic in nature. Again, this –OH groups also contributes to the formation of crystalline region in the polymeric chain, as they facilitate the formation of hydrogen bonding and Van Der Waals interaction. Unlike starch, cellulose is a straight chain polymer and branching is not observed. Cellulose molecules can crystalize into five different polymeric forms: Cellulose I, Cellulose II, Cellulose III, Cellulose IV, and Cellulose X [38]. In most living plants and natural fibers, Cellulose I is the predominant crystalline structure [39]. By the process of mercerization [40] , Cellulose I can be converted to Cellulose II [41]. Cellulose II is more chemically active than Cellulose I, and for this reason chemical industries are more

interested in them. Cellulose II can be used to produce viscose, cellophane, cuprammonium rayon, tire chord rayon etc. [42].

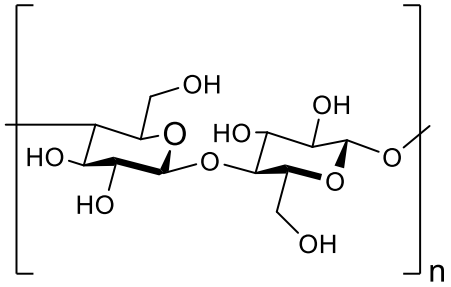

Figure 1.2: Structure of cellulose

Hemicellulosic wall polysaccharides are defined as those that are solubilized with aqueous alkali, but cannot be solubilized by hot water or chelating agents. Typical hemicellulosic wall polysaccharides include xyloglucan, glucomannan, xylan, and glucan. They are usually branched copolymer. Xyloglucan is the most prominent and abundant hemicellulosic polysaccharides in the primary cell wall. In xyloglucan the main repeating backbone unit is $1{,}4-\beta-D$-Glucopyranose, that is, they have a cellulosic backbone and as a side chain $\alpha-D$-Xylopyranose, $\beta-D$- Galactopyranose, $\alpha-L$-Fucopyranose may exist. For glucomannan, the main repeating backbone unit is $1{,}4-\beta-D$-Glucopyranose and $1{,}4-\beta-D$-Mannopyranose. $\alpha-D$-Galactopyranose may exist as a side chain. Xyloglucan, xylans, and mannans are chemically similar to cellulose. This structural similarity between cellulose and hemicellulose leads to the formation of a strong noncovalent bonding between hemicellulose and cellulose microfibrils.

On the other hand, pectic polysaccharides can be solubilized with treatments using aqueous buffers, dilute acids, and calcium chelators. They include homogalacturonan, galacturonans, and rhamnogalacturonans. Usually homogalacturonan (HG) is a linear chain and

the main repeating backbone unit is $1,4-\alpha-D$-Galactopyranosyluronic acid (GalpA) (Figure 1.3) [27]. When the carboxyl groups present in the HG polymers are esterified by methyl groups, they are referred to as pectin and HG with no esterification is referred to as pectic acid. HG may account for up to 60% of the pectin in the primary cell wall. Pectin may contribute to the cell wall plasticity and may act as gelling agent.

Among the cell wall polymers, the structure of lignin is the most complex and the least understood. Lignin is usually deposited on a preformed polysaccharide matrix and provide water proofing, seal and protection of the cell wall. They are also responsible for reducing the porosity of the cell wall. The microfibril diameter in the lignified cell wall is higher than the unlignified cell wall. Lignin is basically an amorphous, three dimensional, aromatic polymer resulting from the polymerization of phenoxy redicals that are derived from three hydroxycinnamyl alcohols [43]. The three monolignols are p-coumaryl alcohol, coniferyl alcohol, and sinapyl alcohol (Figure 1.4). By coupling these three alcohols by a non-enzymatic process, lignin polymer is formed and this process involves at least eleven kinds of intermonomeric linkages. Chemical bonding exists between lignin and plant polysaccharides. Galactose and arabinose may act as linking agent between lignin and hemicelluloses. For more detailed discussion of lignin chemistry and structure these references are recommended [44, 45].

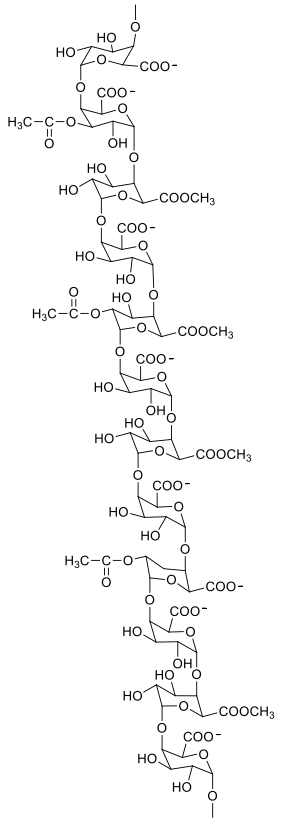

Figure 1.3: Structure of homogalcturonan

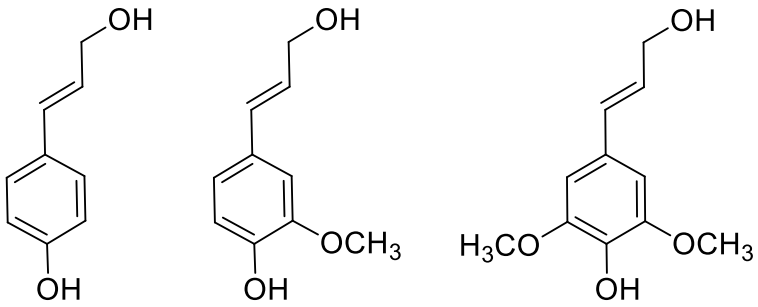

Figure 1.4: Three primary alcohol in lignin

According to classical literature, the secondary wall mainly consists of three layers namely S1, S2 and S3 with a thickness of 0.5-2 μm, 5-10 μm and 0.5-1 μm respectively [17, 46].

Among them the S2 layer is the thickest and around 70% of the Young's Modulus is mainly governed from this part of the structure. However, the transmission electron microscopy of flax fiber suggests that there are more than four layers present in the cell wall [47]. It is a common practice in the literature to describe the morphological feature of a single flax fiber as the same as that of the wood cell, although they are quite different. As the diameter of flax fiber varies widely, so sometimes it is convenient to describe the thickness of different layers in terms of the percentage of its diameter. A relative thickness of 15-20% for S1 and S3, 70-80% for S2, and 1-4% for primary layer is generally reported in the literature [48, 49].

However, high resolution TEM image of flax fiber reveals that S3 layer has three to four sublayer and constitute 20-25% of the diameter [47]. The middle lamella or S2 layer constitutes 55-70% of the total thickness and the outer layer is about 2-10% of the thickness. Thus, this study enables us to hypothesize a seven layer single flax fiber model which is more accurate than the widely used four layer model of flax fiber. Domenges and Charlet [24] also attempted to characterize the internal structure of flax fiber within multiple length scale using focused ion beam method. They also confirmed the presence of more than four layers contrary to the four layer model usually cited in the literature. In a separate study, Charlet et. al. [50] maintained that the assumption of hexagonal cross section is no better than assuming a circular cross section. In addition, the assumption of circular shape provide advantage in terms of simplicity of the analysis. They also proposed a form factor (f) based on the analysis of a large number of cross sectional area of elementary fibers. This form factor assumes a value of one when the cross section is a perfect circle and a value of zero when the cross section is a perfect line. They also proposed the use of a medium sized technical fibers to be used in composite materials for

achieving better properties. Too large a technical fiber would result in higher elementary fiber sliding while too small a technical fiber would limit and complicate the extraction process.

The S2 layer is analogous to a composite lamina where cellulose meso-fibrils, having a diameter of 100-200 nm, are helically arranged in an amorphous matrix of hemicellulose and pectin (Figure 1.5) [21]. The meso-fibrils are a bundle of microfibrils having a diameter between 2-10 nm [51]. These fibrils are at an angle with the fiber longitudinal direction, known as the helix angle of the fibrils. The orientation of the microfibril angle in S2 layer governs the physical and mechanical properties of any natural fibers. The microfibril angle of single wood fibers were investigated widely [52] and it varies from species to species. A few methods that were employed for measuring the microfibril angle of wood fibers such as X-ray diffraction method [53], polarized light microscopy method [54], and near infrared spectrum method [55, 56] are noteworthy. Some researchers have used ultra sound for rupturing the cell wall, and thus were able to observe the fibril angle in the cell wall [57].

Muller et.al. [58] have measured the microfibril angle of flax fiber by micro-small angle X-ray scattering method (μSAXS). He found the fibril angle to be 8.8°. He hypothesized the shape of cellulose microfibril as cylinders and measured the diameter to be 3 nm. This result is consistent with the SAXS study performed by Heyn [59, 60]. Transmission electron microscopy reveals the diameter to be between 2-4 nm. However, X-ray and neutron diffraction experiments reveal the diameter of the cellulose microfibril to be 4.5 nm which is slightly higher than the other techniques [61-63]. Astley et. al.[64] measured the helix angle of flax fiber with small angle X-ray diffraction technique and found that it depends on the degree of water sorption. In dry state the angle is approximately 10 degrees and in wet state the angle is 15 degrees. This angle is quite small when compared to the helix angle of cotton fibers (30°) and coir and some

leaf fibers (more than 40°)[65-67]. Typically, the higher the microfibril angle, the lower is the value of strength and modulus. For this reason, flax fibers with lower helix angles are among some of the strongest and stiffest natural fibers.

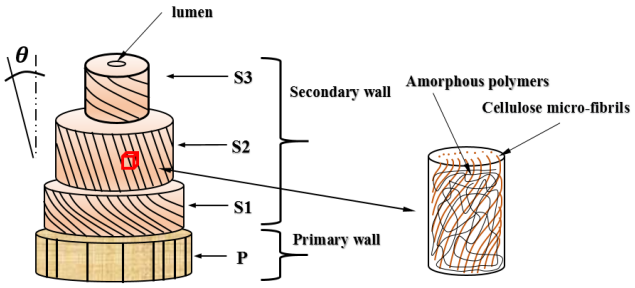

Figure 1.5: Schematic diagram of a single fiber with primary and secondary layers, secondary layer is composed of S1, S2, and S3 layer. A smaller portion of S2 layer is magnified and cellulose micro-fibrils are seen to be dispersed on an amorphous polymeric matrix. Adapted from [70].

The mechanical properties of flax fibers have been investigated widely [65, 68-72]. The tensile strength of flax fiber is in the range of 250-2000 MPa, failure strain is between 1.2 and 3.5 % and Young's modulus varies between 30 and 110 MPa [73-78]. By using X-ray scattering method, Astley et.al. [79] studied the deformation of flax fiber under tension. They performed both small angle and wide angle X-ray scattering experiments on technical flax fibers. They showed that the initial increase in the intensity of wide angle data is due to the strain induced crystallization of the cellulose chain. By performing experiments on other polymeric materials, they concluded that the noncrystalline cellulose chains are also oriented parallel to the cellulose crystals, and for this reason they are not assumed to be perfectly amorphous.

Lefeuvre et.al [80] investigated the variation of mechanical properties such as elastic modulus, failure stress and failure strain among different types of flax fibers. They named the samples M1 and M2. The elastic modulus and failure stress of M1 samples were reported to be

greater than 55 GPa and 1000 MPa while the elastic modulus and failure stress of M2 samples were reported to be 45 GPa and 800 MPa, respectively. They attributed this variation in mechanical property is partly due to the differences in the cell wall composition, that is, on the proportion of amorphous and crystalline materials. They also attempted to perform statistical analysis on different samples.

The different values for elastic modulus and tensile strength reported in the literature is not an absolute value for the true strength and modulus of flax fiber. In fact, there exists many uncertainties and they have a very large standard deviation that may originate from the separating process of the fiber, retting conditions, presence of defects, and the experimenter and the machine itself. The uncertainty may also originate from the measurement of the diameter, as the flax fiber does not have a uniform cross section throughout the whole length of the fiber. Lefeuvre et. al. [81] in a separate study, attempted to quantify this variation of uncertainty from different sources. He mentioned that 78% of the uncertainty of elastic modulus and 93% of the uncertainty of failure stress results from the measurement of the diameter and the cross sectional area of the fiber. Bodros et. al [82] investigated the mechanical properties of flax fiber reinforced biopolymers in conjunction with the glass fiber reinforced biopolymers. Though the properties of glass fiber reinforced bio-composites shows better properties, they suggested that by improving the interfacial adhesion between the flax fiber and the matrix, it is possible to manufacture flax fiber reinforced bio-composite materials, which could be used for structural load applications.

Mechanical properties of flax fiber is influenced by drying and thermal loading. Baley et. al [70] performed thermogravimetric analysis of flax fiber. They subjected the flax fiber at 105° Celsius for 14 h and at 150° Celsius for 5 h. They observed that most of the weight loss occurs during the first few minutes and this weight loss is due to the vaporization of water molecules

present in the fiber surface and in the mesofibrils. At 105° Celsius complete evaporation of water does not occur as some of the water molecules form hydrogen bond with the polysaccharide matrix and are strongly attached to them. However, at 150° Celsius water molecules are completely removed from the fiber. Tensile tests on dried fibers shows the significant loss of elastic modulus, failure stress and failure strain. When composite is prepared with these dried fibers, similar trend is also observed as that of the dried fibers.

The moisture absorption behavior of flax fiber was investigated by Stuart et. al. [83] They subjected the flax fiber to be immersed in a specified amount of time and measured the weight gain of the fiber. They found that for the first few minutes, the weight gain occurs very quickly. After this initial high rate of weight gain, water uptake tendency of flax fiber slows down, and either zero or variable number of water uptake steps are observed during the prolonged exposure of flax fiber in water.

For investigating the fracture mechanism of flax fiber reinforced composite materials, it is necessary to investigate the fracture mechanism of elementary and technical fiber itself. Romhany et. al [22] investigated the failure mode of flax fiber by acoustic emission technique. He maintained that the failure of flax fiber is initiated by the axial or longitudinal fibrillation. The radial micro-cracking may be initiated by a drop in load or at the point of maximum load. This hypothesis was confirmed by acoustic emission (AE) amplitude measurement. High AE amplitudes correspondence to the radial or transverse crack which is mainly observed near the failure stress. They can also be linked to the failure of microfibrils.

The surface of flax fibers contain numerous defects. These defects may originate during the separation process of flax fiber from the flax stem. The location of these defects may act as the potential site for crack initiation and crack propagation. Baley [84] measured the tensile

strength of flax fiber as a function of the number of defects present in the fiber. However, he maintained that no specific relationship exists between these two parameters. In composite materials, these defects may act as the site for the initiation of debonding and the formation of micro-cracks.

Lefeuvre et. al [85] performed a study for analyzing the role of different constituent polysaccharides on the mechanical properties of flax fiber. After extracting the fiber from the flax stem, they successively performed different treatment such as cold water washing, boiling water extraction, EDTA extraction, HCl treatment, NaOH treatment for differentially removing different polysaccharides. They found the failure strength and modulus of the crude fiber having the highest value. As the fiber undergoes different treatments, the hemicelluloses and pectins continue to be removed, and their failure strength and modulus goes on decreasing. During tensile testing, exceeding a specific level of shear stress may initiate breaking of bondage between hemicellulose and cellulose or hemicellulose and pectins. This bond breaking will result in a slippage of the matrix.

Oksman et. al [86] studied the influence of fiber micro-structure on the mechanical properties of polypropylene based bio-composite materials. The reported the tensile strength, elongation, and modulus of flax fiber to be 345-1100 MPa, 2.4%, and 28-100 GPa respectively. They mentioned the sisal fiber to be the toughest among flax, sisal, jute and banana fiber. The flax fibers were easily separated into elementary fibers during extrusion which resulted in better dispersion and higher l/d ratio. However, the fiber length of flax fibers were lower than sisal fibers resulting in a lower impact strength. On the other hand, flax fiber reinforced composites showed best performance in terms of strength and modulus with the addition of coupling agents

compared to sisal, jute and banana fibers. This improved performance can be attributed to the higher fiber matrix adhesion, better dispersion and higher l/d ratio.

The presence of wax and non-cellulosic polysaccharides on fiber surface may hinder proper interfacial bonding between the fiber and the matrix. The degree of retting and the type of retting may also affect the fiber properties. Li et. al [87] investigated the effect of different enzymatic treatments on the mechanical properties of hemp fibers and their composites. By using different characterization techniques such as Fourier transform infrared spectroscopy (FTIR), chemical and thermal analysis of fiber, SEM, X-ray diffraction, they confirmed that enzymatic treatment removed wax, pectin, lignin, and other non-cellulosic compounds from hemp fibers. They also reported a higher strength of composites prepared from these treated hemp fibers. However, when enzyme treated elementary fibers were tensile tested, they showed lower mechanical properties than untreated or raw fibers. These lower strength may be attributed to the partial degradation of cellulose fibrils during the treatment and loss of hemicellulose and pectin. However, this treatment exposed higher amount of –OH groups on the fiber surface. With the presence of maleated polypropylene (MAPP), a coupling agent, these –OH groups could assist in bonding with the matrix resulting in higher strength of composite materials. On the contrary, Bourmaud et. al [75] performed water washing on fiber instead of enzyme treatment for removing wax and debris originating from non-degraded cortical tissues. They prepared three batches of fibers. One batch was just raw fibers. Among the other two batches, one was subjected to distilled water for 72 h at 23 ° Celsius and the other batch was immersed in hot water at 100 ° Celsius for one hour. They observed a detrimental effect of hot water treatment on the fiber that can penetrate several 10 nm into the fiber wall. Room temperature water washing

had a beneficial effect on the fiber resulting in smooth fiber surface and improved mechanical properties.

Pucci et. al [88] studied the capillary wicking of water in flax fabrics. They investigated the capillary effects combined with swelling during spontaneous imbibition of water in both treated and untreated flax fabrics. The maintained that the exposure of the fabrics in a thermal environment before coming in contact with water may decrease the sensitivity to water uptake of flax fiber. This thermal treatment degrades the hemicellulose, which is partially responsible for the hydrophilic nature of flax fiber. In addition, the thermal decomposition of hemicellulose generates free radicals which modify the nature of pectins [89, 90].

The study of the thermal degradation of flax fiber is important as the manufacturing of composite materials often involves the application of heat. Van De Velde and Kiekens [91] studied the thermal degradation of different types of flax fibers such as green flax, medium retted, dew retted and boiled flax by thermogravimetric analysis (TGA). They found that the cellulose content of the fiber is proportional to the loss of mass of the fiber in TGA peak. They also calculated the reaction constant and activation energy of different types of fibers. The fully retted and boiled fibers had the highest degree of thermal stability.

Hu et. al.[92] studied the thermal behavior and interfacial bond strength of dew retted [93-95] and enzyme retted [96-98] flax fibers. From thermogravimetric analysis (TGA), they found that the enzyme retted flax has better thermal stability than dew retted flax. In terms of interfacial shear strength of flax/PP composite and single fiber tensile strength, the enzyme retted flax showed better performance.

With the above literature review, it is apparent that no study was performed assessing the effect of stalk diameter to the strength of individual or technical flax fiber. This study aims to bridge the gap between the existing literature and the lack of knowledge on this specific field.

1.4. References

1. Agarwal, B.D., L.J. Broutman, and K. Chandrashekhara, *Analysis and performance of fiber composites*. 2006: John Wiley & Sons.
2. Mohanty, A.K., M. Misra, and L.T. Drzal, *Natural fibers, biopolymers, and biocomposites*. 2005: CRC press.
3. Stevens, E.S., *Green plastics: an introduction to the new science of biodegradable plastics*. 2002: Princeton University Press.
4. Netravali, A.N. and S. Chabba, *Composites get greener*. Materials today, 2003. **6**(4): p. 22-29.
5. Mueller, D.H. and A. Krobjilowski, *New discovery in the properties of composites reinforced with natural fibers.* Journal of Industrial Textiles, 2003. **33**(2): p. 111-130.
6. Pandey, J.K., et al., *Recent advances in the application of natural fiber based composites.* Macromolecular Materials and Engineering, 2010. **295**(11): p. 975-989.
7. Karus, M., M. Kaup, and S. Ortmann, *Naturfasereinsatz in Verbundwerkstoffen in der deutschen und österreichischen Automobilindustrie Status 2002, Analyse und Trends.* Nova-Institut, Hürth, 2003.
8. Joshi, S.V., et al., *Are natural fiber composites environmentally superior to glass fiber reinforced composites?* Composites Part A: Applied science and manufacturing, 2004. **35**(3): p. 371-376.

9. Grozdanov, A., et al., *Biocomposites Based on Natural Fibers and Polymer Matrix—From Theory to Industrial Products.* Green Biorenewable Biocomposites: From Knowledge to Industrial Applications" edit by Vijau Kumar and Michael R. Kessler, 2015: p. 323-344.
10. YILMAZ, N.D. and N.B. Powell, *Biocomposite Structures as Sound Absorber Materials*. 2015: Apple Academic Press, Canada.
11. Ng, Y.H. and L. Hong, *Acoustic attenuation characteristics of surface-modified polymeric porous microspheres.* Journal of applied polymer science, 2006. **102**(2): p. 1202-1212.
12. Fahy, F.J., *Foundations of engineering acoustics*. 2000: Academic press.
13. Cox, J., *D' Antonio P., Acoustic Absorbers and Diffusers*. 2004, Spon Press, Taylor& Francis Group, London and New York.
14. Dhakal, H., et al., *The low velocity impact response of non-woven hemp fibre reinforced unsaturated polyester composites.* Composite structures, 2007. **81**(4): p. 559-567.
15. Mohanty, A., M. Misra, and G. Hinrichsen, *Biofibres, biodegradable polymers and biocomposites: an overview.* Macromolecular materials and Engineering, 2000. **276**(1): p. 1-24.
16. Bledzki, A. and J. Gassan, *Composites reinforced with cellulose based fibres.* Progress in polymer science, 1999. **24**(2): p. 221-274.
17. Fuqua, M.A., S. Huo, and C.A. Ulven, *Natural fiber reinforced composites.* Polymer Reviews, 2012. **52**(3): p. 259-320.
18. Diederichsen, A. and K. Richards, *Cultivated flax and the genus Linum L.* Flax: the genus Linum, 2003: p. 22-54.

19. Batra, S.K., *Other long vegetable fibers*, in *Handbook of Fiber Chemistry, Third Edition*. 2006, CRC Press.

20. Mukherjee, P. and K. Satyanarayana, *An empirical evaluation of structure-property relationships in natural fibres and their fracture behaviour.* Journal of materials science, 1986. **21**(12): p. 4162-4168.

21. Morvan, C., et al., *Building flax fibres: more than one brick in the walls.* Plant Physiology and Biochemistry, 2003. **41**(11): p. 935-944.

22. Romhany, G., J. Karger-Kocsis, and T. Czigany, *Tensile fracture and failure behavior of technical flax fibers.* Journal of Applied Polymer Science, 2003. **90**(13): p. 3638-3645.

23. Gibson, L.J., *The hierarchical structure and mechanics of plant materials.* Journal of the Royal Society Interface, 2012: p. rsif20120341.

24. Domenges, B. and K. Charlet, *Direct insights on flax fiber structure by focused ion beam microscopy.* Microscopy and Microanalysis, 2010. **16**(02): p. 175-182.

25. Cosgrove, D.J., *Assembly and enlargement of the primary cell wall in plants.* Annual review of cell and developmental biology, 1997. **13**(1): p. 171-201.

26. Carpita, N.C. and D.M. Gibeaut, *Structural models of primary cell walls in flowering plants: consistency of molecular structure with the physical properties of the walls during growth.* The Plant Journal, 1993. **3**(1): p. 1-30.

27. Rose, J.K., *The plant cell wall*. Vol. 8. 2003: CRC Press.

28. Keegstra, K., et al., *The structure of plant cell walls III. A model of the walls of suspension-cultured sycamore cells based on the interconnections of the macromolecular components.* Plant physiology, 1973. **51**(1): p. 188-197.

29. Talbott, L.D. and P.M. Ray, *Molecular size and separability features of pea cell wall polysaccharides Implications for models of primary wall structure.* Plant Physiology, 1992. **98**(1): p. 357-368.

30. McCann, M.C. and K. Roberts, *Changes in cell wall architecture during cell elongation.* Journal of Experimental Botany, 1994. **45**(Special Issue): p. 1683-1691.

31. Ha, M.-A., D.C. Apperley, and M.C. Jarvis, *Molecular rigidity in dry and hydrated onion cell walls.* Plant Physiology, 1997. **115**(2): p. 593-598.

32. Thuault, A., et al., *Interrelation between the variety and the mechanical properties of flax fibres.* Journal of Biobased Materials and Bioenergy, 2013. **7**(5): p. 609-618.

33. Thuault, A., et al., *Numerical study of the influence of structural and mechanical parameters on the tensile mechanical behaviour of flax fibres.* Journal of Industrial Textiles, 2014. **44**(1): p. 22-39.

34. Day, A., et al., *Lignification in the flax stem: evidence for an unusual lignin in bast fibers.* Planta, 2005. **222**(2): p. 234-245.

35. Love, G., et al., *Determination of phenolic structures in flax fibre by solid-state 13C NMR.* Phytochemistry, 1994. **35**(2): p. 489-491.

36. McDougall, G.J., *Isolation and partial characterisation of the non-cellulosic polysaccharides of flax fibre.* Carbohydrate research, 1993. **241**: p. 227-236.

37. Gorshkova, T.A., et al., *Cell-wall polysaccharides of developing flax plants.* Plant Physiology, 1996. **110**(3): p. 721-729.

38. Ugbolue, S., *Structure/property relationships in textile fibres.* Textile Progress, 1990. **20**(4): p. 1-43.

39. Lennholm, H., T. Larsson, and T. Iversen, *Determination of cellulose Iα and Iβ in lignocellulosic materials.* Carbohydrate Research, 1994. **261**(1): p. 119-131.

40. Aboul-Fadl, S., et al., *Effect of mercerization on the relation between single fiber mechanical properties and fine structure for different cotton species.* Textile research journal, 1985. **55**(8): p. 461-469.

41. Kulshreshtha, A., *2—A Review Of The Literature On The Formation Of Cellulose Iv, Its Structure, And Its Significance In The Technology Of Rayon Manufacture.* Journal of the Textile Institute, 1979. **70**(1): p. 13-18.

42. Frushour, B., et al., *Handbook of Fiber Science and Technology: Fiber Chemistry*. 1985, Dekker, New York.

43. Adler, E., *Lignin chemistry—past, present and future.* Wood science and technology, 1977. **11**(3): p. 169-218.

44. Crawford, R.L., *Lignin biodegradation and transformation*. 1981: John Wiley and Sons.

45. Sakakibara, A., *A structural model of softwood lignin.* Wood Science and Technology, 1980. **14**(2): p. 89-100.

46. Peterlin, A. and P. Ingram, *Morphology of secondary wall fibrils in cotton.* Textile Research Journal, 1970. **40**(4): p. 345-354.

47. Thuault, A., et al., *Investigation of the internal structure of flax fibre cell walls by transmission electron microscopy.* Cellulose, 2015. **22**(6): p. 3521-3530.

48. Gassan, J., A. Chate, and A.K. Bledzki, *Calculation of elastic properties of natural fibers.* Journal of materials science, 2001. **36**(15): p. 3715-3720.

49. Arnould, O., et al., *Better insight into the nano-mechanical properties of flax fibre cell walls.* Industrial Crops and Products, 2017. **97**: p. 224-228.

50. Charlet, K., et al., *Multi-scale morphological characterisation of flax: From the stem to the fibrils.* Carbohydrate Polymers, 2010. **82**(1): p. 54-61.

51. Ding, S.-Y., et al., *How does plant cell wall nanoscale architecture correlate with enzymatic digestibility?* Science, 2012. **338**(6110): p. 1055-1060.

52. Wang, H., et al., *An improved fibril angle measurement method for wood fibres.* Wood Science and Technology, 2001. **34**(6): p. 493-503.

53. Stuart, S.-A. and R. Evans, *X-ray diffraction estimation of the microfibril angle variation in eucalypt wood.* Appita journal, 1995. **48**(3): p. 197-200.

54. Leney, L., *A technique for measuring fibril angle using polarized light.* Wood and Fiber Science, 2007. **13**(1): p. 13-16.

55. Barnett, J. and V.A. Bonham, *Cellulose microfibril angle in the cell wall of wood fibres.* Biological reviews, 2004. **79**(2): p. 461-472.

56. Gindl, W., et al., *The relationship between near infrared spectra of radial wood surfaces and wood mechanical properties.* Journal of Near Infrared Spectroscopy, 2001. **9**(4): p. 255-262.

57. Huang, C.-L., *Revealing fibril angle in wood sections by ultrasonic treatment.* Wood and Fiber Science, 2007. **27**(1): p. 49-54.

58. Müller, M., et al., *Direct observation of microfibril arrangement in a single native cellulose fiber by microbeam small-angle X-ray scattering.* Macromolecules, 1998. **31**(12): p. 3953-3957.

59. Heyn, A.N., *Small Particle X-Ray Scattering by Fibers, Size and Shape of Microcrystallites.* Journal of Applied Physics, 1955. **26**(5): p. 519-526.

60. Heyn, A., *Small Particle X-Ray Scattering by Fibers. II. Radial Distribution of Microcrystallites.* Journal of Applied Physics, 1955. **26**(9): p. 1113-1120.

61. Näslund, P., et al., *Diffraction contrast transmission electron microscopy on flax fiber ultrathin cross sections.* Textile Research Journal, 1988. **58**(7): p. 414-417.

62. Fischer, E., et al., *Small-angle neutron scattering of selectively deuterated cellulose.* Macromolecules, 1978. **11**(1): p. 213-217.

63. Müller, M., et al., *Combined X-ray microbeam small-angle scattering and fibre diffraction experiments on single native cellulose fibres.* Journal of applied crystallography, 2000. **33**(3): p. 817-819.

64. Astley, O.M. and A.M. Donald, *A small-angle X-ray scattering study of the effect of hydration on the microstructure of flax fibers.* Biomacromolecules, 2001. **2**(3): p. 672-680.

65. Bourmaud, A., et al., *Relationships between micro-fibrillar angle, mechanical properties and biochemical composition of flax fibers.* Industrial Crops and Products, 2013. **44**: p. 343-351.

66. Baley, C., *Analysis of the flax fibres tensile behaviour and analysis of the tensile stiffness increase.* Composites Part A: Applied Science and Manufacturing, 2002. **33**(7): p. 939-948.

67. Hearle, J., *The fine structure of fibers and crystalline polymers. III. Interpretation of the mechanical properties of fibers.* Journal of applied polymer science, 1963. **7**(4): p. 1207-1223.

68. Charlet, K., et al., *Mechanical properties of flax fibers and of the derived unidirectional composites.* Journal of Composite Materials, 2010. **44**(24): p. 2887-2896.

69. Bos, H., M.J. Van Den Oever, and O.C. Peters, *Tensile and compressive properties of flax fibres for natural fibre reinforced composites.* Journal of Materials Science, 2002. **37**(8): p. 1683-1692.

70. Baley, C., et al., *Influence of drying on the mechanical behaviour of flax fibres and their unidirectional composites.* Composites Part A: Applied Science and Manufacturing, 2012. **43**(8): p. 1226-1233.

71. Shah, D.U., R.K. Nag, and M.J. Clifford, *Why do we observe significant differences between measured and 'back-calculated'properties of natural fibres?* Cellulose, 2016. **23**(3): p. 1481-1490.

72. Andersons, J., et al., *Strength distribution of elementary flax fibres.* Composites science and technology, 2005. **65**(3): p. 693-702.

73. Baley, C. and A. Bourmaud, *Average tensile properties of French elementary flax fibers.* Materials Letters, 2014. **122**: p. 159-161.

74. Spārniņš, E. and J. Andersons, *Diameter variability and strength scatter of elementary flax fibers.* Journal of materials science, 2009. **44**(20): p. 5697-5699.

75. Bourmaud, A., C. Morvan, and C. Baley, *Importance of fiber preparation to optimize the surface and mechanical properties of unitary flax fiber.* Industrial Crops and Products, 2010. **32**(3): p. 662-667.

76. Andersons, J., E. Spārniņš, and E. Poriķe, *Strength and damage of elementary flax fibers extracted from tow and long line flax.* Journal of composite materials, 2009.

77. Andersons, J., E. Poriķe, and E. Spārniņš, *Ultimate strain and deformability of elementary flax fibres.* The Journal of Strain Analysis for Engineering Design, 2011. **46**(6): p. 428-435.

78. Charlet, K., et al., *Influence of an Agatha flax fibre location in a stem on its mechanical, chemical and morphological properties.* Composites Science and Technology, 2009. **69**(9): p. 1399-1403.

79. Astley, O. and A. Donald, *The tensile deformation of flax fibres as studied by X-ray scattering.* Journal of materials science, 2003. **38**(1): p. 165-171.

80. Lefeuvre, A., et al., *Elementary flax fibre tensile properties: correlation between stress–strain behaviour and fibre composition.* Industrial Crops and Products, 2014. **52**: p. 762-769.

81. Lefeuvre, A., et al., *A study of the yearly reproducibility of flax fiber tensile properties.* Industrial Crops and Products, 2013. **50**: p. 400-407.

82. Bodros, E., et al., *Could biopolymers reinforced by randomly scattered flax fibre be used in structural applications?* Composites Science and Technology, 2007. **67**(3): p. 462-470.

83. Stuart, T., et al., *Modelling of wicking and moisture interactions of flax and viscose fibres.* Carbohydrate polymers, 2015. **123**: p. 359-368.

84. Baley, C., *Influence of kink bands on the tensile strength of flax fibers.* Journal of materials science, 2004. **39**(1): p. 331-334.

85. Lefeuvre, A., et al., *Analysis of the role of the main constitutive polysaccharides in the flax fibre mechanical behaviour.* Industrial Crops and Products, 2015. **76**: p. 1039-1048.

86. Oksman, K., et al., *The influence of fibre microstructure on fibre breakage and mechanical properties of natural fibre reinforced polypropylene.* Composites Science and Technology, 2009. **69**(11): p. 1847-1853.

87. Li, Y. and K.L. Pickering, *Hemp fibre reinforced composites using chelator and enzyme treatments.* Composites Science and Technology, 2008. **68**(15): p. 3293-3298.

88. Pucci, M.F., P.-J. Liotier, and S. Drapier, *Capillary wicking in flax fabrics–effects of swelling in water.* Colloids and Surfaces A: Physicochemical and Engineering Aspects, 2016. **498**: p. 176-184.

89. Pucci, M.F., P.-J. Liotier, and S. Drapier, *Capillary effects on flax fibers–Modification and characterization of the wetting dynamics.* Composites Part A: Applied Science and Manufacturing, 2015. **77**: p. 257-265.

90. Pucci, M.F., et al., *Wetting and swelling property modifications of elementary flax fibres and their effects on the Liquid Composite Molding process.* Composites Part A: Applied Science and Manufacturing, 2017. **97**: p. 31-40.

91. Van De Velde, K. and P. Kiekens, *Thermal degradation of flax: The determination of kinetic parameters with thermogravimetric analysis.* Journal of Applied Polymer Science, 2002. **83**(12): p. 2634-2643.

92. Hu, W., et al., *Comparison between dew-retted and enzyme-retted flax fibers as reinforcing material for composites.* Polymer Engineering & Science, 2012. **52**(1): p. 165-171.

93. Morrison Iii, W., et al., *Chemical and physical characterization of water-and dew-retted flax fibers.* Industrial Crops and Products, 2000. **12**(1): p. 39-46.

94. Sharma, H. and G. Faughey, *Comparison of subjective and objective methods to assess flax straw cultivars and fibre quality after dew-retting.* Annals of Applied Biology, 1999. **135**(2): p. 495-501.

95. Pallesen, B.E., *The quality of combine-harvested fibre flax for industrials purposes depends on the degree of retting.* Industrial crops and products, 1996. **5**(1): p. 65-78.

96. Akin, D.E., et al., *Optimization for enzyme-retting of flax with pectate lyase.* Industrial Crops and Products, 2007. **25**(2): p. 136-146.

97. Van Sumere, C.F. and H.S. Sharma, *Analyses of fine flax fibre produced by enzymatic retting.* Aspects Appl Biol, 1991. **28**: p. 15-20.

98. Mooney, C., et al., *Analysis of retted and non retted flax fibres by chemical and enzymatic means.* Journal of Biotechnology, 2001. **89**(2): p. 205-216.

CHAPTER 2. STATISTICAL ANALYSIS

This chapter presents the detailed description of the procedures and methodologies of tensile testing of technical flax fibers. Background theories are introduced at the beginning and statistical analysis such as hypothesis testing and ANOVA analysis are presented thereafter. Next, different probability distributions are employed to fit the data and the distribution with the highest degree of fit is identified. The effect of strain rate on technical fiber is also analyzed. Out of the six samples tested, only the data and graph of one sample is presented in this chapter. The rest of the data and graphs are presented in the appendix.

2.1. Theoretical background

In literature, a bundle of flax fiber is usually referred to as the technical fiber and an individual fiber is called a single fiber or fiber ultimate or elementary fibers. Into a technical fiber, these single fibers are held together by pectic polysaccharides. The strength of elementary fibers were reported to be higher than the technical fibers and with the increase in gauge length, the strength of elementary fibers were reported to decrease. This phenomena is due to the number of defects present in the single fibers. As the gauge length of the fiber increases, the number of defects present in the fiber also increases, which reduces the strength of the fiber. The defects in the elementary fibers are generally referred to as kink bands, dislocations or nodes [1]. They are actually localized distortions of the cell wall. More specifically, when the micro-fibrils in the secondary cell wall get misaligned and oriented perpendicular to the fiber axis, the region is slightly protruded from the plane surface, and they can be seen in plane polarized microscope as thin strips or dark lines. They may originate during the growth or processing (hackling, scutching, and separating) of the fibers. These kink bands are the weakest points in the

elementary fiber. During tensile testing, the origin and propagation of cracks occur from these kink bands.

The amount of damage sustained by the elementary fiber is usually quantified by the presence of the kink bands per unit length. The number of kink bands in a single fiber may vary between 100 and 500 [2], and the spacing between the two adjacent kink bands may be approximately 120 micrometer [3].

2.1.1. Weakest link theory

For understanding the weakest link theory, a chain or shackles consisting of n links or parts may be considered. With the application of a tensile stress σ, the probability of failure of a single link is $F(\sigma)$. The probability of failure of the whole chain $F_n(\sigma)$ is to be determined. The total chain or shackle will fail if a single component or link from that chain is failed. On the other hand, the total chain or shackle is survived if each and every component or link is survived. The probability of non-failure of a single link is $(1-F)$. As the failure of a link does not affect the failure of another link, they are independent events. As a result the probability of non-failure of two successive link is

$$(1-F).(1-F) = (1-F)^2$$

Similarly, the probability of non-failure of the n links is

$$(1-F).(1-F).(1-F) \ldots \ \ldots (1-F) = (1-F)^n$$

The probability of non-failure of the whole chain is $(1-F_n)$.As a result,

$$(1-F_n) = (1-F)^n$$

$$F_n(\sigma) = 1-(1-F(\sigma))^n$$

At this point, the task is reduced to finding a suitable function for $F(\sigma)$. According to Weibull [4], any distribution function may be written in the following form

$$F(\sigma) = 1 - e^{-\varphi(\sigma)}$$

From which, the following relations are obtained.

$$1 - F(\sigma) = 1 - \left(1 - e^{-\varphi(\sigma)}\right) = e^{-\varphi(\sigma)}$$

$$\{1 - F(\sigma)\}^n = e^{-n.\varphi(\sigma)}$$

$$1 - \{1 - F(\sigma)\}^n = 1 - e^{-n.\varphi(\sigma)}$$

Therefore, the probability of failure of the whole chain is,

$$F_n(\sigma) = 1 - e^{-n.\varphi(\sigma)} \tag{2.1}$$

Equation (2.1) represents the mathematical expression of the weakest link theory.

2.1.2. Failure of brittle materials

It is a known fact that the elastic modulus of any material is its intrinsic property. It does not depend on the size or shape of the material but that to the atomic bonds present in the material. Depending on the strength of these atomic bonds, the magnitude of the elastic modulus of a material is determined. If $r_0$is the interatomic distance, e is the electric charge of an electron, and K be a constant, the elastic modulus of ionic solids can be represented by the following equation [5]

$$E = \frac{Ke^2}{{r_0}^4} \tag{2.2}$$

That is, elastic modulus varies according to the negative fourth power of interatomic distance of an ionic material. Ionic bonds are generally observed in ceramic materials. In metals, the situation is more complex and requires the use of wave mechanics. However, the negative fourth power dependence of the interatomic bond length upon the elastic modulus is also observed in metals. In short, the electronic structure of a material has significant influence on the elastic modulus and other properties of a material.

The theoretical breaking or fracture strength and shear strength of a material can be derived from the elastic modulus of a material. That is, it can be related to the interatomic bond strength of a material. We obtain the following relationship:

$$\sigma_{th} = \sqrt{\frac{E\gamma}{r_0}} \approx \frac{E}{\pi} \tag{2.3}$$

$$\tau_{th} = \frac{Gb}{2\pi r_0} \approx \frac{G}{2\pi} \tag{2.4}$$

where, E and G are Young's modulus and shear modulus of the material, r_0 is the interatomic distance and γ is the surface energy of the material.

However, prediction from these equations, about the strength of materials reveals extremely high values, which is seldom achieved in reality. The reason for this mismatch between the theory and the reality may be attributed to the presence of flaws and defects in the material. The size, shape, and orientation of these defects may vary from specimen to specimen. As a result, the strength of individual specimen with similar dimensions generally do not possess the exact same numerical values. It has been experimentally shown that the distribution of tensile stress for ductile material follows a normal distribution and the standard deviation around the mean is very small. That is, the width of the bell-shaped curve is very narrow. On the other hand, for brittle materials, the distribution of strength around the mean is very high and they possess a large standard deviation. In addition, the standard deviation is not symmetric about the mean and there is a large tail on the high strength side, that is, a non-Gaussian distribution. The reason may be attributed to the presence of crack with different shape, size, and orientation inside a specimen and varying degree of distribution of crack from specimen to specimen.

Theoretically, for the failure of a material, the interatomic bonds should be broken. But materials fail with much lower applied stress than this theoretical bond strength. As the crack tips

are very sharp, they may act as the site for stress concentration, and the localized stress in the crack tip may exceed the interatomic bond strength of the material. According to Griffith [6], the critical stress required for the crack to propagate in the plane stress situation is

$$\sigma_c = \sqrt{\frac{2E\gamma}{\pi a}} \tag{2.5}$$

where, E is the elastic modulus, γ is the surface energy, and a is the crack length.

When the crack length a reaches a certain critical length such that, the strain energy release of the system is higher than the newly created surface energy of the two crack faces, unstable crack propagation will occur. This is often the case for brittle materials such as ceramics.

However, in ductile materials, blunting of the crack tip occurs due to the plastic deformation and this bluntness of the tip helps preventing stress concentration. The localized stress at the crack tip does not exceed the interatomic bond strength of the material. As a result, the presence of crack in ductile materials has a less pronounced effect and almost all of the sample fail in the same manner, as opposed to the brittle materials. For this reason, their failure strength has a narrow distribution.

Waloddi Weibull first proposed a distribution, now familiar by the name Weibull distribution [7], which can explain the failure strength of brittle materials. A body is considered with a volume of V which contains flaws in it. The flaws are randomly distributed in the volume V and does not interact with one another. The volume V is assumed to made up of n elements with volume V_0. Each smaller volume element V_0 has the same flaw distribution. The volume V is subjected to an applied stress σ. For the survival of the entire volume, each individual element has to survive.

If $P(\sigma)$ be the probability of survival of the entire volume and $P(V_0)$ be the probability of survival of the small volume element, it is possible to write,

$$P(\sigma) = P(V_0).P(V_0).P(V_0) \ldots \ldots P(V_0) = P(V_0)^n$$

Taking logarithm,

$$\ln P(\sigma) = n \ln P(V_0)$$

$$P(\sigma) = \exp(n \ln P(V_0))$$

It is assumed that the occurrence of flaws in volume V_0 occurs as a Poisson process [8]. Poisson random variable represent the number of some kind of occurrences per unit of the region of opportunity for those occurrences. Weibull defined a "risk of rupture" as

$$R = -[\ln P(V_0)]$$

$$P(V_0) = \exp(-R)$$

The condition for finding R has to be a monotonically increasing function. At low stress the survival probability would be 1 and at high stress it would be 0. Weibull assumed a value of R as a function of the following form,

$$R = \left(\frac{\sigma - \sigma_u}{\sigma_0}\right)^m$$

$$P(V_0) = \exp\left[-\left(\frac{\sigma - \sigma_u}{\sigma_0}\right)^m\right]$$

If the probability of failure is defined as $F(\sigma)$ then it follows that

$$F(\sigma) = 1 - P(V_0) = 1 - \exp\left[-\left(\frac{\sigma - \sigma_u}{\sigma_0}\right)^m\right] \quad (2.6)$$

If $\sigma_u = 0$ then equation (2.6) becomes,

$$F(\sigma) = 1 - \exp\left[-\left(\frac{\sigma}{\sigma_0}\right)^m\right] \quad (2.7)$$

Combining the results from the weakest link theory, it is possible to write

$$P(\sigma) = P(V_0)^n = P(V_0)^{\frac{V}{V_0}}$$

$$\ln P(\sigma) = \frac{V}{V_0} \ln P(V_0)$$

$$P(\sigma) = \exp\left[\frac{V}{V_0} \ln P(V_0)\right] = \exp\left[-\frac{V}{V_0}\left(\frac{\sigma}{\sigma_0}\right)^m\right] \tag{2.8}$$

In terms of probability of failure,

$$F(\sigma) = 1 - \exp\left[-\frac{V}{V_0}\left(\frac{\sigma}{\sigma_0}\right)^m\right] \tag{2.9}$$

Equation (2.8) is a combination of weakest link theory and Weibull model and usually employed in the statistical analysis of brittle materials.

2.1.3. Weibull model for single flax fiber

Usually fibers possess smaller volume compared to its length. As a result, it is more reasonable to use length element, instead of a volume element. A single fiber of length L is considered and is comprised of n elements of length L_0. That is, $n = \frac{L}{L_0}$. As a result, the Weibull equation for a single fiber failure would be,

$$F(\sigma) = 1 - \exp\left[-\frac{L}{L_0}\left(\frac{\sigma}{\sigma_0}\right)^m\right] \tag{2.10}$$

Usually, L_0 is taken as 1. Equation (2.10) can be written as,

$$F(\sigma) = 1 - \exp\left[-L\left(\frac{\sigma}{\sigma_0}\right)^m\right] \tag{2.11}$$

m is called the shape parameter or Weibull modulus and $\hat{\sigma} = \sigma_0 L^{-\frac{1}{m}}$ is called the scale parameter. The average of the distribution is defined as

$$\sigma_{avg} = \hat{\sigma}\Gamma(1 + \frac{1}{m}) \tag{2.12}$$

For conventional materials, typically the value of the shape parameter m takes a value between 5 and 25. Lower values are the characteristic of brittle failures. When the value of m is higher, it implies that the data has a very small dispersion about the mean, that is, a very low standard deviation. On the other hand, a lower value of m implies that the data are widely dispersed about the mean and possess a very high standard deviation. Ductile materials usually possess higher m values and ceramics possess lower m values due to their unexpected nature of failure of similar specimens because of the presence of cracks. For biological materials the value of m is even lower, because they possess much higher variability than other conventional materials.

The application of Weibull model in describing the failure of flax fibers rest on two assumptions:

1. The fibers fail in a brittle manner
2. The strength is determined by the presence of critical flaws and the fiber will follow a weakest link model.

Taylor series expansion of equation (2.11) gives,

$$F(\sigma) = (\frac{\sigma}{\sigma_0})^m + O(\sigma^m) \tag{2.13}$$

$O(\sigma^m)$ represents the term σ^{2m} and higher order. This equation reveals that the probability of failure of an individual fiber increases in proportion to the load σ raised to the power m. This implication also conforms to the reality and experimental results. As the load increases, the probability of failure also increases.

From the weakest link theory it is predicted that, the mean strength $\hat{\sigma}$ will diminish in proportion to $L^{-\frac{1}{m}}$ as the length of the fiber L increases. In reality, this feature is often observed when the change in length is one to three orders of magnitude higher.

2.1.4. Weibull model for technical flax fibers

Flax fibers are often present in the form of a bundle of fibers instead of being an individual fiber. This small bundle of single flax fibers are called technical fibers. Technical fiber dimension (equivalent diameter) may vary between 50-150 μm while the dimension (equivalent diameter) of a single flax fiber is approximately 10-20 μm. Often, in a carefully extracted technical flax fiber, 5-10 single flax fibers exist. In a flax fiber bundle, the individual fibers are bonded together by pectic polysaccharides, waxes, and other non-cellulosic materials. When an individual fiber in such a bundle breaks, it carries no load near the break region. However, further away from the break, the load returns to normal due to the shear traction on the fiber surface. This shear traction on flax fiber bundle occurs due to the inter-fiber adhesion and cementing of the pectic polysaccharide matrix. The region which is unable to carry the load near the breakage is called the ineffective length. For statistical analysis of technical fibers, the total length of fiber bundle should be several order of magnitude higher than its ineffective length. When a single flax fiber is broken, the load carried by that fiber is transferred to the adjacent fibers in the lateral direction. Two distinct situation may arise: a) the transferred load may have redistributed uniformly on all lateral survivors, b) the transferred load may have locally redistributed onto only two or three immediate neighbors. From a statistical viewpoint, the nature of this load sharing among non-failed fibers is very important. S.L Phoenix in his treatise described two major load sharing rules [9].

A technical flax fiber may be considered as a chain of bundles of length L as shown in the Figure 2.1. There are p fibers in a bundle. There are n bundles of length δ in the technical fiber. As a result, $n\delta = L =$ technical fiber length.

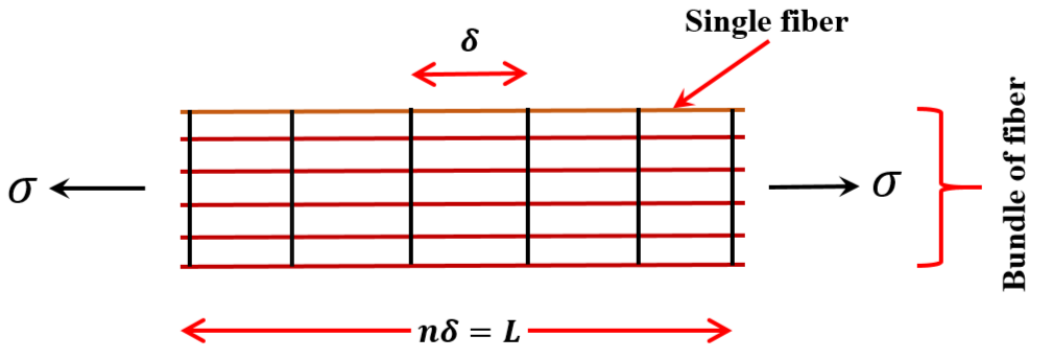

Figure 2.1: A technical flax fiber

As the strength of individual fiber elements are independent and identically distributed random variables, so are the strength of individual bundles. Failure of the chain of bundle occurs with the failure of the weakest bundle, and thus, by the weakest link rule

$$M(\sigma) = 1 - [1 - B(\sigma)]^n \quad \sigma \geq 0 \tag{2.14}$$

where, $M(\sigma)$ is the probability of failure of the bundle and $B(\sigma)$ is the probability distribution function. Difficulty arises in finding a proper $B(\sigma)$. Because the function for the statistical distribution of technical fiber depends on the load sharing rule, that is, how the load is transferred to the non-failed neighbours and the distribution function $F(\sigma)$ for individual fibers. S. L Phoenix [10], by using the load sharing rule and performing asymptotic analysis, showed that, when the bundle is comprised of a small number of individual fibers (5-10), which is usually the case for technical flax fibers, showed that the chain of bundles also follows a Weibull distribution with,

$$M(\sigma) \approx 1 - \exp\left\{-L\left(\frac{\sigma}{\sigma_0^*}\right)^{pm}\right\} \tag{2.15}$$

where,

$$\hat{\sigma} = \sigma_0^* L^{-\frac{1}{pm}}$$

From a theoretical standpoint, the technical fiber should have a much lower variability in strength than single fibers as the value of shape parameter is $(p.m)$ which is greater than the value for single fibers m. The size effect for technical fibers should be less pronounced than single fibers as the mean length would decrease in proportion to $L^{-\frac{1}{pm}}$ instead of $L^{-\frac{1}{m}}$. The value of $L^{-\frac{1}{m}}$ diminishes much faster than the value of $L^{-\frac{1}{pm}}$.

2.1.5. Probability distributions

As the experimental data would be analyzed in terms of different probability distributions, a short overview of the distributions are presented in this section.

2.1.5.1. Discrete and continuous random variables. A discrete random variable is one whose possible values constitute a finite set or whose values can be listed in an infinite sequence. On the other hand, a continuous random variable is one which can assume any value between intervals. It may be defined in the following way:

A random variable X is said to be continuous if it's set of possible values is an entire interval of numbers. If A and B are lower and upper limit of an interval, then a continuous random variable X can assume any number between A and B.

2.1.5.2. Probability density function. Let X be a continuous random variable. Then a probability distribution or probability density function (pdf) of X is a function $f(x)$ such that for any two numbers a and b with $a \leq b$,

$$P(a \leq X \leq b) = \int_a^b f(x)dx \tag{2.16}$$

That is, the probability that X takes on a value in the interval $[a, b]$ is the area under the graph of the density function. The graph of $f(x)$ is often referred to as the density curve.

For $f(x)$ to be a legitimate pdf, it must satisfy the following two conditions:

1. $f(x) \geq 0$ for all x

2. $\int_{-\infty}^{\infty} f(x)dx =$ area under the entire graph $f(x) = 1$

2.1.5.3. Cumulative distribution function. The cumulative distribution function $F(x)$ for a continuous random variable X is defined for every number x such that,

$$F(x) = P(X \leq x) = \int_{-\infty}^{x} f(y)dy \tag{2.17}$$

For each x, $F(x)$ is the area under the density curve to the left of x.

2.1.5.4. Normal distribution. A continuous random variable X is said to have a normal distribution with parameters μ and σ, where $-\infty < \mu < \infty$ and $\sigma > 0$, if the pdf of X is,

$$f(x; \mu, \sigma) = \frac{1}{\sqrt{2\pi}\sigma} e^{\frac{-(x-\mu)^2}{2\sigma^2}} \quad , \qquad -\infty < x < \infty \tag{2.18}$$

It can be shown that the expected value $E(X) = mean = \mu$ and the variance $V(X) = \sigma^2$, so the parameters are the mean and the standard deviation of X.

The normal distribution with parameter values $\mu = 0$ and $\sigma = 1$ is called a standard normal distribution. A random variable which has a standard normal distribution is called a standard normal random variable and is denoted by z.The pdf of z is

$$f(z; 0,1) = \frac{1}{\sqrt{2\pi}} e^{\frac{-(z)^2}{2}} \quad , -\infty < z < \infty \tag{2.19}$$

2.1.5.5. Gamma distribution. The graph of any normal distribution is bell shaped and symmetric about the mean. However, in certain situations, the distribution is not symmetric

about the mean. To describe this type of skewed phenomena, a set of non-symmetric pdf is used. They are called gamma family. For $\alpha > 0$, the gamma function $\Gamma(\alpha)$ is defined as,

$$\Gamma(\alpha) = \int_0^\infty x^{\alpha-1} e^{-x} dx \tag{2.20}$$

A continuous random variable X is said to have a gamma distribution if the pdf of X is

$$f(x;\alpha,\beta) = \begin{cases} \frac{1}{\beta^\alpha \Gamma(\alpha)} x^{\alpha-1} e^{-\frac{x}{\beta}} & x \geq 0 \\ 0 & otherwisw \end{cases} \tag{2.21}$$

where the parameters α and β satisfy $\alpha > 0$ and $\beta > 0$.

The standard gamma distribution has $\beta = 1$, so the pdf of a standard gamma random variable is given by,

$$f(x;\alpha) = \begin{cases} \frac{1}{\Gamma(\alpha)} x^{\alpha-1} e^{-x} & x \geq 0 \\ 0 & otherwisw \end{cases} \tag{2.22}$$

The mean and the variance of a random variable X having the gamma distribution $f(x;\alpha,\beta)$ are

$$E(x) = \alpha\beta \; and \; V(x) = \alpha\beta^2 \tag{2.23}$$

When X is a standard gamma random variable, the cumulative distribution function (cdf) of X is,

$$F(x;\alpha) = \int_0^x \frac{1}{\Gamma(\alpha)} y^{\alpha-1} e^{-y} dy \;\; , x > 0 \tag{2.24}$$

which is called the incomplete gamma function.

2.1.5.6. Exponential distribution. X is said to have an exponential distribution if the pdf of X is,

$$f(x;\lambda) = \begin{cases} \lambda e^{-\lambda x} & x \geq 0, \lambda > 0 \\ 0 & otherwise \end{cases} \tag{2.25}$$

The exponential pdf is a special case of the gamma pdf where $\alpha = 1$ and $\beta = \frac{1}{\lambda}$

The mean and the variance are as follows:

$$E(X) = \alpha\beta = \frac{1}{\lambda} \quad V(X) = \frac{1}{\lambda^2} \tag{2.26}$$

2.1.5.7. Weibull distribution. A random variable X is said to have a Weibull distribution with parameters α and β if the of X is

$$f(x;\alpha,\beta) = \begin{cases} \frac{\alpha}{\beta^{\alpha}} x^{\alpha-1} e^{-(\frac{x}{\beta})^{\alpha}} & x \geq 0 \\ 0 & x < 0 \end{cases} \tag{2.27}$$

The cdf of a Weibull random variable having parameters α and β is,

$$F(x;\alpha,\beta) = \begin{cases} 1 - e^{-(\frac{x}{\beta})^{\alpha}} & x \geq 0 \\ 0 & x < 0 \end{cases} \tag{2.28}$$

2.1.5.8. Lognormal distribution. A non-negative random variable X is said to have a lognormal distribution if the random variable $Y = \ln(X)$ has a normal distribution. The resulting pdf of a lognormal random variable when $\ln(X)$ is normally distributed with parameters μ and σ is,

$$f(x;\mu,\sigma) = \begin{cases} \frac{1}{\sqrt{2\pi}\sigma} e^{\frac{-(\ln(x)-\mu)^2}{2\sigma^2}} & x \geq 0 \\ 0 & x < 0 \end{cases} \tag{2.29}$$

The mean and the variance of the distribution is

$$E(X) = e^{\mu+\frac{\sigma^2}{2}} \; and \; V(X) = e^{2\mu+\sigma^2}(e^{\sigma^2} - 1) \tag{2.30}$$

2.2. Experimental

2.2.1. Materials

Flax fibers were provided by Composite Innovation Center, Winnipeg, Canada. Flax plants of the variety Bethune and Prairie Grande were grown in two different locations in Manitoba, Canada in 2015. Flax stems were harvested and collected before they were able to ret. Next measurements were made on these flax stems in order to separate them into two distinct categories. The criteria was that if the diameter of flax stems were less than 1.5 mm, they were

categorized as small stems (small diameter). On the other hand, if the diameter of flax stems were larger than 1.65 mm, they were categorized as large stems (large diameter). Combining these different criteria such as stem diameter, location of growth, and variety, six batch of samples were prepared: Arborg Large (Arb L), Arborg Small (Arb S), Melita Large (Mel L), Melita Small (Mel S), Prairie Grande Large (PG L), and Prairie Grande Small (PG S). Table 2.1 shows this categorization more specifically.

Table 2.1: Formation of different samples

Sample Name	Location	Variety	Stem Size	% Medium Stems
Arborg Large	Arborg	Bethune	Large	16%
Arborg Small	Arborg	Bethune	Small	16%
Melita Large	Melita	Bethune	Large	8%
Melita Small	Melita	Bethune	Small	8%
PG Large	Melita	Prairie Grande	Large	14%
PG Small	Melita	Prairie Grande	Small	14%

Prior to enzyme retting, straw stems were gently crimped using a wooden tool so that the enzyme solution can penetrate easily into the stems. This facilitates proper enzyme retting. Straw stems were enzyme retted using a pectinase enzyme (Bioprep 3000L), EDTA and buffer solution. The straws were soaked in the enzyme solution for 5 minutes and then removed from the soaking tub. The unrinsed straws were placed in sealed bags and incubated at 55° C for two hours. Next the straws were soaked in an EDTA and buffer solution for 30 minutes and incubated again at 55° C for 22 hours. The straw was then rinsed thoroughly with tap water to remove the remaining enzyme/EDTA solution. The straws were spread out flat to dry in a fume hood at room temperature for 12 hours. Next the fibers were decorticated from the stem using the same wooden crimping tool used in the pre-crimp step.

2.2.2. Tensile testing

Tensile tests were performed on technical flax fibers having a diameter range of 35-150 μm. A gauge length of 20 mm were selected for proper handling of the fiber specimen. A Deben micro-tensile tester, which is more generally used for in-situ observation of a specimen under tension in electron microscope, was selected for the testing. The maximum load that can be measured with the machine is 180 N with a load cell linearity of 1.5%. Force and position resolution of the machine were 0.001 N and 0.0001 mm respectively. Displacement rate of the crosshead were selected to be 0.75 mm/min. ASTM standard D3822 was followed for determining the mechanical properties of the fibers.

On the other hand, the instrument used in Composite Innovation Center (CIC) was a load cell and a screw based linear actuator to measure and produce stress, respectively. The combination is sold as a LEX810 tensile tester from Diastron. The equipment has a load cell capacity of 10N with a load cell linearity of 0.08%. The speed range for the CIC tensile tester is 0.01-60 mm/min. The positional accuracy is 10 micron and the maximum elongation is 50 mm. The gauge length used for flax fiber in CIC was 4 mm. For the diameter measurement, a rotational laser scanner was used.

At least 50 fibers were tested from each of the six samples mentioned above. Before performing the tensile test, diameter of each fiber was measured using a Zeiss Axiovert 40 MAT inverted optical microscope with an attached camera of Progress C10 Plus. The diameter of each fiber specimen was measured in three different locations and then averaged for each sample. Figure 2.2 shows a typical diameter measurement of the technical fiber. A circular cross-section was assumed and the average diameter was used for calculating the area. The effect of lumen was neglected. Thomason et.al [11] maintained that the assumption of a circular cross-section

overestimates the true cross-section of flax fibers and proposed a common scale factor in order to correct the circular area to a more elliptical shape. In this study, a factor of 1.5 was used in order to correct for the circular area assumptions. All the testing of flax fibers were performed in a temperature and humidity controlled laboratory ($21°C \pm 1°C$, 18%RH$\pm$3%).

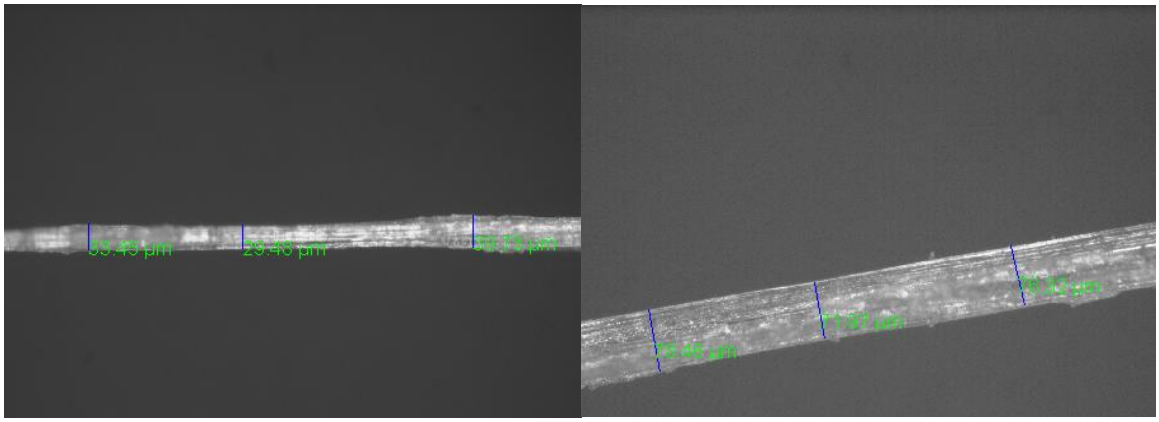

Figure 2.2: Diameter measurement with optical microscope

2.3. Results and discussion

2.3.1. Variation in ultimate strength

Variation of strength in technical flax fibers are discussed in terms of Prairie Grande large and small samples. Prairie Grande is an oilseed flax and it was released in 2007, by Agriculture and Agrifood, Manitoba, Canada. Better disease resistance properties has made it a useful cultivar in Canada and North American countries. In Figure 2.3, the strength distribution of PG Large and PG Small samples are shown. For each sample, fifty specimens were tested and their mechanical properties were determined. The range of strength of the PG Large sample is seen to be much lower than the strength of PG Small sample. The mean and the median strength of PG Large sample are 440 MPa and 336 MPa, respectively. On the other hand, the mean and the median strength of the PG Small sample are 637 MPa and 498 MPa, respectively. This

implies that the small diameter fibers possess higher strength than the large diameter fibers. The reason may be that the small diameter flax stem has to be stronger to withstand a higher wind resistance than a large diameter flax stem and as such the PG Small samples possess higher strength. A more detailed analysis of the Figure 2.3 is shown in Table 2.2. The minimum, maximum, first quartile, third quartile, mean and standard deviation of strength of all the six samples are also shown in Table 2.2.

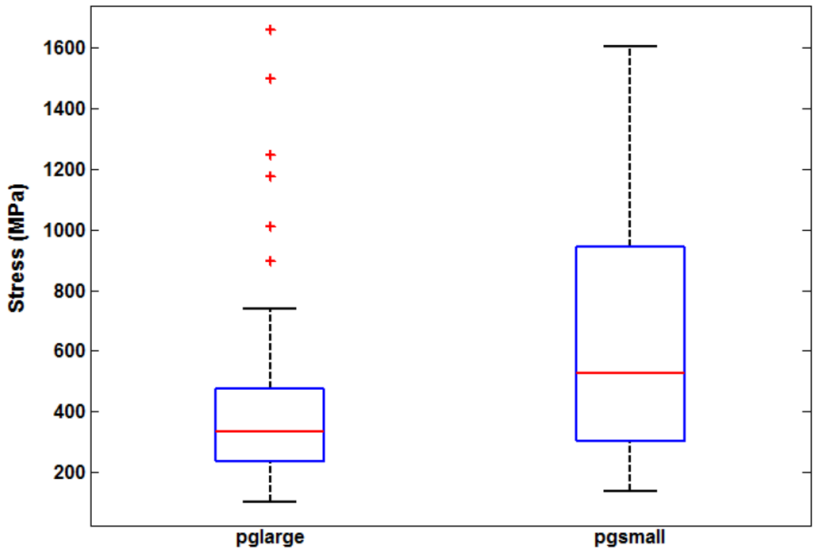

Figure 2.3: Distribution of Stress for Prairie Grande Large and Small sample.

Table 2.2: Tensile strength of the six samples of flax fibers

	Arborg Small (MPa)	**Arborg Large (MPa)**	**Melita Small (MPa)**	**Melita Large (MPa)**	**PG Small (MPa)**	**PG Large (MPa)**
Minimum	169	104	78	49	136	103
First quartile(Q1)	313	232	232	141	294	233
Median	467	348	466	222	498	336
Third quartile (Q3)	766	496	793	323	954	480
Maximum	1138	851	1115	430	1603	739
Mean	567	445	536	341	637	440
Standard deviation	367	329	394	355	414	354

In reference to the mechanical properties of wood cell, Burgert et.al [12] maintained that the stress-strain diagram may be either biphasic or triphasic. Biphasic refers to two distinct slopes: steep initial slope followed by a moderate slope. Triphasic refers to three slopes: the first two slopes are similar to biphasic but the third slope is due to the additional stiffening at the end of the testing. This two types of stress-strain occurs when the micro-fibril angle (MFA) in S2 layer is relatively large. It is also known that the MFA is larger in young cell than in mature cell. So, this type of curve is more typical of young cell than mature cell. The stiffness of the micro-fibrils are two order of magnitude higher than the hemicellulose and pectin matrix in which they are embedded in. When a tensile load is applied, the matrix reaches its yield point ahead of the micro-fibrils, which results in a viscous flow of the matrix and gliding of the cellulose micro-fibrils (CMFs). This gliding of CMFs may cause repeatitive breaking or bridging of hydrogen bonds between the CMFs and the hemicellulose matrix like a stick-slip or velcro. This phenomena helps to retain the mechanical properties of single fibers though the plastic deformation has occurred in the matrix. The degree of lignification or the lignin content in secondary cell wall may increase the shear stiffness of the cell.

It is previously mentioned that the micro-fibrils in the S1 and S3 layers are arranged in circumferential directions. The analogy might be the metal bands surrounding a barrel. The outer S1 layer prevents buckling of the cell due to the axial compressive loads. The inner S3 layer helps preventing radial tensile stress.

This type of model for wood cell was confirmed by the experimental investigation of Keckes et. al [13]. They performed in-situ synchroton experiment on single wood cell. They measured the change of MFA as the tensile load was applied on the fiber. They concluded that it is the matrix that mainly undergoes shear deformations and the micro-fibrils sustain little

deformations. With the increase in strain, the magnitude of the micro-fibril angle decreases and they found a linear relationship between the strain and the MFA.

The mechanical behavior of individual wood cells are very similar to that of the bundle of cells or tissue. However, the tissue usually breaks at smaller strains. The cells are initially stiff up to a yield point, then permanent deformation starts and stiffness drops for a moment, but increases again before the failure. They also pointed out that, by microfocusing on the cell, the deformation of the single wood cell was not uniform over the entire cell length. Some regions sustained sustained large deformation resulting in a very low MFA angle, whereas other places remained almost undeformed. However, in tissue or in bundle, the amount of this inhomogeneity is reduced due to the cell-cell interactions. In case of tissue or foil or bundle, the effect of strain hardening is less obvious as they fail at smaller strains.

In reference to the tensile properties of elementary flax fibers, Lefeuvre et.al [14] mentioned three distinct types of stress-strain curve while performing tensile test. One is fairly linear stress-strain curve, other two is biphasic and triphasic stress-strain curve. They found that within a sample, when the number of triphasic stress-strain curve predominates, the sample shows better mechanical properties. Also the triphasic stress-strain curve has a higher strain than the other two types of curve. The average mechanical properties such as strength, failure strain and modulus of all the six technical flax fiber samples tested in this study are summarised in Table 2.3.

All these six samples were also tested in Composite Innovation Centre (CIC), Winnipeg, Canada to justify the results. The strength values found in CIC are also presented in Table 2.3

Table 2.3: Summary of the mechanical parameters of flax fibers

Name	Number of sample tested	Diameter (μm)	Elastic modulus (GPa)	Failure strength (MPa)	Failure strain mm	CIC failure stress
PG large	50	100 ±28	46±31	440±354	0.9±0.2	775±341
PG small	50	82±27	60±31	637±414	0.9±0.3	813±371
Arborg large	50	92±33	41±23	483±406	1.1±0.5	636±307
Arborg small	50	61±24	52±35	567±367	1.2±0.5	907±423
Melita large	50	99±30	40±19	362±320	0.8±0.4	565±280
Melita small	50	66±24	50±27	542±432	0.9±0.4	811±290

It can be observed from Table 2.3 that the distribution of strength of flax fibers possess a higher standard deviation than conventional materials. This can be explained form the structure of a single cell wall. Figure 2.4 shows the force displacement (comparable to stress-strain curve) curve of a few representative specimens. All the stress-strain curves of the 50 specimen tested fall under this 8 category . It can be seen that considerable variation exists among this 8 individual force-displacement curve. Type 1 (T1) curve shows biphasic nature, that is, they have two distinct slopes. However, the second slope has an increasing trend rather than a decreasing one which is usually the case for single wood cell. The reason may be attributed to the difference in microfibril angle between the single wood cell and single flax fiber. The range of microfibril angle in wood cell varies between 25° and 50° [13]whereas for flax fiber it varies between 10-15°. In flax fiber, the microfibrils straiten more rapidly than the single wood fibers and these straitened microfibrils contribute to the increasing slope or stiffening effect. In this study, a decresing biphasic curve is rarely encountered. T1 and T5 is also biphasic in nature but in different shape and value. T2, T3 and T6 are essentially triphasic in nature but in different shape and magnitude. T2 has much higher breaking force than T3 and T6. T4 represents the linear stress-strain curve. T8 stands alone from other literature and may be only found in technical fiber

testing. The serrated portion of the curve represents the failure of a few individual single fibers and the entire load is carried by only one or two nonfailed single fibers. As a result the stiffness is also decreased in the last part of the graph.

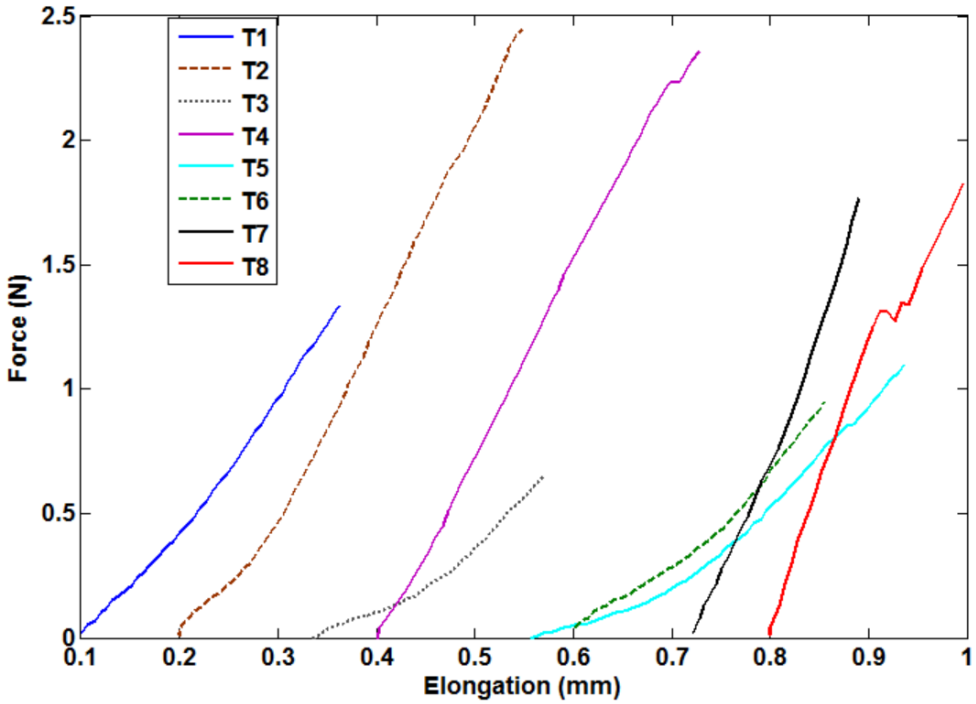

Figure 2.4: Different types of force displacement curves.

In an effort to explain the differences between the average failure strength and failure strain, all the stress-strain curves of Arborg Small and Arborg Large samples were carefully studied. It was found that in all 50 stress-strain curve of Arborg Small sample, 51% of the curves were triphasic, 22% were biphasic and 26% were linear. On the otherhand, of all the stress-strain curve of Arborg Large sample, 22% of the curves were triphasic, 28% were biphasic and 48% were linear. A higher percentage of triphasic curves may partially account for the higher strength and slightly higher strain encountered in arborg small samples. Because, triphasic curves generally have higher elongation and strength than their linear counterpart. The same trend is assumed to be present in all other samples.

In addition, hypothesis testing and analysis of variance (ANOVA) was performed to prove that the difference between the mean strength of large diameter and the small diameter samples were statistically significant.

When the probability distribution of a random variable is known (the random variable follows a normal distribution, gamma distribution or Weibull distribution), it is easy, by using the formula mentioned above, to compute the mean, variance, and probabilities associated with the random variables. However, in most practical cases, this information is not available. The true mean and standard deviation of a population are unknown quantities that have to be determined. The population mean and standard deviation (true mean and standard deviation) are usually denoted by μ and σ, respectively. On the other hand, sample mean and standard deviation are denoted by $\bar{x}$ and s and these are numerically calculated from the sample. The information contained in this sample statistics are used to make inferences about the population parameters. The term statistic refers to a sample quantity and the term parameter refers to a population quantity. A random sample is chosen from a large population and the sample mean is found to be $\bar{x}$. If another random sample is chosen, a different mean would be found. If these sampling experiments were repeated a very large number of times, an approximate probability distribution of all the sample means $\bar{x}$ would be found. If $\bar{x}$ is a good estimator of μ, then all the values of $\bar{x}$ would cluster around μ. This probability distribution of $\bar{x}$ is called a sampling distribution. In order to make an inference about a population parameter, the sample statistic is used which has a sample distribution that is unbiased and possess a small standard deviation. There are two theorems regarding the sampling distribution of $\bar{x}$:

1. If a random sample of n observations is selected from a population with a normal distribution, the sampling distribution of $\bar{x}$ will be a normal distribution.

2. If a random sample of n (n being sufficiently large) observations is selected from a population with mean μ and standard deviation σ, the sampling distribution of $\bar{x}$ will be approximately a normal distribution with mean $\overline{\mu_x} = \mu$ and standard deviation $\sigma_x = \frac{\sigma}{\sqrt{n}}$. The larger the sample size, the better will be the normal approximation to the sampling distribution of $\bar{x}$.

When $n \geq 30$, it is sufficient to say that the normal approximation is reasonable. The standard normal z_{value} corresponding to the sample mean $\bar{x}$ is,

$$\mathrm{z_{value}} = \frac{\text{Normal random variable} - \text{Mean}}{\text{standard deviation}} = \frac{\bar{x} - \overline{\mu_x}}{\sigma_x} = \frac{\bar{x} - \overline{\mu_x}}{\frac{\sigma}{\sqrt{n}}}$$

When using student's t-statistics, the following formula is used

$$\mathrm{t_{value}} = \frac{\bar{x} - \overline{\mu_x}}{\frac{s}{\sqrt{n}}} \tag{2.31}$$

where, the population standard deviation σ is replaced by the sample standard deviation s. T-statistic has a sampling distribution very similar to z-statistic: mound shape, symmetric, and zero mean. However, t-statistic contains two random quantities ($\bar{x}$ and s), whereas z-statistic contains only one random variable ($\bar{x}$).

A statistical hypothesis is a statement about the numerical value of a population parameter. For performing a hypothesis testing, two hypothesis is defined. The null hypothesis, denoted H_0, represents the hypothesis that will be accepted unless the data provide convincing evidence that it is false. The alternative hypothesis or research hypothesis, denoted H_a, represents the hypothesis that will be accepted only if the data provide convincing evidence of its truth. The researcher usually wants to prove this alternative hypothesis.

For technical flax fibers in this study, to prove that the small diameter sample has higher strength than the large diameter sample, the following hypothesis is formed:

$$H_0: \mu_1 = \mu_2$$

$$H_a: \mu_1 \neq \mu_2$$

where,

$$\mu_1 = \text{strength of small diameter sample}$$

$$\mu_2 = \text{strength of large diameter sample}$$

If one wants to prove $\mu_1 > \mu_2$, it would be a one tailed t-test. The formula for calculating t_{value} is as follows:

$$\mathrm{t_{value}} = \frac{\mu_1 - \mu_2}{\sqrt{\frac{s_1^2}{n_1} + \frac{s_2^2}{n_2}}}$$

where,

$$s_1 = \text{standard deviation of small diameter sample}$$

$$s_2 = \text{standard deviation of large diameter sample}$$

$$n_1 = \text{degree of freedom of small diameter sample}$$

$$n_2 = \text{degree of freedom of large diameter sample}$$

For a 95% confidence interval, the t_{value} is 1.96. The corresponding significance level or p-value is 0.05. For a two mean hypothesis testing, the null hypothesis H_0 is rejected if the t_{value} is greater than 1.96 or the p-value is below 0.05. This means that the sample means are different and statistically significant. For Arborg Small and Arborg Large sample:

$$\mu_1 = 567\ MPa$$

$$\mu_2 = 483\ MPa$$

$$s_1 = 367\ MPa$$

$$s_2 = 406\ MPa$$

$$n_1 = 50$$

$$n_2 = 50$$

$$\mathrm{t_{value}} = \frac{567 - 483}{\sqrt{\frac{367^2}{50} + \frac{406^2}{50}}} = 1.08$$

$$\mathrm{p - value} = 0.142662 > 0.05$$

The result shows that the mean of the large diameter and small diameter samples are not statistically significant. This is because of the higher standard deviation of the two samples that arises from the measurement of the fiber diameter by optical microscope. The diameter of flax fibers are not perfectly circular, rather more of an elliptical shape. They have a major diameter and a minor diameter. The measurement of diameter with optical microscope results in either a major diameter or a minor diameter which overestimates or underestimates the actual cross-section. This error in the measurement of cross-sectional area directly affects the measurement of the strength and modulus of the fiber. However, CIC (Composite Innovation Center) employed a totally different approach for measuring the diameter of the fiber which resulted in a smaller standard deviation for the measurement of the strength and modulus.

In CIC, measurement of diameter was performed using a laser scanner Mitutoyo LSM6000-500s which is attached to Diastron FDAS760 specimen holder. A laser beam shines a certain region of the fiber. A portion of the laser beam is interrupted by the fiber. Based on the shadow cast, a detector reads the size of the fiber. The fiber is rotated 360° around its axis to capture numerous 2D measurements. These measurements can be used to determine the minimum and maximum diameter of the fiber which allows the determination of an elliptical

cross section. The range of the laser is 5-2000 microns. That is, approximately a length of 2000 microns of the fiber can be measured by the laser beam.

Figure 2.5 shows a sample measurement of the fiber diameter by the rotational laser scanner. The minimum fiber diameter is approximately 38 μm and the maximum fiber diameter is 130 μm. The length of the fiber scanned was approximately 1450 μm. Figure 2.6 shows the overall set-up of the laser scanner. A laser emitter and a detector is placed across the fiber. The fibers are mounted on a tab and there are tabs for holding those tabs. The specimen holder can have a 360° rotation while moving along the fiber axis. Based on the minimum and maximum diameter measured from the laser scanner, a roundness factor was determined.

$$\text{roundness factor} = \frac{\text{maximum diameter}}{\text{minimum diameter}} = \frac{130}{38} = 3.42$$

The formula for calculating the cross-sectional area assuming an elliptical shape is as follows:

$$\text{area A} = \pi \frac{d_{max}}{2} \frac{d_{min}}{2}$$

If a circular cross section was assumed using the maximum diameter of the fiber, then the area would be overestimated. On the other hand, using the minimum diameter would underestimate the area. Hence, the roundness factor helps to determine the variability that would arise from the assumption of a circular cross section.

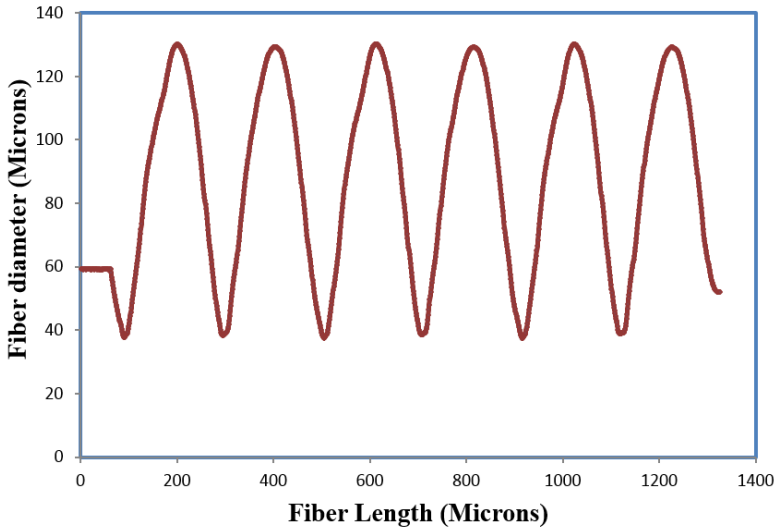

Figure 2.5: Output from a laser scanner showing the variation of diameter over its length

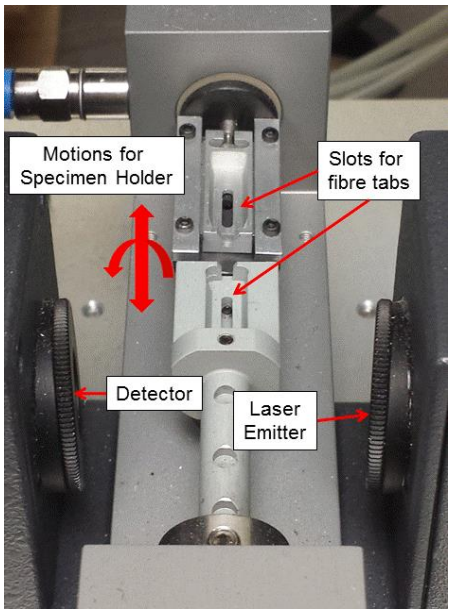

Figure 2.6: Equipment setup for a laser scanner. The laser emitter and detector is placed across the fiber

Figure 2.7 represents the boxplot representation of the roundness value for all the six samples. These roundness values were calculated using the above mentioned formula based on the maximum and minimum diameter. The prairie grande small (MPS) has the highest mean

roundness value. On the other hand, arborg small has the lowest mean roundness value. Table 2.4 summarizes the minimum, maximum, first quartile, third quartile, mean and standard deviation of roundness value for all the six samples.

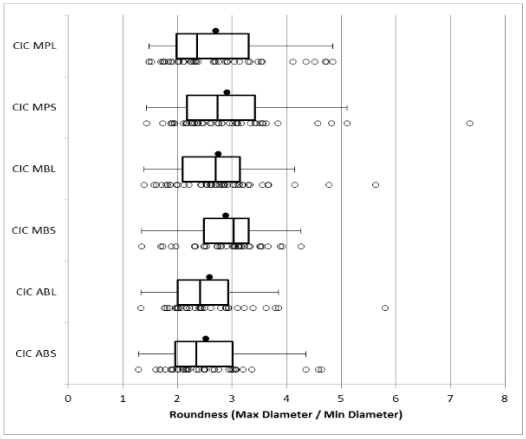

Figure 2.7: Boxplot representation of the roundness of fiber for all the six samples

Table 2.4: Summary of the roundness values for all the six samples of flax fiber

	CIC Arborg Small	CIC Arborg Large	CIC Melita Small	CIC Melita Large	CIC PG Small	CIC PG large
Minimum	1.3	1.3	1.3	1.4	1.4	1.5
First quartile (Q1)	2.0	2.0	2.5	2.1	2.2	2.0
Median	2.3	2.4	3.0	2.7	2.7	2.4
Third quartile (Q3)	3.0	2.9	3.3	3.1	3.4	3.3
Maximum	4.3	3.8	4.3	4.2	5.1	4.8
Mean	2.5	2.6	2.9	2.7	2.9	2.7
Standard deviation	0.8	0.8	0.7	0.8	1.1	1.0

After performing these improvements in the diameter measurement, the standard deviation of all the samples were greatly reduced. The hypothesis testing of these data sets reveals the following results. For CIC arborg small and large samples:

$$\mu_1 = 907\ MPa$$

$$\mu_2 = 636\ MPa$$

$$s_1 = 423\ MPa$$

$$s_2 = 307\ MPa$$

$$n_1 = 50$$

$$n_2 = 50$$

$$\mathrm{t_{value}} = \frac{907 - 636}{\sqrt{\frac{423^2}{50} + \frac{307^2}{50}}} = 3.66$$

$$\mathrm{p - value} = 0.000304 < 0.05$$

This value implies that the difference between the mean of small diameter and large diameter sample is statistically significant.

To confirm this analysis, ANOVA (analysis of variance) was also performed and the results are summarized in Table 2.5. From Table 2.5, it can be observed that the between treatment mean square (1.3669e+06) is many times larger than the within treatment mean square (1.3141e+05). This indicates that it is unlikely that the treatment means are equal. More formally, the $F - ratio$ can be calculated

$$F_0 = \frac{1.3669\mathrm{e} + 06}{1.3141\mathrm{e} + 05} = 10.4017$$

This value of F_0 can be compared to the value of an appropriate upper tail percentage point of the $F_{1,72}$ distribution. From the F-statistic table, it is found that $F_{0.05,1,72} = 3.97$. As $F_0 = 10.40 >$ 3.97, null hypothesis H_0 is rejected. From this analysis, it can be concluded that the treatment means differ, that is, the mean of arborg large and arborg small samples are significantly different.

Table 2.5: Summary of ANOVA analysis

Source of Variation	Sum of Squares	Degrees of Freedom	Mean Square	F_0	$P-Value$
Arborg Strength	1.3669e+06	1	1.3669e+06	10.4017	0.0019
Error	9.4617e+06	72	1.3141e+05		
Total	1.0829e+07	73			

2.3.2. Variation in ultimate strain

For brittle synthetic fibers such as glass fibers, knowledge of the strength and Young's modulus is sufficient for determining the failure strain of the fiber. Because the stress-strain curve of glass fiber shows a linear elastic behavior. However, for flax fibers, knowledge of strength and Young's modulus is not enough to determine the failure strain. Their initial stress-strain curve shows a non-linear behavior and the Young's modulus also possess a greater spread. On the other hand, experimental determination of failure strain does not involve measurement of cross-sectional area. The gauge length of the fiber can be measured from the grip separation with reasonable accuracy. The extension of the fiber is measured from the crosshead displacement given that the fiber is straight and taut. As a result, failure strain values are more reliable than strength values. Virk et. al have proposed the failure strain as design criteria for composite materials. Figure 2.8 compares the distribution of the failure strain of PG Large and PG Small sample in the form of boxplot graph. Table 2.6 summarizes the minimum, maximum, first quartile, third quartile, mean, median and the standard deviation of failure strain of all the six samples tested in this study. It can be observed from Figure 2.7 that the PG small sample has higher range of failure strain than the PG large sample. PG small also possess higher standard deviation compared to PG large sample.

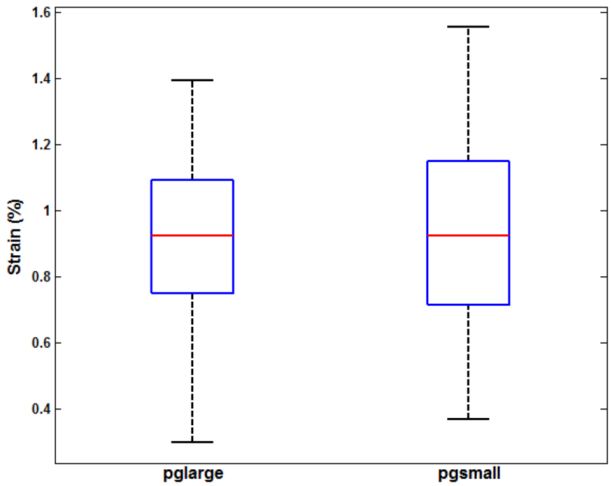

Figure 2.8: Distribution of strain of PG Large and PG Small samples.

Table 2.6: Summary of ultimate strain (%) analysis of flax fiber

	Arborg Small	**Arborg Large**	**Melita Small**	**Melita Large**	**PG Small**	**PG Large**
Minimum	0.4	0.3	0.3	0.2	0.4	0.3
First quartile (Q1)	0.8	0.7	0.6	0.4	0.7	0.7
Median	1.2	1.1	1.0	0.7	0.9	0.9
Third quartile (Q3)	1.5	1.4	1.2	1.1	1.2	1.1
Maximum	2.2	2.1	1.6	1.4	1.6	1.4
Mean	1.1	1.1	0.9	0.7	0.9	0.9
Standard deviation	0.4	0.4	0.3	0.4	0.3	0.2

However, the mean of the failure strain of both the samples is 0.9 mm/min. From a design perspective, a higher failure strain is desirable. Because, a higher failure strain would be able to accommodate a higher deformation upon application of load before failure. Arborg Large and Arborg Small sample has the highest value of failure strain.

To quantify the variation or dispersion of failure strain, Weibull statistical analysis was performed. The Weibull plot of PG small and PG large is presented in Figure 2.9. Maximum likelihood method was employed for finding the Weibull scale and shape parameter. PG small sample has a scale parameter of 1.03 and a shape parameter of 3.59. On the other hand, PG large

sample has a scale parameter of 0.99 and a shape parameter of 4.45. A higher value of shape parameter represents that the data has lower dispersion. As a result, PG large sample has lower dispersion than PG small sample.

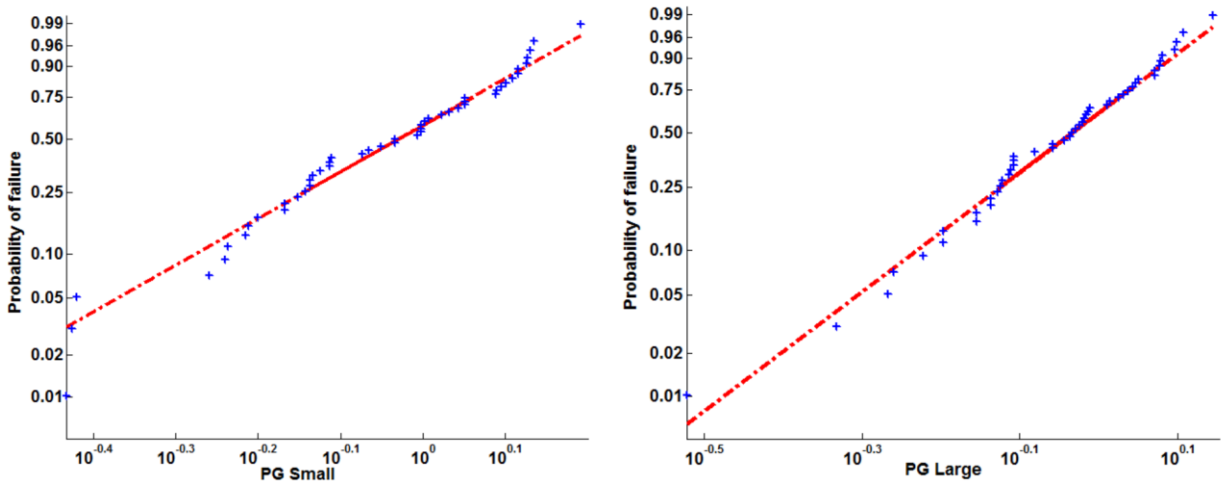

Figure 2.9: Weibull plot for PG Small and PG Large sample

2.3.3. Variation in Young's modulus

Though the elastic modulus of a material is its intrinsic property, flax fibers exhibit a wide range of modulus. This is because each and every fiber is different in its morphology and constituent materials. The micro-fibril angle is not constant throughout the whole length of the fiber and there may be discontinuities in the arrangement of these fibrils which may affect the modulus of flax fiber.

Figure 2.10 compares the distribution of Young's modulus for both PG Large and PG Small samples. The range of elastic modulus of PG large is lower than the range of PG Small sample. The mean and median of PG Large are 46 GPa and 36 GPa, respectively. On the other hand, the mean and the median of the PG Small sample are 60 GPa and 55 GPa, respectively. The mean of the elastic modulus for PG Small sample is higher than the PG Large sample. That is, small diameter fibers, on an average, are stiffer than the large diameter fibers. However, PG

Small possess a higher standard deviation than PG Large sample. Table 2.7 summarizes the minimum, maximum, first quartile, third quartile, mean, median, and standard deviation of all the six samples studied in this thesis.

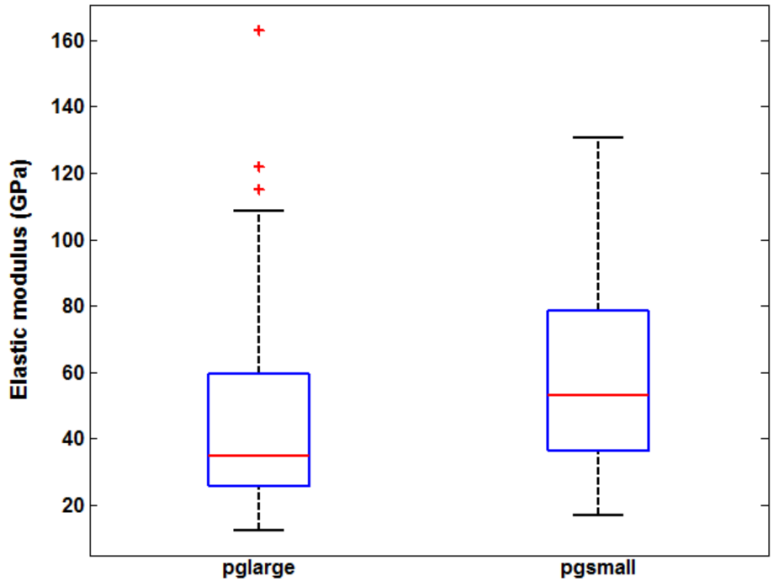

Figure 2.10: Distribution of Young's modulus of PG Large and PG Small samples.

Table 2.7: Summary of elastic modulus (GPa) analysis of flax fiber

	Arborg Small	**Arborg Large**	**Melita Small**	**Melita Large**	**PG Small**	**PG large**
Minimum	14	10	10	14	17	13
First quartile Q1	29	27	31	24	35	26
Median	43	33	48	35	53	35
Third quartile Q3	78	53	71	47	80	60
Maximum	147	92	109	67	130	109
Mean	62	41	53	39	61	46
Standard deviation	46	22	27	21	31	31

To quantify the variation in elastic modulus, Weibull statistical analysis was also performed on both PG Large and PG Small samples. The scale and the shape parameter of PG Small sample is 68.38 and 2.14, respectively. On the other hand, the scale and the shape

parameter of PG Large sample is 52.29 and 1.64, respectively. Unlike the shape parameter of failure strain, the PG small sample has a higher value of shape parameter and thus, they have a lower overall dispersion. Figure 2.11 shows the Weibull plot for elastic modulus distribution of PG Small and PG Large sample.

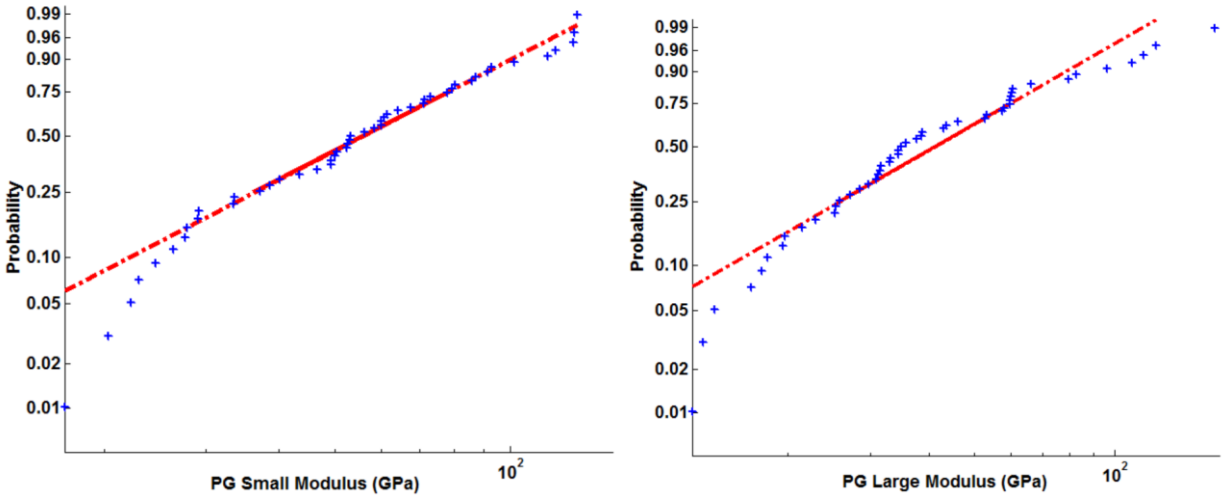

Figure 2.11: Weibull plot for elastic modulus distribution of PG small and PG large sample.

2.3.4. Variation in failure time

Figure 2.12 compares the distribution of failure time for both PG Large and PG Small samples. The range of failure time for PG Small sample is higher than PG Large sample. The mean and the median of the failure time are also slightly higher for PG Small sample and the magnitude is approximately 15 seconds. PG Small sample contains a higher percentage of tri-phasic stress-strain curve. Tri-phasic curves take longer time to fail as their deformation is higher than the biphasic or linear stress-strain curve. From a design perspective, a longer failure time is desirable as it would allow a higher amount of deformation. On an average, the small diameter sample possess a higher failure time than large diameter sample.

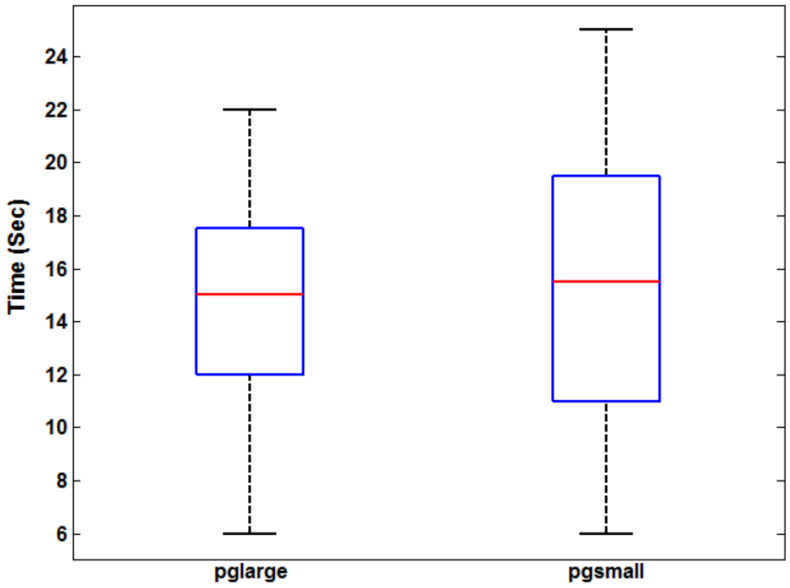

Figure 2.12: Distribution of failure time for PG Large and PG Small sample.

2.3.5. Variation in diameter

Figure 2.13 compares the distribution of diameter between PG Large and PG Small sample. The range of diameter of PG Large sample is higher than the range of PG Small sample. The mean diameter for PG Small sample is 82 μm while the mean diameter for PG Large sample is 100 μm. The standard deviation of both sample is almost same and it is 28 μm. The measurement of diameter directly affects the measurement of strength and modulus of the fiber. About 93% of the error in estimating strength and modulus comes from the diameter measurement. However, an appropriate measurement of the fiber diameter is still considered a challenge. Because the diameter varies widely over its length. Over a 20 mm gauge length, an optical microscope can measure the diameter of the fiber with a span of less than 1 mm. The presence of lumen may also complicate the measurement. Though the effect of lumen is neglected, their influence might be significant in young flax.

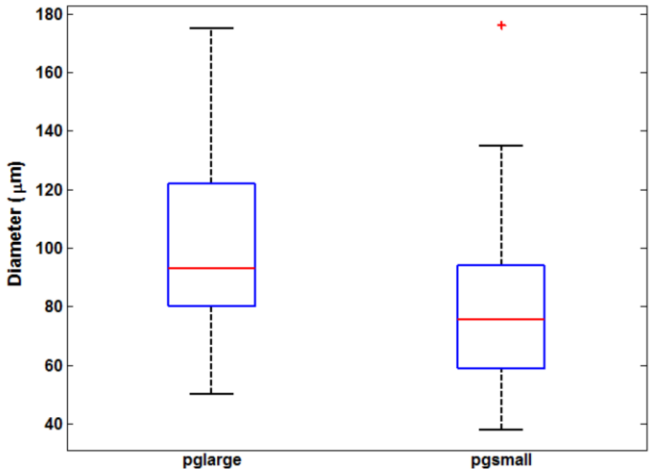

Figure 2.13: Distribution of diameter for PG Small and PG Large sample

2.4. Comparison among the samples

Figure 2.14 compares the mean strength of all the six samples studied in this thesis. Standard deviation of each sample is also shown in the graph. In all the cases, small diameter sample exhibits higher strength than their large diameter counterpart. Among all the six samples, PG Small has the highest strength.

Figure 2.15 compares the mean elastic modulus among the six different samples. The elastic modulus also shows similar trend as that of the strength, that is, the small diameter sample possess higher mean stiffness than their large diameter counterparts. Among all the samples, PG small has the highest amount of stiffness.

Figure 2.16 compares the mean ultimate strain among six different samples. For the variety Arborg and Melita, the trend is similar to that of strength and elastic modulus, that is, small diameter fiber exhibits higher mean ultimate strain. However, for the variety Prairie Grande the trend is different. Both small and large diameter sample has the same mean ultimate

strain. PG Large and Small sample also possess lowest amount of standard deviation in their ultimate strain which is beneficial from the perspective of bio-composites manufacturing.

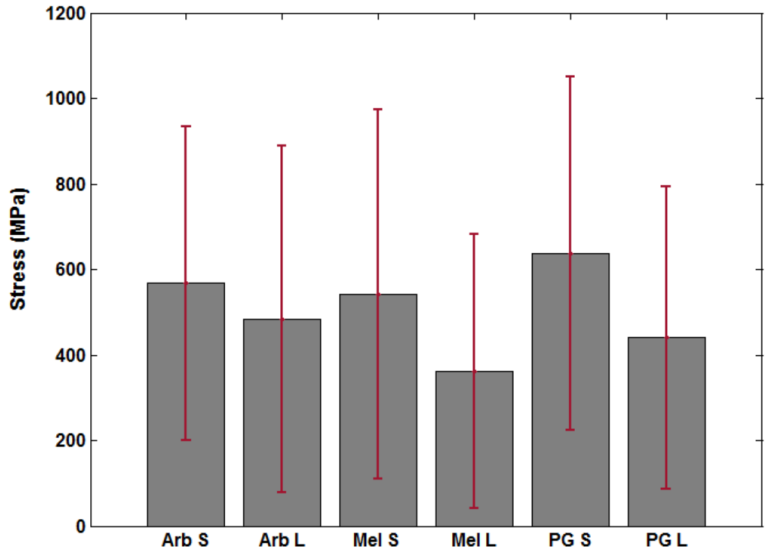

Figure 2.14: Comparison of strength among different samples

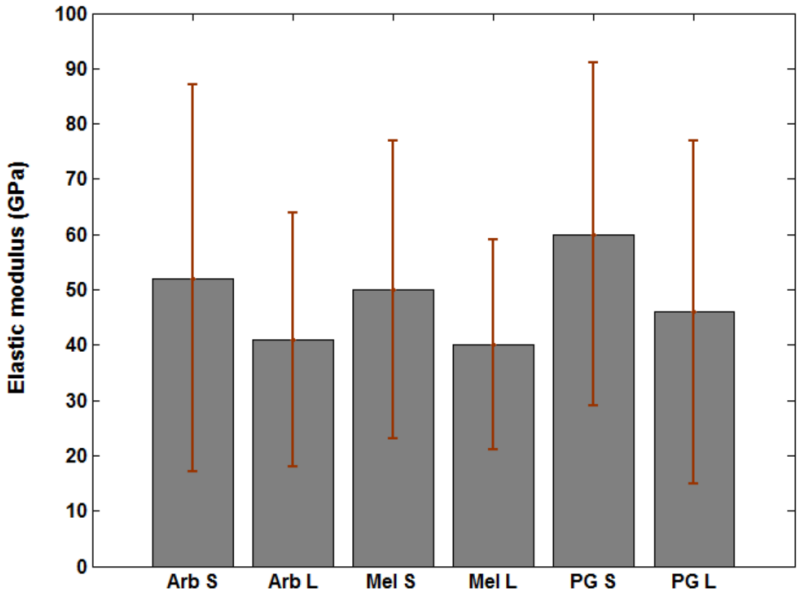

Figure 2.15: Comparison of elastic modulus among different samples

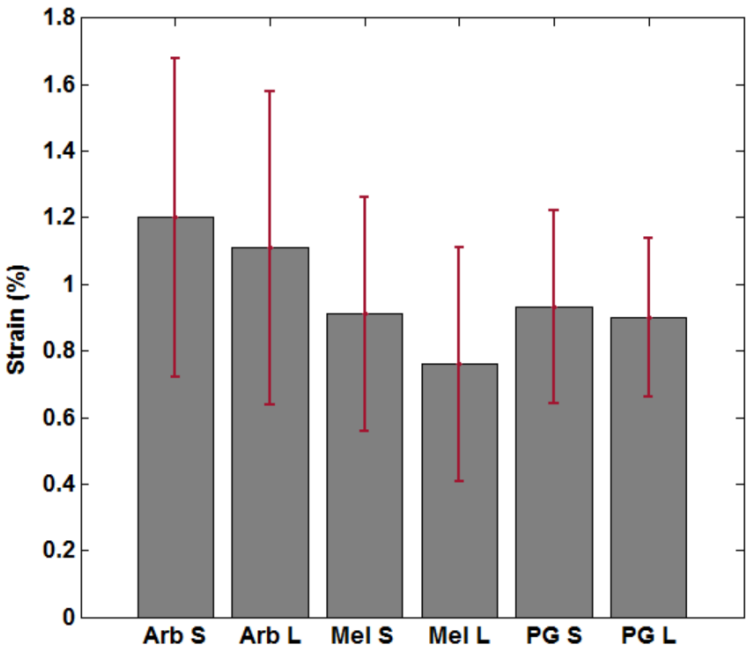

Figure 2.16: Comparison of failure strain among different samples

Figure 2.17 compares the strength of all six samples with 20 mm gauge length (NDSU) and 4 mm gauge length (CIC). It can be observed that the general trend is similar for both 20 mm gauge length and 4 mm gauge length, that is, the strength of small diameter fiber is always greater than the strength of large diameter fiber. In addition, 4 mm gauge length has higher mean strength than 20 mm gauge length. According to the weakest link theory, this trend is expected to happen. Because, the 4 mm gauge length fiber contains smaller amount of flaws compared to the 20 mm gauge length fiber. As the number of flaws decreases in a certain length of fiber, the probability of failure also decreases and the strength of the fiber increases. The flaws and kink bands are the potential site for crack initiation and stress contration. As a result, a reduction in the site for crack initiation and stress concentration would result in a increase in strength.

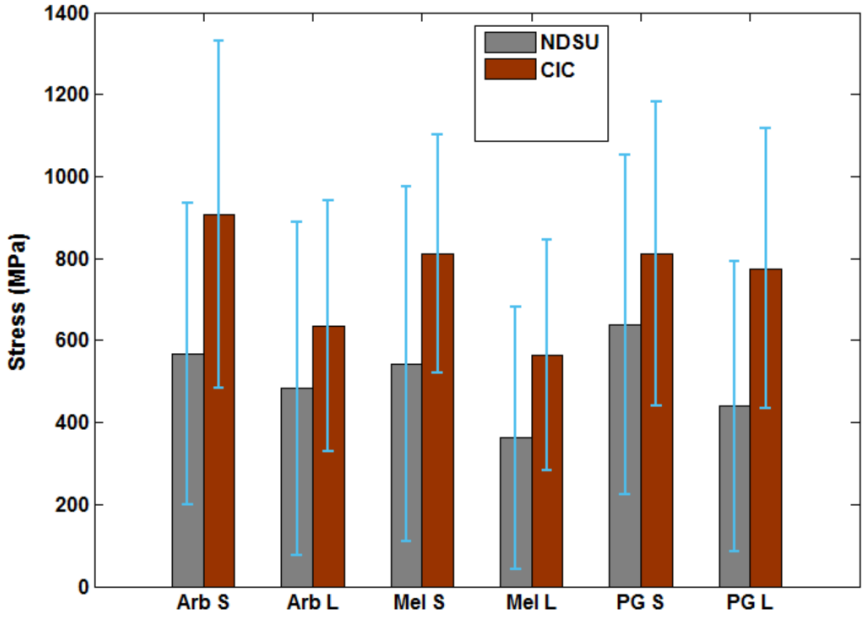

Figure 2.17: Comparison of strength between 20 mm (NDSU) and 4 mm samples (CIC).

2.5. Investigation on probability distributions

To investigate the best statistical distribution which can fit the failure strength of flax fiber, a number of distribution such as lognormal, gamma, Weibull and others were investigated. The parameter of each distribution was determined by maximum likelihood method (MLM) considering a 95% confidence interval. The distribution plot was then superimposed on the experimental data and visually inspected which one fits best. More formally, Anderson-darling test (AD value) and $P-value$ were employed to discern the best fit. A lower AD value and a higher $P-value$ represents better fit.

Figure 2.18 depicts the superposition of lognormal distribution with the experimental strength data (PG small). The parameter of the distribution, mean and standard deviation, were found to be 648 and 491 by maximum likelihood method, respectively. The AD value and P-

value for this distribution is 0.383. Though the middle portion of the data fit the distribution, the lower and upper portion of the data significantly deviates from the distribution.

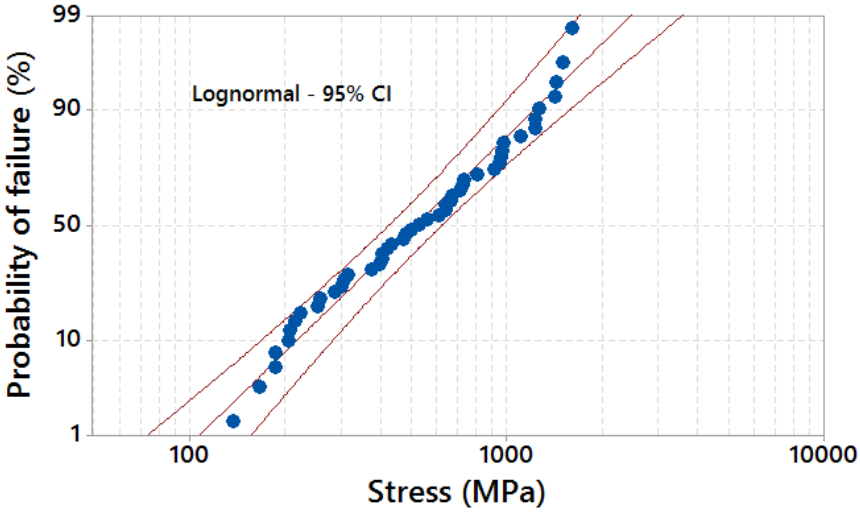

Figure 2.18: Probability plot of lognormal distribution

Figure 2.19 depicts the superposition of exponential distribution with the experimental strength data. The parameter of the distribution β was determined to be 637 MPa by maximum likelihood method. For exponential distribution, the mean and the standard deviation is the same quantity and equal to β. The AD value and P-value for this distribution fit is 2.936 and 0.003, respectively. Though the higher values of the experimental data fit the distribution, significant deviation occurs at the lower end values.

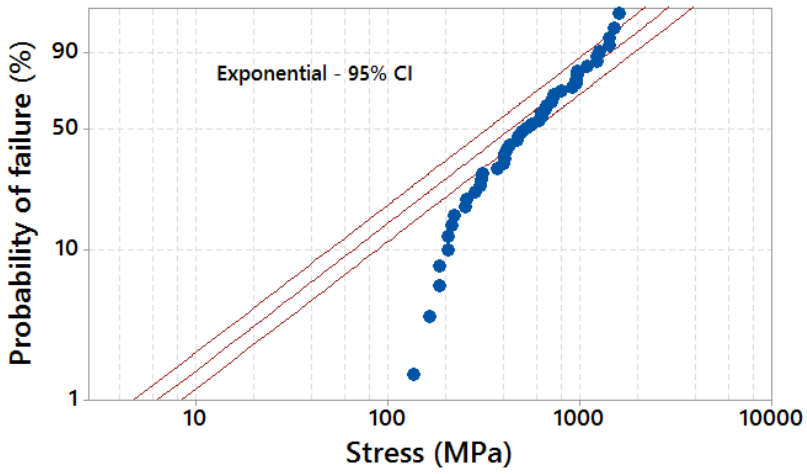

Figure 2.19: Probability plot of exponential distribution

Figure 2.20 depicts the superposition of gamma distribution with the experimental strength data (PG Small). The parameter of gamma distribution α and β are found to be 2.54 and 250, by maximum likelihood method. The mean and the standard deviation are 637 and 399, respectively. The AD value and P-value for this distribution fit is 0.435 and 0.25, respectively. Most of the experimental data deviate from the distribution. The upper and lower end values show higher deviation than the middle values.

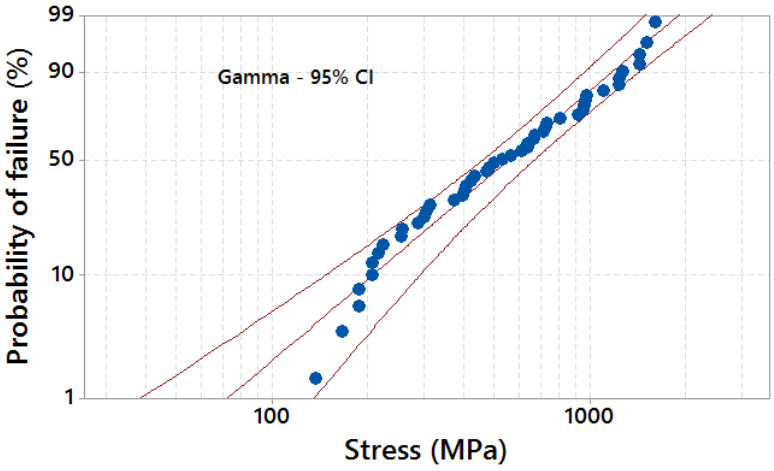

Figure 2.20: Probability plot of gamma distribution

Figure 2.21 shows the superposition of 2 parameter Weibull distribution with the experimental strength data. The parameters of the Weibull distribution, the scale parameter and the shape parameter, are found to be 717 MPa and 1.68, respectively by maximum likelihood method. The mean and the standard deviation of the distribution is predicted to be 641 MPa and 391 MPa, respectively. The AD value and P-value for this distribution fit is 0.503 and 0.209, respectively. The higher end values of the experimental data agrees well with the distribution. However, the middle portion of the data and the lower end values show deviation from the distribution.

Figure 2.22 depicts the superposition of Loglogistic distribution with the experimental strength data. This distribution has been used for modeling the probability of survival for cancer patients and is similar in shape to the lognormal distribution [15]. The AD value and P-value for this distribution fit is 0.458 and 0.212, respectively. Most of the experimental data agrees well with the distribution, especially the middle values. However, the lower and upper end values show deviation from the distribution.

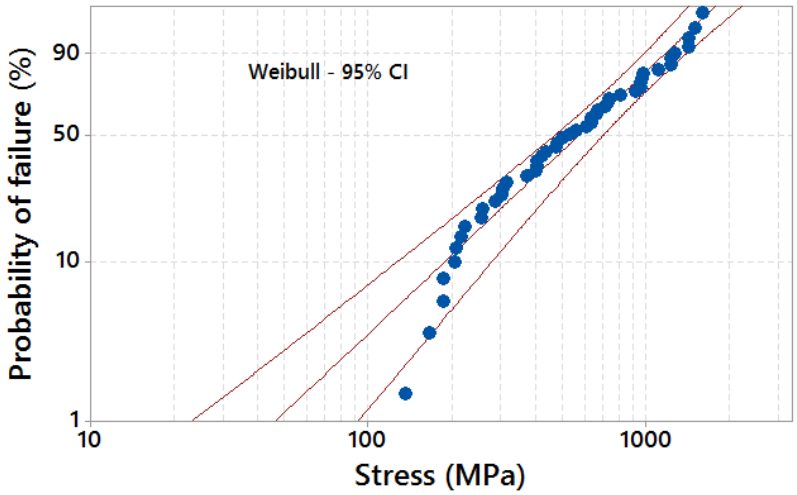

Figure 2.21: Probability plot of 2 parameter Weibull distribution

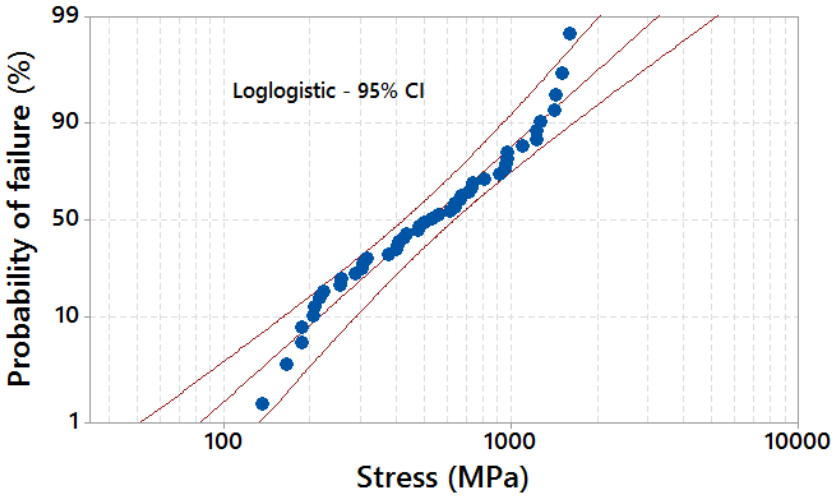

Figure 2.22: Probability plot of Loglogistic distribution

Figure 2.23 depicts the superposition of 3-parameter Weibull distribution with the experimental strength data. The scale parameter and the shape parameter are found to be 530 MPa and 1.16, respectively by maximum likelihood method. The three parameter Weibull distribution has an additional parameter called threshold parameter which is found to be 133 MPa. This threshold parameter gives an indication that it is unlikely to fail a technical flax fiber under this threshold stress. The mean and the standard deviation predicted by this distribution is found to be 635 MPa and 432 MPa, respectively. The AD value and P-value for this distribution fit is 0.250 and 0.5, respectively. Most of the experimental data agrees well with the distribution including the lower and upper end values. Compared to all other distribution analyzed in this study, 3-parameter Weibull distribution shows the highest degree of fit.

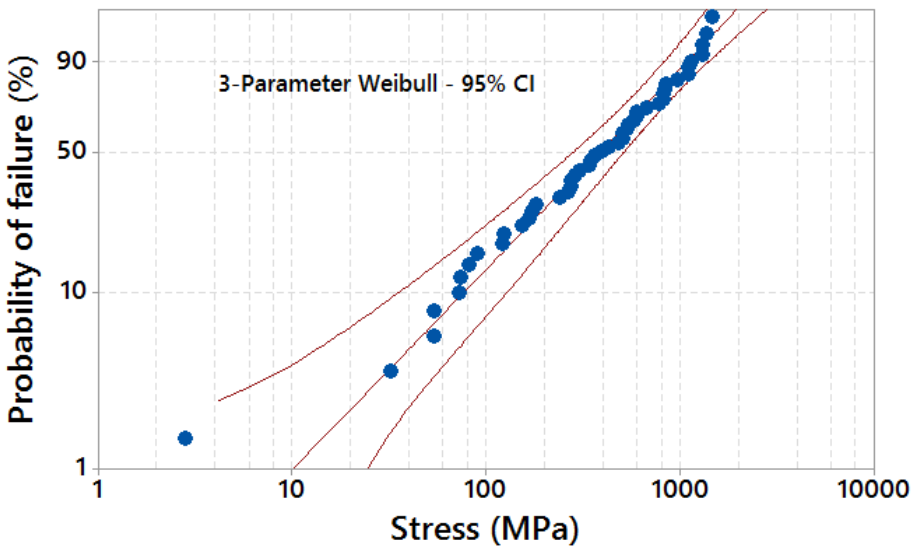

Figure 2.23: Probability plot of 3-parameter Weibull distribution

Figure 2.24 shows the distribution of strength of PG small sample with different gauge length. In this study, 20 mm and 4 mm gauge length of the technical flax fiber was considered. According to the weakest link theory, as mentioned earlier, with the increase in gauge length, the probability of failure also increases. Because, a larger gauge length would contain a higher amount of flaws. This trend is clearly demonstrated in Figure 2.24 by employing Weibull distribution. As for example, a stress level of 500 MPa for a 4 mm gauge length fiber has a probability of failure of 0.2 (black dots). On the other hand, with the same stress level for a 20 mm gauge length fiber has a probability of failure of 0.4 (blue dots). The red lines shows the associated fit of the Weibull distribution. The parameters of the distribution were determined by linear least square method and maximum likelihood method. In addition to the effect of gauge length, there might be an effect of diameter measurement as the NDSU used an optical microscope and the CIC used a laser scanner. A reduction factor and circular cross section was used at NDSU while an elliptical cross-section was used at CIC.

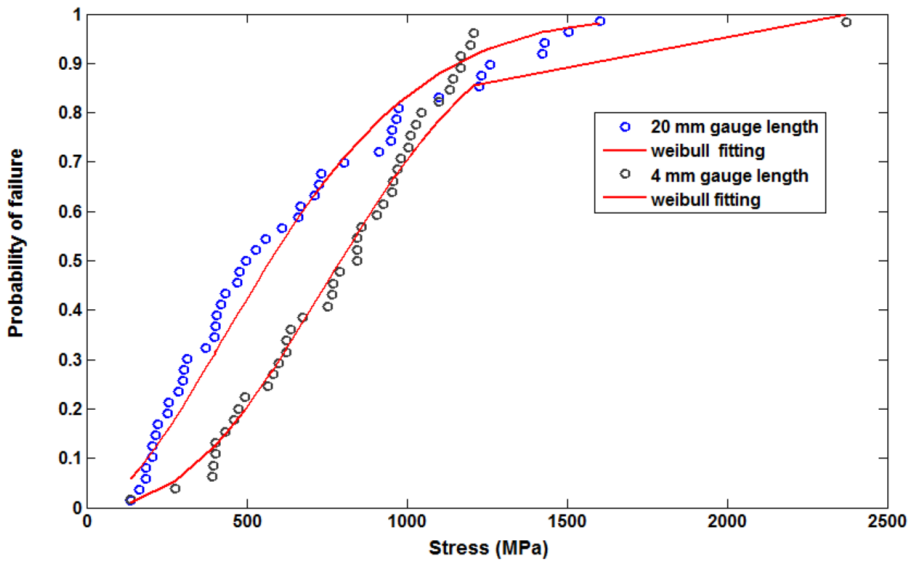

Figure 2.24: Manifestation of the weakest link theory by 2-parameter Weibull distribution

Figure 2.25 shows the superimposed 2- parameter and 3- parameter Weibull distribution on the experimental strength data. Though the 2-parameter Weibull distribution well approximates the failure stress of flax fiber, a three parameter Weibull distribution can have a better approximation of the strength data. In case of the 2-parameter Weibull distribution, a slight deviation occurs in approximating the lower end values of the experimental data. However, the three parameter Weibull distribution can capture those values as well. For the middle range values (230-700 MPa), two parameter Weibull distribution may underestimate the probability of failure, whereas a three parameter Weibull distribution will provide a more accurate description of the probability of failure of flax fibers. From a design perspective, in some cases, overestimation may be acceptable which provide a factor of safety. However, underestimation in strength values may lead to catastrophic failure. In most of the cases, a three parameter Weibull distribution well approximates the strength values, and in some cases overestimates, but never highly underestimates. For this reason, a three parameter Weibull distribution is more reliable than a two parameter Weibull distribution.

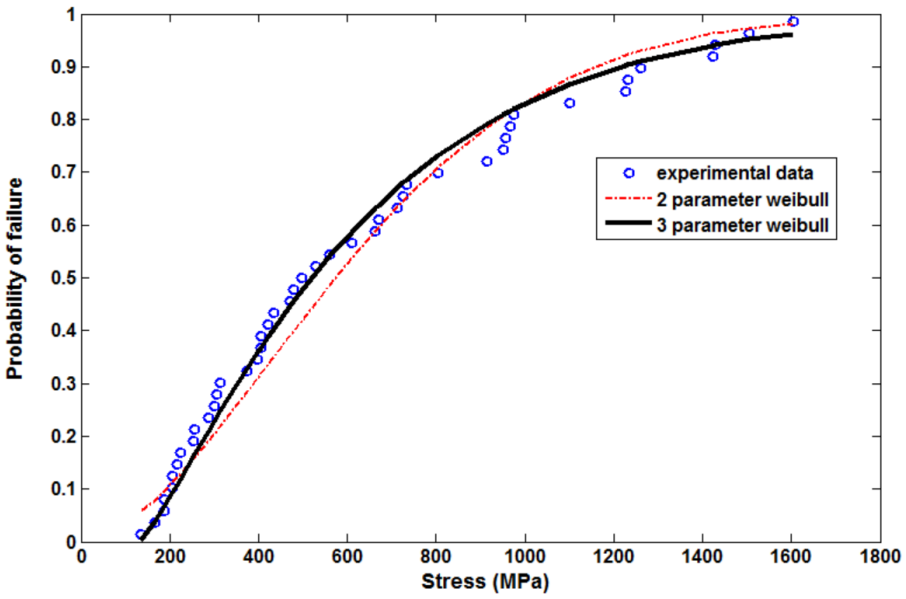

Figure 2.25: 2- parameter and 3- parameter Weibull distribution fit

2.6. Strain rate testing of technical flax fiber

For determining the effect of strain rate on technical flax fiber, a separate study was performed. Three different displacement rate were selected and at least 50 technical flax fiber were tested under with each displacement rate. A motor speed of 5 mm/min, 15 mm/min, and 30 mm/min were used which correspond to 0.25 mm/min, 0.75 mm/min and 1.6 mm/min displacement rate. A gauge length of 20 mm were used. For determining the strain rate, displacement rates are divided by the gauge length. Therefore, the strain rate used in the experiment are 0.01 min^{-1} , 0.03 min^{-1}, and 0.08 min^{-1} . Table 2.7 summarizes the results for strain rate testing in this study.

Schwartz et.al [16] investigated the effect of strain rate and gauge length on the failure of ultra-high strength polyethylene fibers. For investigating the effect of strain rate, they fixed the gauge length at 50 mm and used the strain rates at 0.004, 0.1, 0.4, and 1 min^{-1}. For investigating the effect of gauge length, they fixed the strain rate at 0.1 min^{-1}, and used the gauge lengths of

10, 50, 100, and 200 mm. They found that with the increase in strain rate, the failure strength increases and the fibers transition from viscoelastic to elastic nature. The failure surface becomes more fibrillated as the strain rate increases. Okoli et.al [17, 18] studied the effect of strain rate on fiber reinforced composites (glass fiber/Epoxy). They found that with the increase in strain rate, the failure strength of the composite increases. They reasoned that this increase stems from the increase in strength of glass fibers from high strain rate, as glass fibers are strain rate sensitive. The amount of energy absorbed during the failure process is also increased with the increase in strain rate.

Figure 2.26 shows the distribution of failure strength of technical flax fibers at different strain rate. Flax fibers, being a natural polymeric materials, is expected to show strain rate sensitivity. However, the mean of this three sets of samples is not statistically significant. That is, the strain rate sensitivity is not observed within the specified limit of strain rate tested. One reason for this behavior is that the strain rate used in this experiment (0.01-0.08 min^{-1}) does not vary appreciably that would produce the increase in failure strength. For the strain rate 0.08 min^{-1}, the failure strength of flax fibers showed very limited scatter and the range is very short. The highest range of failure strength is observed with the strain rate of 0.03 min^{-1}. With regards to glass fiber, Cansfield et.al [19] found that the strain rate of 0.2 $\text{min}^{-1}(3.10^{-3}s^{-1})$ is the threshold at which the glass fibers starts to show appreciable increase in strength and the distinct yield point that is visible on stress-strain curve, starts to disappear.

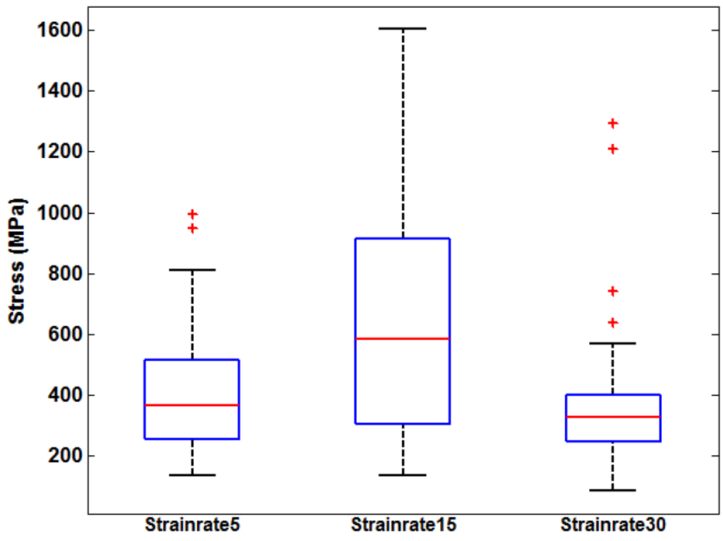

Figure 2.26: Distribution of stress for different strain rate

Figure 2.27 and Figure 2.28 shows the distribution of failure strain and elastic modulus with different strain rates, respectively. With 0.08 min^{-1} strain rate, the failure strain gets maximum value. However, the mean failure strain is highest for 0.03 min^{-1}strain rate. The mean of the failure strain of three different sets of samples does not vary to an appreciable amount and they are not statistically significant. The mean of the elastic modulus for strain rate 0.03 min^{-1} is the highest for three sets of samples. As the structure of a single flax fiber is very different from a glass fiber or regular polymeric materials [20], therefore, it is not expected that they would follow the same trend. The failure strength, failure strain, and elastic modulus of a technical flax fiber with different strain rate may be affected in the following way:

1. A fiber may fail due to higher strain or higher stress or both. That is, a fiber may reach a high value of strain without reaching a high value of stress. In this case, the failure would be governed by the higher strain. For a 0.08 min^{-1} strain rate, highest failure strain is observed but the failure strength is lower than the 0.03 min^{-1} strain rate. In this case,

failure is governed by high strain of the fiber. Due to the higher strain rate, the fibers quickly reaches a value of strain that it can no more accommodate without reaching a sufficiently higher strength, and failure occurs.

2. A fiber may reach a high value of stress without reaching a high value of strain. This may happen when the fiber has a high modulus. Or, when the slope of the force elongation curve is high. In this case, a fiber will quickly reach a high value of stress while maintaining a low value of strain. And the failure would be governed by higher strength. For 0.03 min^{-1} strain rate, the microfibrils of the flax fibers get sufficient time to untwine and rearrange. Therefore, the failure strength and elastic modulus (Figure 2.26 and 2.28) reaches a higher value than other two strain rates. For this strain rate (0.03 min^{-1}) failure is governed by higher strength.
3. A fiber may reach both higher value of strength and higher value of strain simultaneously. And the failure would be governed by this combined effect. This may happen when the strain rate is very low and the time to failure is very high usually 50-60 seconds (Figure 2.29). For 0.01 min^{-1} strain rate, this trend is clearly observed. The fibers have a moderate failure strength and moderate failure strain, but a lower moduli. This lower moduli helps the flax fibers to attain moderate strength and strain simultaneously.

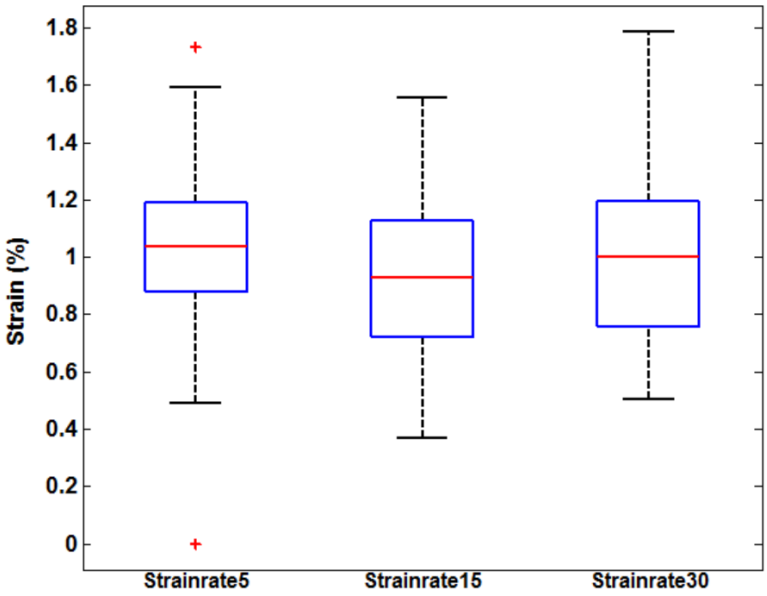

Figure 2.27: Distribution of failure strain at different strain rates

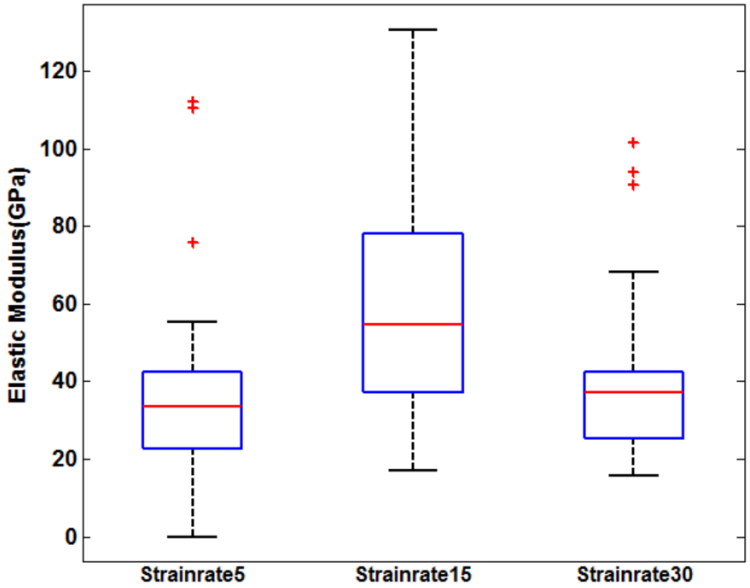

Figure 2.28: Distribution of elastic modulus at different strain rates

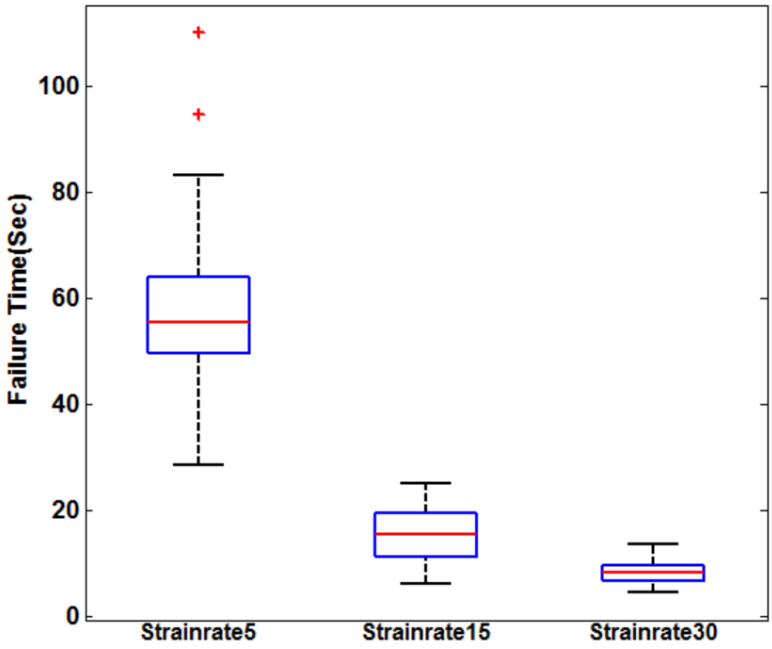

Figure 2.29: Distribution of failure time at different strain rates

Table 2.8: Summary of the results of strain rate testing

	PG small 5 (0.01 min^{-1})	**PG small 15 (0.03 min^{-1})**	**PG small 30 (0.08 min^{-1})**
Failure Strength (MPa)	389±203	637±414	364±244
Failure Strain (mm/mm)	1.055±0.24	0.93±0.29	1.02±0.31
Elastic Modulus (GPa)	37±20	60±31	38±20
Failure Time (Sec)	55±18	15±4.6	8.2±2.24
Number of Discard	2	5	8

2.7. References

1. Andersons, J., E. Spārniņš, and E. Poriķe, *Strength and damage of elementary flax fibers extracted from tow and long line flax.* Journal of composite materials, 2009.

2. Khalili, S., et al., *Fibernodes in flax and other bast fibers.* Journal of applied botany, 2002. **76**(5-6): p. 133-138.
3. Baley, C., *Influence of kink bands on the tensile strength of flax fibers.* Journal of materials science, 2004. **39**(1): p. 331-334.
4. Weibull, W., *A statistical distribution function of wide applicability.* Journal of applied mechanics, 1951. **18**(3): p. 293-297.
5. Meyers, M.A. and K.K. Chawla, *Mechanical behavior of materials*. Vol. 2. 2009: Cambridge University Press Cambridge.
6. Griffith, A.A., *The phenomena of rupture and flow in solids.* Philosophical transactions of the royal society of london. Series A, containing papers of a mathematical or physical character, 1921. **221**: p. 163-198.
7. Zok, F.W., *On weakest link theory and Weibull statistics.* Journal of the American Ceramic Society, 2017. **100**(4): p. 1265-1268.
8. Phoenix, S.L. and R.G. Sexsmith, *Clamp effects in fiber testing.* Journal of Composite Materials, 1972. **6**(3): p. 322-337.
9. Phoenix, S., et al., *Statistical Models for the Tensile Strength of Yarns and Cables.* Mechanics of Flexible Fiber Assemblies Series of Applied Science, 1980(38): p. 113-141.
10. Hearle, J.W., *Mechanics of flexible fibre assemblies*. 1980: Kluwer Academic Publishers.
11. Thomason, J., et al., *Fibre cross-section determination and variability in sisal and flax and its effects on fibre performance characterisation.* Composites Science and Technology, 2011. **71**(7): p. 1008-1015.

12. Burgert, I. and P. Fratzl, *Plants control the properties and actuation of their organs through the orientation of cellulose fibrils in their cell walls.* Integrative and comparative biology, 2009. **49**(1): p. 69-79.

13. Keckes, J., et al., *Cell-wall recovery after irreversible deformation of wood.* Nature materials, 2003. **2**(12): p. 810-813.

14. Lefeuvre, A., et al., *Elementary flax fibre tensile properties: correlation between stress–strain behaviour and fibre composition.* Industrial Crops and Products, 2014. **52**: p. 762-769.

15. Bennett, S., *Log-logistic regression models for survival data.* Applied Statistics, 1983: p. 165-171.

16. Schwartz, P., A. Netravali, and S. Sembach, *Effects of strain rate and gauge length on the failure of ultra-high strength polyethylene fibers.* Textile Research Journal, 1986. **56**(8): p. 502-508.

17. Okoli, O. and G. Smith, *Failure modes of fibre reinforced composites: The effects of strain rate and fibre content.* Journal of Materials Science, 1998. **33**(22): p. 5415-5422.

18. Huang, W., W. Xu, and Y. Xia, *Effect of strain rate on the mechanical behaviors of SiC fiber.* Journal of materials science, 2005. **40**(2): p. 465-468.

19. Cansfield, D., et al., *Tensile-Strength Of Ultra High Modulus Linear Polyethylene Filaments.* Polymer Communications, 1983. **24**(5): p. 130-131.

20. Gorwade, C., et al. *Finite element analysis of the high strain rate testing of polymeric materials*. in *Journal of Physics: Conference Series*. 2012. IOP Publishing.

CHAPTER 3. FAILURE ANALYSIS OF FLAX FIBERS

The use of flax fiber as a reinforcement in bio-composite materials requires a proper understanding of their fracture behavior from an individual fiber down to the constituent micro-fibrils. For investigating the failure mechanism of individual and technical flax fibers, a tensile test bench was integrated with the electron microscope, and the entire process of fiber failure was investigated through the capture of SEM movie. After that the fractographic analysis was performed on the failure surface of single fibers as well as meso-fibrils that failed at a displacement rate of 0.25 mm/min, 0.75 mm/min, and 1.6 mm/min. The analysis also enabled visualization of a few internal details of flax fiber such as the arrangement of meso-fibrils and micro-fibrils. It was shown that the crack bridging mechanism and successive fiber pull-out contributed to the high work of fracture of flax fiber and the value may reach as high as (10^6) J/m^2.

3.1. Literature review

The failure strength and failure strain of flax fibers have been investigated widely [1-5]. The compressive strength of flax fiber is about 80% of its tensile strength whereas polymeric or glass fiber has much lower compressive strength, about 20% of the tensile strength [2]. However, their internal variability (arising from plant varieties, growing conditions, separating procedures such as dew retting, enzyme retting), and their high water absorption properties - all continue to act as barriers for widespread adoption of natural fibers, more specifically flax fibers, in industrial and structural applications such as reinforcing agents in composite materials. In this respect, the analysis of the failure mechanism of technical as well as elementary flax fibers have become important. Andersons et.al.[6] attempted to investigate the effect of mechanical defects on the strength distribution of elementary flax fibers. He proposed that a modified Weibull

distribution instead of a two-parameter Weibull distribution can approximate the strength with greater accuracy. Mclaughlin et. al.[7] studied the fracture mechanism of different plant fibers by SEM micrograph and tensile testing of single cells and found that the work of fracture depends on the helix angle as well as the cellulose content of the fiber. Nilsson et.al[8] studied the influence of dislocations (Figure 3.1) on the tensile behavior of flax and hemp fibers by finite element analysis. They assumed the elementary flax fiber as a thick walled cylinder and modeled only the secondary layer. For the simplicity of analysis a circular cross-section was assumed and it was considered that cellulose micro-fibrils are embedded in a hemicellulose matrix. The effect of lignin and pectin were neglected. Thygesen et.al [9] studied the effect of growth and storage conditions on the distribution of dislocations on hemp fibers. They found that the dislocations are present in the fiber even before harvest and mechanical isolation. Different growing conditions such as wind and arid were found to produce similar effects on dislocations. The storage of fiber in different moisture conditions also affects the presence of dislocations. They also indicated that these dislocations tend to reduce the strength of fibers. Davies and Bruce [10] studied the effect of damage or dislocations and relative humidity on the tensile properties and stiffness of flax fibers. They observed that the overall effect of damage was to decrease the tensile strength and stiffness of flax fiber. They mentioned that the relative humidity did not have much influence on the tensile strength but decreases the stiffness of flax fiber. Bos et. al.[11] investigated the fracture surface of elementary fibers by straining a loop of elementary fiber. He showed that failure in primary wall is brittle, whereas in secondary wall crack bridging occurs. However, to the author's knowledge, no study has been performed analyzing the dynamic failure of flax fiber in tension. To remedy this shortcoming, in-situ observation on the failure mechanism of technical and elementary flax fibers have been investigated in the present study.

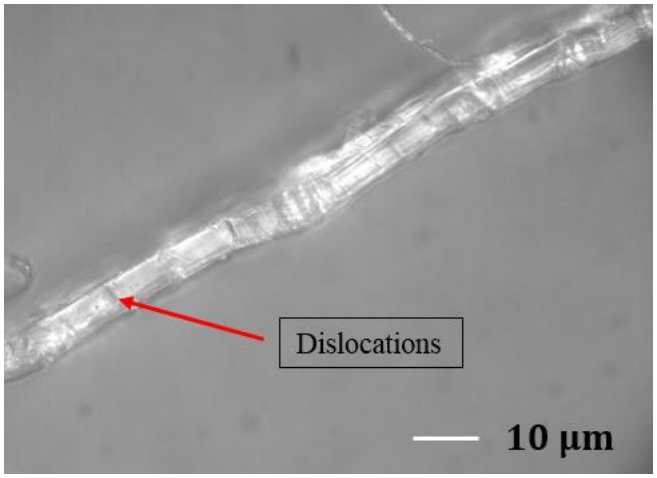

Figure 3.1: Kink bands or dislocations are visible on a single flax fiber

3.2 Experimental

The flax fibers used in this study were linseed flax, farmed and harvested at Melita, Manitoba, Canada and provided by Composite Innovation Center (CIC), Winnipeg, Canada. Flax plants were planted on May 22, 2015 and harvested on August 13, 2015. The average height of the plants was 60 cm at harvest. When harvested, the flax plants were observed to be very dry and mature with greater than 50% brown seed bolls.

After harvest, enzyme retting was performed for extracting the fibers from the cuticularized epidermis and the woody core. The fibers were of shiny golden color. The technical fibers were carefully hand separated for tensile testing. The diameter of the fibers were measured by a Zeiss Axiovert 40MAT inverted optical microscope. The diameter was measured at three different locations of the fiber and then the average was taken. The main uncertainty that arises in flax fiber characterization is due to the diameter and area measurement as the fibers are not circular in shape, but rather more of an elliptical shape [12].

For performing the tensile tests, ASTM standard D3822/D3822M was followed. The tensile testing was performed with a Deben Microtest tensile test bench with maximum load cell

capacity of 180 N. The fibers were clamped at both ends of the machine. The gauge length of the fibers was fixed at 20 mm with a displacement rate of 0.75 mm/min. 50 specimens were tested in this study to investigate the distribution of failure stress, failure strain and Young's modulus of the technical fibers.

Next, 10 technical fibers were tested and scanning electron microscopy was performed on the fractured surface of the fibers that failed at three different displacement rate: 0.25 mm/min, 0.75 mm/min, and 1.6 mm/min. The fractured samples were carefully mounted on aluminum mounts using carbon tabs and then coated with a conductive layer of carbon in a high-vacuum evaporative coater (Cressington 208c, Ted Pella Inc., Redding, California). The images for fractographic analysis were obtained with a JEOL JSM-7600F scanning electron microscope (JEOL USA Inc., Peabody, Massachusetts).

3.3 Results and discussion

A typical stress-strain curve for a flax fiber is shown in Figure 3.2. When a flax fiber is loaded in tension, from 0 to 0.1% strain, the curve shows fairly linear behavior (Figure 3.2). From 0.1 to 0.6% strain, the curve shows non-linear behavior and strain softening occurs. This is analogous to the yield point of a metal specimen pulled in tension. After this non-linear region, strain hardening occurs and the curve behave in a fairly linear fashion once again. At a strain of approximately 1.3%, the fiber fails suddenly in a brittle manner. The plastic zone is much larger than the linear elastic region. However, the non-linear portion of the figure is not always distinguishable in some of the specimens and failure strength varies between 200 and 1600 MPa. A single flax fiber may be thought of as a composite laminate with four lamina naturally adhered together [13]. Inside a single lamina (Figure 3.3), cellulose micro-fibrils (CMFs) are scattered on a hemicellulose matrix, consisting mainly of xylan or xyloglucan matrix. These hemicelluloses

(HC) are attached to the surface of cellulose micro-fibrils by non-covalent and hydrophobic bonding such as hydrogen bonds. Pectin acts like a gel and holds together these entire C-HC network [14]. In addition to the non-covalent bonding, cellulose micro-fibrils are also physically entangled with the hemicellulose and pectin matrix. Though the HCs are not crystalline, they are also not random in orientation and mostly lie parallel to the CMFs or at some preferred angles.

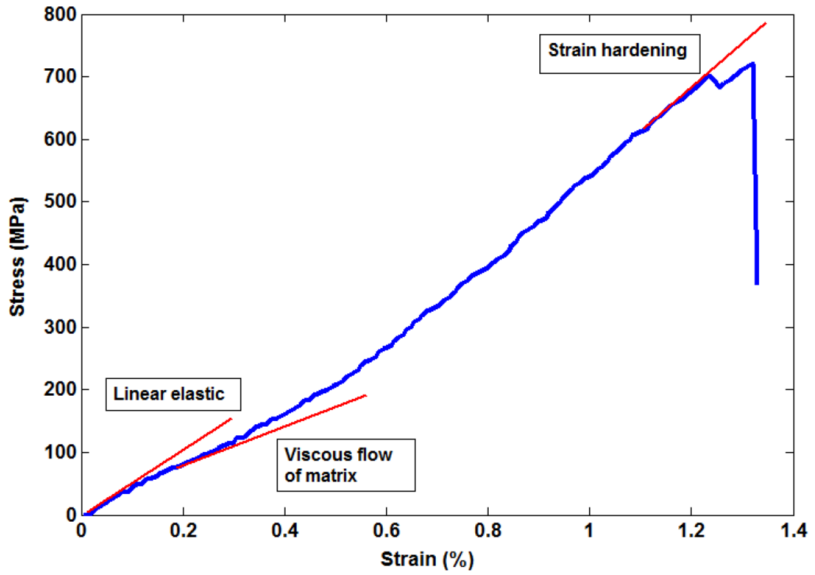

Figure 3.2: Typical stress-strain curve of a single flax fiber. Three distinct regions can be identified: Linear elastic region, matrix flow region and strain hardening region. A large plastic deformation can be observed beyond the elastic limit.

As pointed out by Hughes et. al[15] , the stress-strain curve of flax fiber reinforced composite materials shows linear elastic behavior up to 0.05% strain. After this point, a slight drop in modulus is observed (known as strain softening) and strain hardening occurs before the ultimate breakage of the fiber. Similar trend is also observed for a single or technical flax fiber as shown in Figure 3.2. Within the linear elastic region, the cellulose micro-fibrils and the hemicellulose and pectin network try to disentangle from each other upon the application of load and this extension occurs without any breakage of the bonding. As a result, upon the removal of

the load, the stress-strain curve follows the previous path without any hysteresis. Beyond the linear elastic region, the load is high enough to break some of the non-covalent bond and as the load continues to increase, the matrix reaches its yield point ahead of the cellulose micro-fibrils. There is a viscous flow of the matrix without any fracture and gliding of cellulose micro-fibrils occur. Some of the hydrogen and hydrophobic bonds break. A few hemicellulose and pectin chains are also broken. There is a change in modulus in the stress-strain curve. However, at other portion of the matrix, the hydrogen bonds are reestablished, the stress is locked, and there is no backflow. As the load increases, some of the amorphous molecules also get oriented in a specific direction and tend to be crystalline. CMFs are also arranged parallel to the fiber axis and a larger force is required to break these chains. This shows up in the graph as strain hardening region.

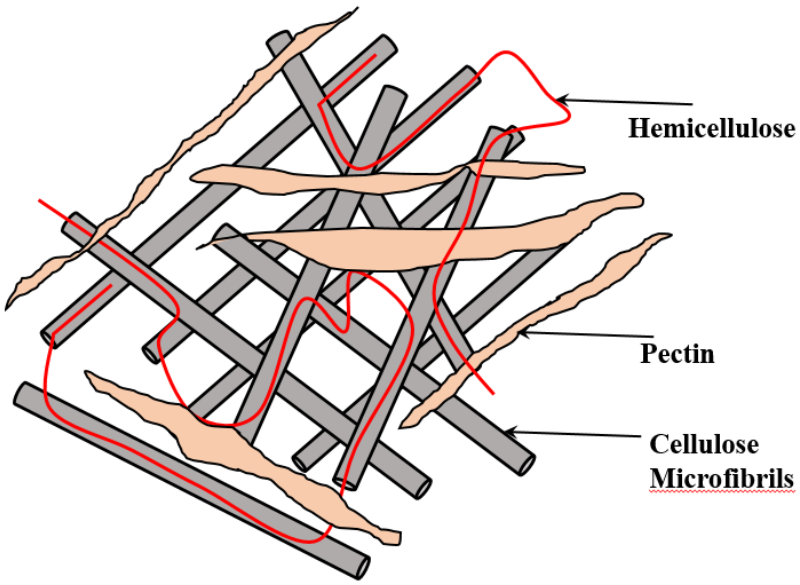

Figure 3.3: Schematic diagram of the arrangement of CMF, HC and Pectin. Adapted from [16, 17]

In Figure 3.4a, the force-elongation curve of a flax fiber is shown. The area under this curve represents the total energy absorbed during the fracture and it is calculated to be 0.2956 N-

mm. Figure 3.4b shows the viscoelastic nature of flax fiber. This curve was generated by successive loading and unloading of a single technical fiber with a diameter of 110 μm. For the first cycle, the slope of the loading curve is lower than the unloading curve, that is, the modulus increases after the fiber is strained. The area enclosed by the loading-unloading curve represents the hysteresis loss of the cycle. In cycle 2, 3 and 4 the slope of the loading and the unloading curve is almost similar. However, with each successive cycle the slope of the loading curve gradually increases. The slope of the loading curve of cycle 4 is approximately twice than that of the cycle1. However, in cycle 3 and 4 the slope of the loading and the unloading curve is nearly similar indicating that there might be a threshold for strain hardening of flax fibers above which there will not be a marked difference in the modulus.

3.4. In situ failure analysis through SEM

For dynamically investigating the failure mechanism of flax fiber, a tensile test bench was placed inside the scanning electron microscopy. With the help of the SEM imaging system, a video was recorded over a period of 1 minute and 11 seconds while the fiber was being pulled in tension, until the failure of the fiber occurred. The speed of the imaging system was 30 frames/sec. The SEM motion picture reveals three distinct phases of fiber failure, 1. initial rotation of fiber bundle, 2. segregation of the single fibers from the bundle, and 3. ultimate failure of the fiber.

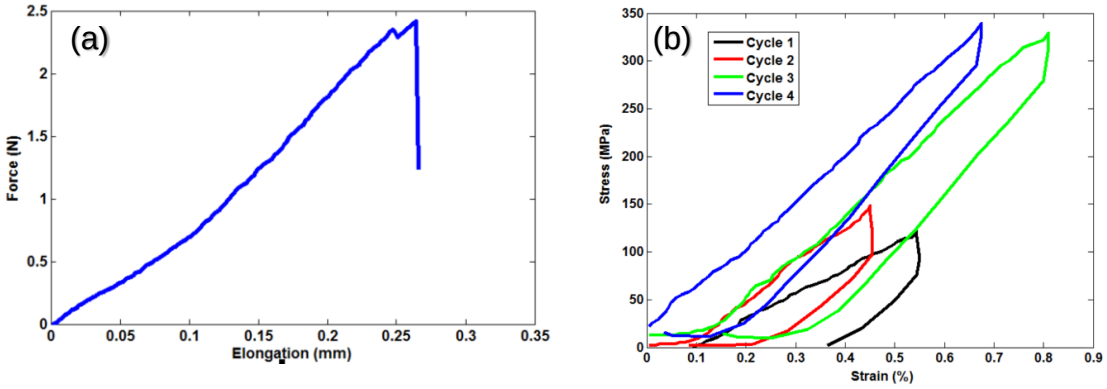

Figure 3.4: (a) Force-Elongation curve and (b) hysteresis curve. Area under the force elongation curve represents the total energy absorbed during the fracture. Hysteresis curve shows the gradual increase in modulus during each successive loading unloading cycle.

3.4.1. Initial rotation of the fiber bundle

At the beginning of the application of the tensile load, the technical fiber undergoes a certain degree of rotation as revealed in the video captured by the SEM. The reason of this rotation of the fiber bundle may be attributed to the presence of the helically arranged meso-fibrils located mainly at the S2 layers within the single fibers. The micro-fibrils in the primary layer are randomely oriented. On the other hand, micro-fibrils in the S1 and S3 layer are arranged in circumferential direction [18]. As a result, micro-fibrils from the primary, S1 and S3 layers have negligible contribution to this rotation effect. This rotation occurs approximately upto 0.3 % of the total strain of the fiber. When an axial load is applied to the both ends of technical fiber, the micro-fibrils within the single fiber tend to straighten and align with the fiber longitudinal axis. However, as the micro-fibrils are not free to move and are naturally adhered to the polysaccharide matrix, the net effect is to impart rotation and twist on the fiber bundle. This phenomena may in part explain the failure of flax fiber reinforced polymer matrix composites.

The surface of cellulosic fibers are rife with –OH molecules which imparts the property of being strongly hydrophilic. On the other hand, the polymeric matrix is strongly hydrophobic.

For this reason the interfacial adhesion between the flax fiber and the polymeric matrix tends to be weak [19-21]. Hence, when flax fiber reinforced composites are exposed to tension along the fiber axis, the rotation and twist of the fiber bundle further weaken the interfacial adhesion, contributing to the typically overall lower strength of flax fiber reinforced composite materials.

3.4.2. Segregation of single fibers from the bundle

As the magnitude of tensile force increases, single fibers are observed to segregate from the bundles adhered together by pectin (Figure 3.5a-b). At this moment, the diameter of the fiber bundle increases perpendicular to the direction of applied load which is the result of separation of single fibers. As the force continues to increase, the single fibers tend to slide past one another contributing to the lower strength of flax fiber reinforced composite materials. The strength and modulus of single flax fiber has been reported to be approximately of 0.7-1.5 GPa and 50 GPa, respectively [22]. However, these strength and moduli values are not fully realized when the fibers are impregnated into polymer matrix composites [4]. This is due to the fact that in composites, the fibers are not present in the form of single fibers, but rather they are fiber bundles. Also these fibers are not continuous fibers like glass or other synthetic fibers. Due to their finite length, they need to be spun into yarn which provide them the property of being continuous and impart flexibility in their use during the manufacture of composite materials. However, this spinning requires twisting the fibers to make use of the frictional forces to hold the individual technical fibers together. This twist also generates additional kink bands or dislocations in the fiber. It is a known that the site of kink band or dislocations have higher energy and show more chemical reactivity than other region of the fiber [23]. Sometimes the polymer chain of cellulose micro-fibrils are partially broken at these sites weakening the strength of the fiber. After the manufacture of composite materials, these sites can act as region of stress

concentration which can lead to crack initiation and crack propagation in polymer matrix upon the application of load. Additionally when flax fibers are used in manufacturing composite materials via injection molding with thermoplastic polymers, they are exposed to temperatures of approximately 200° C. The tensile properties of flax fibers are reduced with an increase in temperature which was confirmed by the investigation of Hornsby et. al [24]. This reduction in strength due to increased temperature occurs because of the difference in thermal coefficient of expansion of cellulose, hemicellulose, lignin and pectin. Again their tensile strength and modulus is increased with the absorption of moisture [3]. At about 200° C, some of the moisture present in the fiber evaporates and porosity and defects are created in the fiber. As a result, after the manufacture of composite materials, these two factors: temperature and moisture tend to contribute to overall lower strength of composite materials. This sliding phenomena, along with all the factors mentioned above, aids in understand the apparent discrepancy between the higher strength and modulus of a single fiber and the relatively lower strength and modulus of their composites.

3.4.3. Ultimate failure of the fiber

It was found in the SEM motion picture that the ultimate failure of a fiber bundle occurs without any significant prior indication of failure. In a specific fiber bundle, with more or less uniform diameter, it is hard to predict the specific location of failure. This is due to a higher variation in the distribution of defects throughout the length of the fiber known as dislocations, kink bands, slip planes or nodes. These defects may originate during the growth of the flax plant and they may be in the form of misalignment of cellulose micro-fibrils [25]. The decortication process or the separation process of fibers from the stalk of the plant, introduces mechanical defects in the form of kink bands which can be observed through polarized light microscopy as

thin strip that are perpendicular to the fiber axis. These kink bands tend to reduce the strength of flax fiber [26, 27].

It was also found that not all elementary fibers fail at the same time and locations, but rather they fail at different locations and different points in time. After failure, near the fractured area, some elementary fibers within the bundle were seen to buckle and bristle such as can be seen in Figure 3.6a-b. In some other cases, the bundle break with a snapping sound and had limited brooming of the elementary fibers as shown in Figure 3.5a-b.

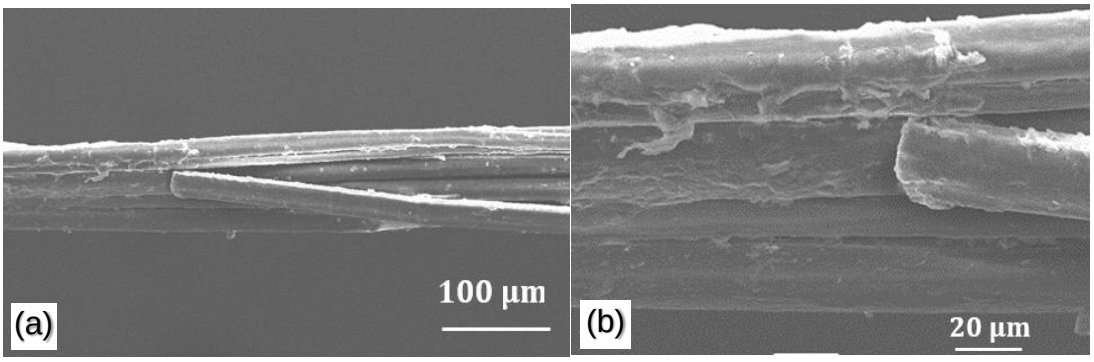

Figure 3.5: (a) Breaking of technical fiber with lower magnification and (b) with higher magnification. The single fiber broke with no prior indication of failure. There is limited brooming or bristling at the failed region of the fiber.

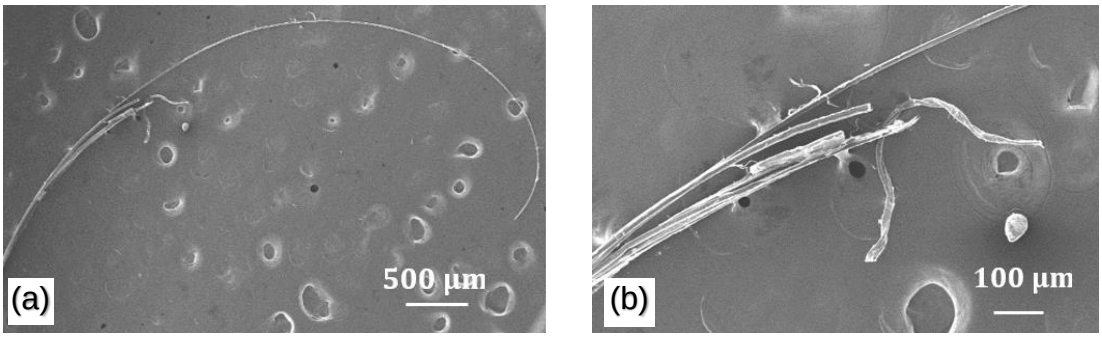

Figure 3.6: (a) Buckling of fiber after failure with lower magnification and (b) with higher magnification Individual fibers are seen to break at different region.

3.5. Fractographic analysis of single fibers

The study of fracture surface of the failed fiber provides useful information about the failure mechanism and failure mode of that fiber. In this respect, a wide array of SEM images of the fractured surface of flax fibers were collected from different angles that failed at three different displacement rate: 0.25 mm/min, 0.75 mm/min and 1.6 mm/min.

Figure 3.7a-b shows the side view of the fracture surface of a single or elementary flax fiber that failed in tension at a displacement rate of 0.25 mm/min. These two images also reveal some of the intricate details of the elementary flax fiber as the primary wall is ripped away. The cylindrical shaped meso-fibrils, sometimes erroneously called as micro-fibrils in the literature, are exposed. These meso-fibrils reside in S2 layer and have a diameter of 1-2 μm . And the angle these meso-fibrils make with the fiber longitudinal axis is erroneously called micro-fibril angle. However, the dimensions of micro-fibrils are in the nanometer range and they reside as a bundle inside these meso-fibrils. To avoid confusion, we would refer to these micro-fibrils as nano-fibrils in this paper.

The fractured surfaces that can be seen in Figure 7a are very rough, which is the characteristics of a tensile failure [28]. In compressive failure, the surfaces are usually flat and shiny. The way the primary wall is removed from the secondary wall bears the evidence of certain degree of counterclockwise rotation. In Figure 7b, a crack has propagated in the longitudinal direction and delamination of the meso-fibrils from the hemicellulose matrix can be observed. The meso-fibrils are seen to be pulled out from the matrix in longitudinal direction as well as in the transverse direction. Though these meso-fibrils make an angle of 10° with the longitudinal axis, the angle seem to disappear at the fractured region and the meso-fibrils are almost parallel with the axis.

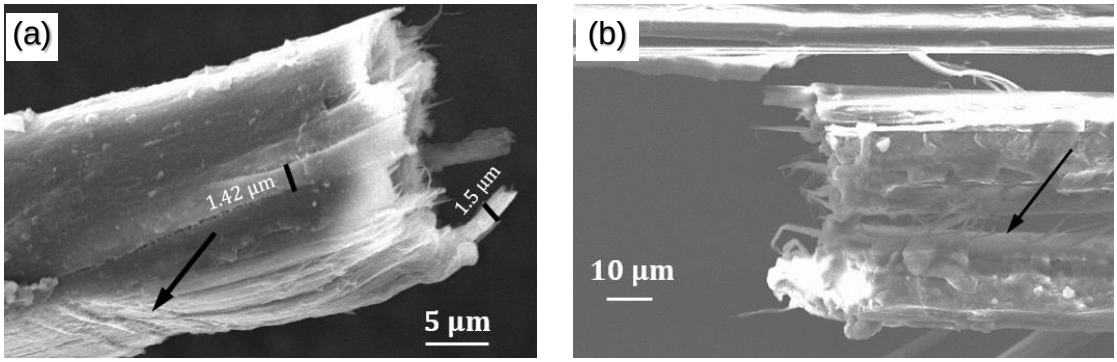

Figure 3.7: Side view of the fractured surface of an elementary flax fiber. Primary wall cringing is visible (arrow). (a) Meso-fibrils are also visible, (b) Meso-fibrils are seen to be aligned with fiber axis after the fibers are exposed to tension until failure

Figure 3.8a-c shows the fracture surface of a meso-fibril. These images were captured when meso-fibrils were exposed after breaking a single fiber with 0.25 mm/min displacement rate. The radial steps or chevron (arrow) indicates the presence of rotational failure (Figure 3.8a). When a glass fiber is subjected to torsion, a helical crack is created and propagates along the surface. The crack initiates at some defects or voids furthest from the center of the fiber as stress is maximum at that point. This crack propagation usually occurs at 45° angle with respect to the fiber longitudinal axis [29, 30]. In other words, due to the applied shear stress, two principal stresses are created in a small element of the fiber: one is compressive and another is tensile. Fracture mainly occurs due to this tensile principal stress [31]. In a similar way, this radial step region might be a potential site for crack initiation and crack propagation. After a crack initiates at that region, it then propagates further downward creating two dissimilar region: region A and region B (Figure 3.8b). The roughness of the fractured region often indicates the type of fracture mode dominating the failure. A very rough and highly fibrous surface generally represent tensile failure, and a flat, less fibrous (that is, the end of the fibrils are relatively in the same plane), generally reflects compression failure [28, 32]. So the region A is more indicative of a compression failure and region B infers more of tensile failure. It may be puzzling how

compressive stress is generated in a tensile specimen. However, this phenomena is discussed elsewhere in the literature [28, 33, 34]. When a unidirectional composite is loaded in tension, a compressive stress may generate due to the backward motion of the partially failed region of the fiber in tension. The dynamic stress wave generated in the process may be of such magnitude that it exceeds the compressive strength of the single flax fiber. In this way, a compressive failure may occur and a region of compressive failure may be created in the fiber. This behavior only occurs in unidirectional composite materials that are loaded in tension [32]. As flax fiber is regarded as a natural composite, this type of phenomena would not be uncommon to occur [35]. Again in terms of the speed or velocity of the crack propagation, region A indicates the slower rate of crack propagation. The nano-fibrils in region A get sufficiently more time to break and just sufficient energy to propagate the crack. Therefore, these fibrils reside nearly in the same plane. On the other hand, as the speed of crack propagation increases, there is some surplus energy which causes the fiber to be abruptly pulled out, and nano-fibrils in region B are no more in the same plane and shows up as rugged surfaces. In addition to these compression and tensile effects, there may have an effect of matrix anisotropy during failure. Meso-fibrils reside in a matrix of hemicellulose and pectin which is highly anisotropic. The anisotropy of the hemicellulose and pectin may arise due to the inhomogeneous deposition of these cell wall polymers during the cell wall formation [36]. The molecular arrangement of hemicellulose and pectin itself are anisotropic. Though hemicelluloses are short chain amorphous polysaccharides [37], different functional groups present in these polymers are oriented in different directions, which has been confirmed by the investigation of Stevanic et. al [38]. This conformational mismatch imparts anisotropic behavior in these polymers under mechanical stress, that is, their properties are different in longitudinal and transverse direction [38-41]. In addition, pectin

molecules are crosslinked with hemicellulose molecules and their properties are different than hemicelluloses. As a result, the matrix of a flax fiber, which is composed of hemicellulose, lignin, and pectin (with different properties), become highly anisotropic. This anisotropy of the matrix may have imparted a twisting moment on the fiber which is evidenced by the presence of the chevron in the radial direction.

Furthermore, in region A, the end of the nano-fibrils are observed to be microscopically bent (Figure 3.8c), and are not normal to the surface. This is due to the micro-buckling of the nano-fibrils. As region A is thought to be in compression, this compressive stress generates an in-plane shear stress which pushes these nano-fibrils sideways rather than being perfectly straight.

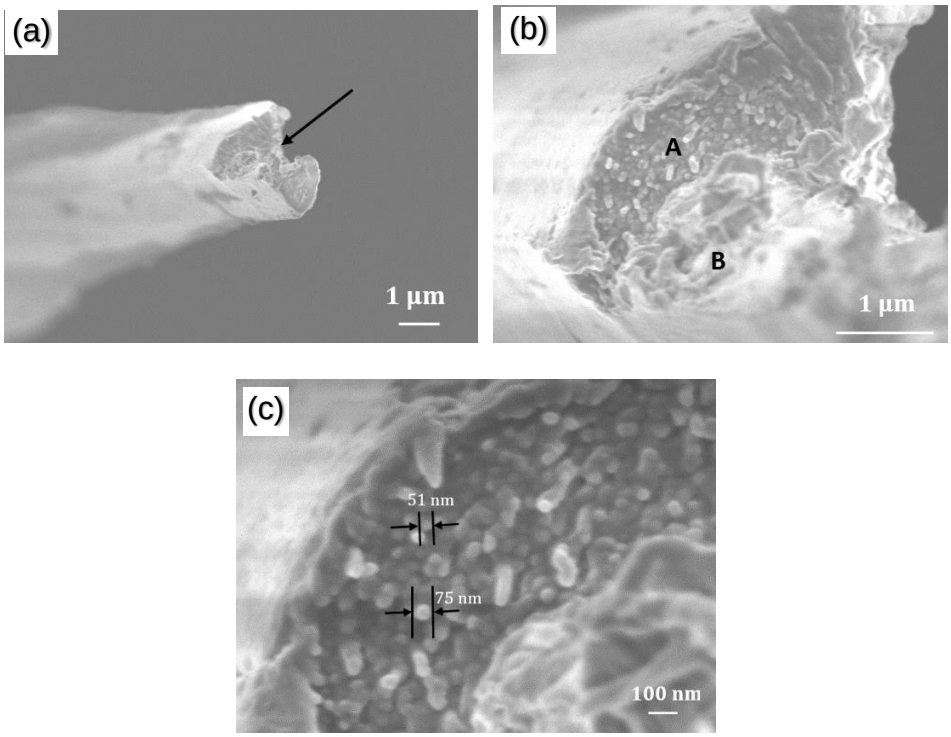

Figure 3.8: Cross sectional view of the fractured surface of a meso-fibril failed at 0.25 mm/min displacement rate. (a) Meso-fibril failure surface is shown and the chevron (arrow) indicates the presence of rotation during failure, (b) magnified view of the same surface is shown. Region A represents low speed crack propagation and region B represents high speed crack propagation, (c) magnified view of the region A is shown, individual nanofibrils are observed, microbuckling of these nanofibrils can also be seen.

Figure 3.9a shows the fractured region of a meso-fibrils that failed at 0.75 mm/min strain rate. Micro-fibrils are seen to stick out form the meso-fibrils in different direction which reflects the high speed of failure. Figure 3.9b shows the splitting of the fiber end both in longitudinal and cross-sectional direction. Evidence of microbuckling is also present at the end of these meso-fibrils. Nano-fibrils are visible in Figure 3.9c. All of these nano-fibrils got straitened and became parallel to the axis of meso-fibrils after the failure. Debonding of these nano-fibrils is also evident in the image (arrow).

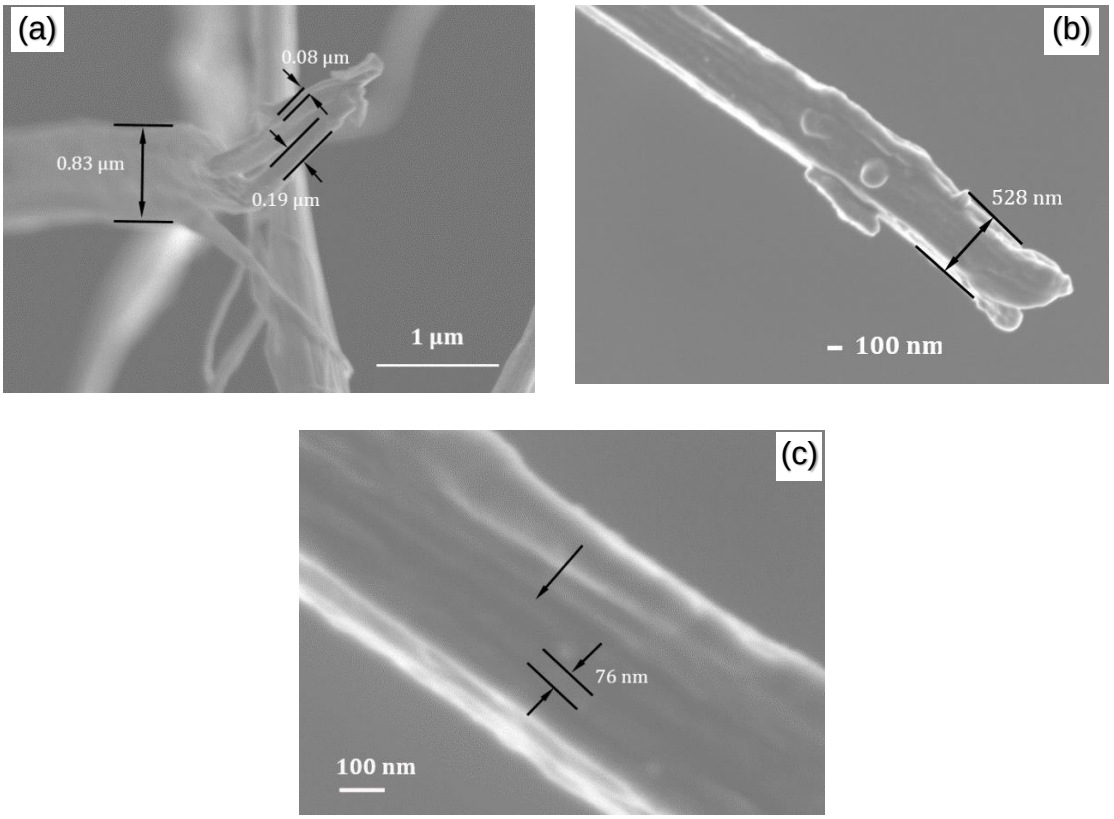

Figure 3.9: Fractured surfaces of a meso-fibril failed at 0.75 mm/min displacement rate is shown. (a) nano-fibrils pull out from a meso-fibril can be seen, (b) side view of a meso-fibril is shown, traces of matrix element is seen to adhere on the fibril surface, (c) magnification of the same meso-fibril is shown, individual nanofibril can be seen and they are aligned with the meso-fibril axis.

Figure 3.10a shows the fracture surface of a single flax fiber pulled at 1.6 mm/min displacement rate which is pretty high for biological specimens. The two circles indicate the potential site of crack initiation and the arrow indicates the direction of crack propagation. At the beginning, the velocity of the crack was slow and as a consequence, a relatively smoother surface was created in region A. As the crack continues to propagate, the velocity becomes higher and higher leaving the surface rougher and rougher creating many ridges and rivers in region B. A magnified image is shown in Figure 3.10b. In region C a crack is visible.

A magnified view of region C is shown in Figure 3.10c. Crack bridging phenomena usually arises in polymer matrix composites where the fiber and the matrix are both brittle [42, 43]. This crack bridging reduces the stress intensity factor ahead of the crack tip and thus increases the magnitude of applied stress for unstable crack propagation. Similar crack bridging phenomena is observed in the failure surface of flax fibers which also suggests the brittle nature of the nano-fibrils and the hemicellulose matrix.In the image, crack bridging by the nano-fibrils can be observed and the nano-fibrils have been pulled out of the hemicellulose matrix. The nano-fibrils seem to bifurcate near the meso-fibrils. However, the meso-fibrils are not very clean and significant amount of matrix material is seen to adhere to the meso-fibril surface. This crack bridging phenomena indicates a poor fiber matrix bond strength of flax fiber. However, this crack bridging by nanofibrils acts as an energy absorbing mechanism and helps to prevent faster crack propagation in the fiber.

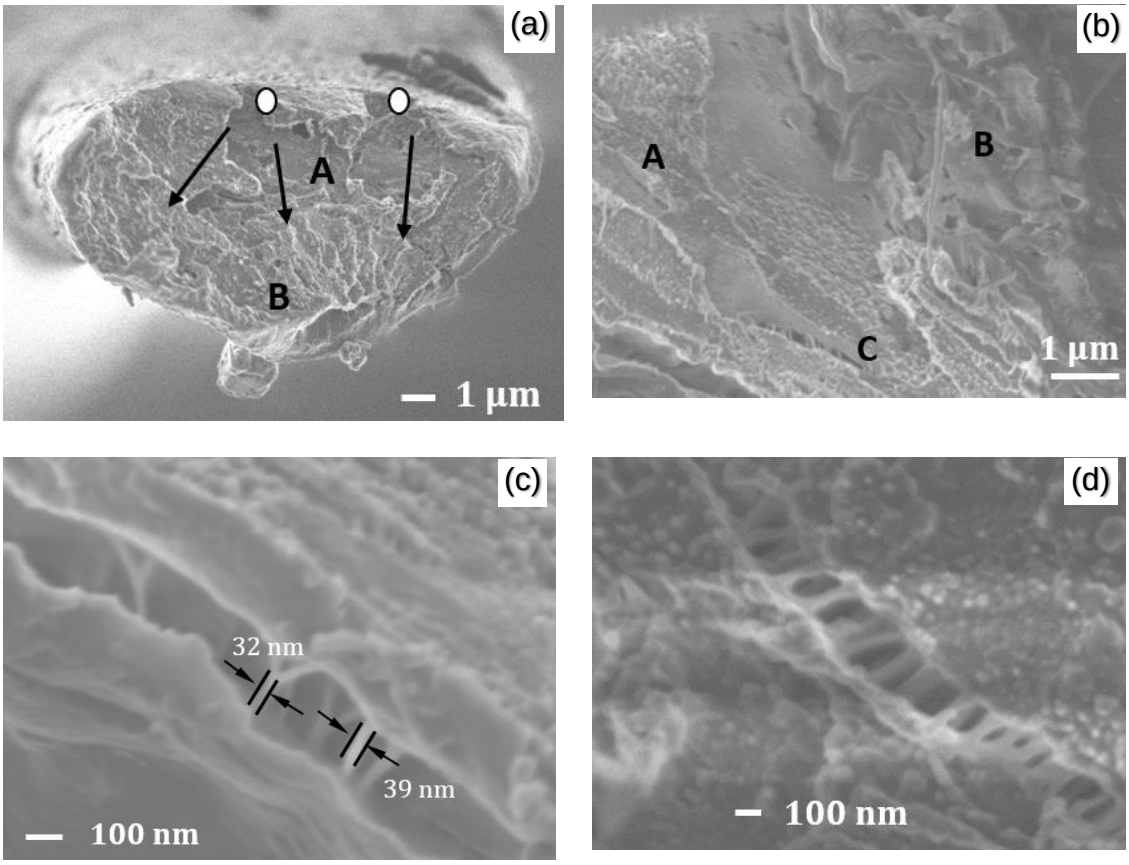

Figure 3.10: Cross sectional view of the fractured surface of an elementary fiber failed at 1.6mm/min displacement rate is shown, (a) the white circle represents the potential site for crack initiation and arrow represents the direction of crack propagation, (b) magnified view of the same surface is shown, three distinct regions are visible, region A represents the region of low speed crack propagation, region B represents the region of high speed crack propagation, region C shows a crack opening, (c) magnified view of region C is shown, bifurcation of nanofibrils can be observed, (d) crack bridging by nano-fibrils are observed, nanofibrils are at an angle with the crack wake confirming the presence of shear deformation.

From Figure 3.10d it is clear that the pulled out nano-fibrils are not perpendicular to the crack wake surface, but rather they are slightly bent. This indicates that the crack bridging stress is a combination of the stress arising from debonding of nano-fibrils as well as the stress arising from the bending and shear of these nano-fibrils. It is assumed that the failure mechanism for polymer matrix composites is also applicable for the failure of flax fibers. As a result, with the increase in the angle of inclination of these nano-fibrils, the bridging stress would be reduced and

the nanofibrils would no longer be able to resist the faster propagation of crack. However, in flax fiber the angle of inclination of these nano-fibrils is high enough to achieve a higher bridging stress, thus resisting faster crack propagation and imparting toughness and strength during their fracture.

The work of fracture of flax fiber was calculated to be $2.94(10^7)\ J/m^2$ from Figure 3.4a using the formula provided by Giorgio Jeronimidis [44] which is two order of magnitude higher than the cellulosic single cell of wood $(10^5)\ J/m^2$ [45]. This high value of work of fracture of the bundle of single cells of flax fiber is explained by the above fracture surface analysis and can be summarized as follows:

The spiral angle of flax fiber contributes to the energy absorbing mechanism by untwining the angle during tensile testing. A fiber with a higher spiral angle would be tougher as they would be able to take advantage of the buckling mode of failure of mesofibrils and nanofibrils but would have a lower stiffness. On the other hand, if the meso-fibrils are perfectly aligned with the fiber axis, the stiffness of the fiber would increase, however, the toughness would be decreased as there would be little bending and shear mode of failure.

The hierarchical fiber pull out mechanism contributes to the high work of fracture of flax fibers. That is, initially, after the breakage of the primary wall, meso-fibrils are pulled out of the matrix, then nano-fibrils are pulled out of the mesofibrils. These nano-fibrils, with a diameter of 50-70 nanometer, might be made of smaller fibrils. These smaller fibrils pull out might also occur which would be subjected to further investigation. It was suggested by G. Jeronimidis and Julian Vincent[46] that if one calculates the toughness of a fibrous composite using the same volume fraction as an wood fiber, the toughness would be ten times less than actually observed from a wood fiber. Because for fibrous composite, the only toughening mechanism is the

presence of frictional force during fiber pull-out. However, during hierarchical fiber pull-out of flax fiber, frictional force is coming from different layers.

Micro-buckling and crack bridging phenomena also contributes to the high work of fracture of flax fiber. Though the contribution of crack bridging phenomena was not accounted for the high work of fracture of flax fiber in previous study, Figure 3.10d strongly corroborates their presence during fracture. The nanofibrils between the crack wake participates in the smooth transfer of stress. In addition, for wood cell, it was found that with the decrease in temperature, the toughness increases, which is opposite to most materials [46]. In lower temperature, the fibers would be less viscous which would result in improved transfer of stress to the crack tip and would contribute to the high work of fracture.

In summary, at the beginning a literature review is performed regarding the failure of flax fiber. The successive loading and unloading cycle of flax fiber shows the gradual increase in Young's modulus which represents the visco-elastic nature of flax fiber. The dynamic failure of flax fiber is investigated with the help of SEM movie while the fiber was being pulled in tension. Three distinct phases of fiber failure was identified: 1. initial rotation of the fiber, 2. segregation of single fibers from the bundle, 3. ultimate failure; and their implications with respect to the failure of composite materials are explained. The fractographic analysis of the failure surface of single fibers and meso-fibrils is performed in detail. It is proposed that the spiral angle, hierarchical fiber pull out, microbuckling and crack bridging- all contribute to the high work of fracture of flax fiber. The fractographic approach of the failure of flax fiber reveals some of the intricate details of the structure of flax fiber such as the arrangement of mesofibrils and nanofibrils and also supports the findings of Thuault et. al [47] about the presence of more than four layers in flax fibers. This study would be helpful in understanding the fracture mechanism

of plant fibers in general, and flax fiber in particular. By dispersing the single cells of flax fiber on thin films or polymeric coatings in appropriate way, it might be possible to get tougher films or coatings. This study may also provide some insight for the manufacture of bio-mimetic fibers. By winding nano fibers in a helical fashion around a hollow polymeric cylinder, and combining several of these cylinders by joining them with adhesives into a single cylinder, it might be possible to get stiffer yet tougher fibers. The resulting composites would have higher toughness and strength in comparison to conventional composite materials.

3.6. References

1. Charlet, K., et al., *Mechanical properties of flax fibers and of the derived unidirectional composites.* Journal of Composite Materials, 2010. **44**(24): p. 2887-2896.
2. Bos, H., M.J. Van Den Oever, and O.C. Peters, *Tensile and compressive properties of flax fibres for natural fibre reinforced composites.* Journal of Materials Science, 2002. **37**(8): p. 1683-1692.
3. Baley, C., et al., *Influence of drying on the mechanical behaviour of flax fibres and their unidirectional composites.* Composites Part A: Applied Science and Manufacturing, 2012. **43**(8): p. 1226-1233.
4. Shah, D.U., R.K. Nag, and M.J. Clifford, *Why do we observe significant differences between measured and 'back-calculated'properties of natural fibres?* Cellulose, 2016. **23**(3): p. 1481-1490.
5. Andersons, J., et al., *Strength distribution of elementary flax fibres.* Composites science and technology, 2005. **65**(3): p. 693-702.

6. Andersons, J., E. Poriķe, and E. Spārniņš, *The effect of mechanical defects on the strength distribution of elementary flax fibres.* Composites Science and Technology, 2009. **69**(13): p. 2152-2157.

7. McLaughlin, E.C. and R.A. Tait, *Fracture mechanism of plant fibres.* Journal of Materials Science, 1980. **15**(1): p. 89-95.

8. Nilsson, T. and P.J. Gustafsson, *Influence of dislocations and plasticity on the tensile behaviour of flax and hemp fibres.* Composites Part A: Applied Science and Manufacturing, 2007. **38**(7): p. 1722-1728.

9. Thygesen, L.G. and M.R. Asgharipour, *The effects of growth and storage conditions on dislocations in hemp fibres.* Journal of Materials Science, 2008. **43**(10): p. 3670-3673.

10. Davies, G.C. and D.M. Bruce, *Effect of environmental relative humidity and damage on the tensile properties of flax and nettle fibers.* Textile Research Journal, 1998. **68**(9): p. 623-629.

11. Bos, H. and A. Donald, *In situ ESEM study of the deformation of elementary flax fibres.* Journal of materials science, 1999. **34**(13): p. 3029-3034.

12. Thomason, J., et al., *Fibre cross-section determination and variability in sisal and flax and its effects on fibre performance characterisation.* Composites Science and Technology, 2011. **71**(7): p. 1008-1015.

13. Burgert, I. and J.W. Dunlop, *Micromechanics of cell walls*, in *Mechanical integration of plant cells and plants*. 2011, Springer. p. 27-52.

14. Cosgrove, D.J., *Assembly and enlargement of the primary cell wall in plants.* Annual review of cell and developmental biology, 1997. **13**(1): p. 171-201.

15. Hughes, M., J. Carpenter, and C. Hill, *Deformation and fracture behaviour of flax fibre reinforced thermosetting polymer matrix composites.* Journal of Materials Science, 2007. **42**(7): p. 2499-2511.

16. McCann, M.C. and K. Roberts, *Changes in cell wall architecture during cell elongation.* Journal of Experimental Botany, 1994. **45**(Special Issue): p. 1683-1691.

17. Lloyd, C.W., *The cytoskeletal basis of plant growth and form*. 1991: London, etc.: Academic Press.

18. Gibson, L.J., *The hierarchical structure and mechanics of plant materials.* Journal of the Royal Society Interface, 2012: p. rsif20120341.

19. Van de Velde, K. and P. Kiekens, *Thermoplastic polymers: overview of several properties and their consequences in flax fibre reinforced composites.* Polymer testing, 2001. **20**(8): p. 885-893.

20. Joffe, R., J. Andersons, and L. Wallström, *Strength and adhesion characteristics of elementary flax fibres with different surface treatments.* Composites Part A: Applied Science and Manufacturing, 2003. **34**(7): p. 603-612.

21. Ivanov, Y., V. Cheshkov, and M. Natova, *Polymer Composite Materials—Interface Phenomena & Processes*. Vol. 90. 2001: Springer Science & Business Media.

22. Martin, N., et al., *Influence of the degree of retting of flax fibers on the tensile properties of single fibers and short fiber/polypropylene composites.* Industrial Crops and Products, 2013. **49**: p. 755-767.

23. Hughes, M., *Defects in natural fibres: their origin, characteristics and implications for natural fibre-reinforced composites.* Journal of materials science, 2012. **47**(2): p. 599-609.

24. Hornsby, P., E. Hinrichsen, and K. Tarverdi, *Preparation and properties of polypropylene composites reinforced with wheat and flax straw fibres: part I fibre characterization.* Journal of materials science, 1997. **32**(2): p. 443-449.

25. Baley, C., *Influence of kink bands on the tensile strength of flax fibers.* Journal of materials science, 2004. **39**(1): p. 331-334.

26. Thygesen, L.G., *The effects of growth conditions and of processing into yarn on dislocations in hemp fibres.* Journal of materials science, 2011. **46**(7): p. 2135-2139.

27. Hughes, M., et al., *An investigation into the effects of micro-compressive defects on interphase behaviour in hemp-epoxy composites using half-fringe photoelasticity.* Composite Interfaces, 2000. **7**(1): p. 13-29.

28. Clements, L.L., *Fractography of unidirectional graphite-epoxy as a function of moisture, temperature and specimen quality.* Journal of materials science, 1986. **21**(6): p. 1853-1862.

29. Slámečka, K., et al., *A Fractographic Study of Bending/Torsion Fatigue Failure in Metallic Materials with Protective Surface Layers.* Advances in Materials Science and Engineering, 2016. **2016**.

30. McCoy, R., *SEM fractography and failure analysis of nonmetallic materials.* Journal of failure analysis and prevention, 2004. **4**(6): p. 58-64.

31. Quinn, G.D. and G.D. Quinn, *Fractography of ceramics and glasses*. 2007: National Institute of Standards and Technology Washington, DC.

32. Greenhalgh, E., *Failure analysis and fractography of polymer composites*. 2009: Elsevier.

33. Clements, L.L., *Reply to comment on "Fractography of unidirectional graphite-epoxy as a function of moisture, temperature and specimen quality".* Journal of Materials Science Letters, 1989. **8**(5): p. 618-618.

34. Purslow, D., *Comment on "Fractography of unidirectional graphite-epoxy as a function of moisture, temperature and specimen quality".* Journal of materials science letters, 1989. **8**(5): p. 617-617.

35. Fratzl, P., I. Burgert, and H.S. Gupta, *On the role of interface polymers for the mechanics of natural polymeric composites.* Physical Chemistry Chemical Physics, 2004. **6**(24): p. 5575-5579.

36. Baskin, T.I., *Anisotropic expansion of the plant cell wall.* Annu. Rev. Cell Dev. Biol., 2005. **21**: p. 203-222.

37. Ebringerová, A. *Structural diversity and application potential of hemicelluloses*. in *Macromolecular Symposia*. 2005. Wiley Online Library.

38. Stevanic, J.S. and L. Salmén, *Orientation of the wood polymers in the cell wall of spruce wood fibres.* Holzforschung, 2009. **63**(5): p. 497-503.

39. Simonović, J., et al., *Anisotropy of cell wall polymers in branches of hardwood and softwood: a polarized FTIR study.* Cellulose, 2011. **18**(6): p. 1433-1440.

40. Youssefian, S., J. Jakes, and N. Rahbar, *Variation of Nanostructures, Molecular Interactions, and Anisotropic Elastic Moduli of Lignocellulosic Cell Walls with Moisture.* Scientific Reports, 2017. **7**.

41. Bidhendi, A.J. and A. Geitmann, *Relating the mechanics of the primary plant cell wall to morphogenesis.* Journal of experimental botany, 2015. **67**(2): p. 449-461.

42. Leung, C.K. and V.C. Li, *Effect of fiber inclination on crack bridging stress in brittle fiber reinforced brittle matrix composites.* Journal of the Mechanics and Physics of Solids, 1992. **40**(6): p. 1333-1362.

43. Cartié, D.D., B. Cox, and N. Fleck, *Mechanisms of crack bridging by composite and metallic rods.* Composites Part A: Applied Science and Manufacturing, 2004. **35**(11): p. 1325-1336.

44. Jeronimides, G., *The fracture of wood in relation to its structure.* Leiden botanical series, 1976. **3**(1): p. 253-265.

45. Gordon, J. and G. Jeronimidis, *Work of fracture of natural cellulose.* Nature, 1974. **252**(5479): p. 116-116.

46. Vincent, J.F., *Structural biomaterials*. 2012: Princeton University Press.

47. Thuault, A., et al., *Investigation of the internal structure of flax fibre cell walls by transmission electron microscopy.* Cellulose, 2015. **22**(6): p. 3521-3530.

CHAPTER 4. MEASUREMENT OF SURFACE ENERGY OF FLAX FIBERS

Fiber surface free energy is an important parameter for predicting the interfacial bond strength of fiber-matrix adhesion of composite materials. For manufacturing bio-composite materials, however, the measurement of the surface energy of individual single fibers ($10 - 15\ \mu m$) by traditional method such as contact angle measurement of liquid, is complicated due to their higher surface roughness, formation of chemical bonds, wicking characteristics etc. This paper demonstrate a novel method for determining the dispersive component of surface free energy (γ_d) of single flax fiber by directly measuring the adhesion force between the probe tip and the fiber surface. Johnson-Kendal-Roberts (JKR) theory was employed to correlate the adhesion force and the tip radius, which was characterized by Field Emission Scanning Electron microscopy. Finally, the value of γ_d was determined to be $32.9 \pm 2.1\ \mathrm{mJ/m^2}$ and its significance with respect to other methods was analyzed.

4.1. Literature review

To achieve better mechanical performance of composite materials, higher interfacial bonding is the key, which can be achieved by increasing physical adhesion between fiber and matrix, and/or by forming a strong chemical bonding and by higher mechanical interlocking. Though the higher roughness of flax fiber provide enhanced mechanical interlocking with the polymeric matrix, the hydrophilicity of the fiber surface may contribute to the weaker interfacial bonding between fiber and matrix[1-3].

Fiber surface free energy (γ) is an important parameter for quantifying the interfacial bond strength between the fiber and the matrix. One approach for measuring the surface free

energy of a solid flat surface is to measure the contact angle formed by a liquid droplets on the solid surface. The contact angle is a manifestation of the degree of overcoming the cohesive energy of the liquid by the solid-liquid interfacial energy. If the solid-liquid interfacial energy is high enough, the contact angle formed by the liquid on a solid surface would be low and vice-versa [4, 5]. However, the contact angle approach for measuring the surface energy rests on a few assumptions. 1. The solid surface is not chemically affected by the liquid, 2. The contact angles to be measured are true equilibrium angles, 3. The difference between the interfacial surface energy at vacuum(γ_{sl}^{0}) and at saturation(γ_{sl}), known as the spreading pressure (π_e), is negligible. For most low energy surfaces, on which adsorption is relatively small, (π_e), is negligible. 4. Errors due to orientational entropy effects are not important, and 5. The solid is free from defects, dislocations, edges, and corners [6]. Schellbach et. al [7] proposed a new method for measuring the contact angle of natural fibers. They placed two similar diameter fibers in parallel with a spacing of 0.2-1 mm so that a water droplet placed on them can form a bridge or column. The meniscus of the liquid bridge was imaged and analyzed for measuring the contact angle. It was claimed that this method provides better estimates of contact angle than widely used tensiometry[8] and capable of measuring both advancing and receding contact angle.

Another method for measuring the surface energy is the inverse gas chromatography (IGC)[9]. Unlike gas chromatography (GC) [10]where the sample is vaporized and acts as a mobile phase, the sample in IGC works as a stationary phase and placed inside a column usually in the powdered form. A probe (usually gas or vapor) with known properties is injected through the column and the retention time of the probe is measured. This retention time is related to the bulk or thermodynamic properties of the material. If the retention time is longer, the sample material has a higher surface energy and vice versa. However, for IGC, the fibers has to be

grounded in powder form and tend to provide high end values of the surface energy of the materials[11, 12].

Measuring the zeta potential of natural fibers using streaming potential method is a powerful way to measure the surface properties of natural fibers. In this method, an electrolyte solution is pumped through the fiber bundle (capillary system) which generates a current or potential due to the motion of ion resulting from the shear off of the electrochemical double layer [13]. This potential is measured as a function of time and P^H using two electrodes. A zeta potential measuring device essentially consists of a measuring cell with electrodes, a device for producing and measuring hydrostatic pressure, a device for measuring streaming potential and a conductivity meter. The details of the measurement procedure can be found elsewhere in the literature [14, 15]. However, the measurement of zeta potential provides reliable information about interaction energy only when the results are corroborated by other physico-chemical methods and the factors influencing the double layers are sufficiently known. Often, the surface conductivity is neglected which introduces error in zeta potential measurement, particularly when the fibers are hydrophilic[16]. Moreover, the measurement may be affected by the degree of fiber swelling. Bismark et. al [17] studied the effect of surface modifications such as dewaxing, alkali treatment, and methyl methacrylate grafting on sisal and coir fibers through zeta potential measurement technique. The rate of decay of zeta potential depends on the degree of hydrophilicity. With the modification of fiber surfaces (such as dewaxing), the fibers become more hydrophilic, and as a result, zeta potential decreases more rapidly.

Bellmann et. al [18] performed streaming potential experiments by an Electro Kinetic Analyzer (AKA) which was specially developed for the measurement of fibrous samples. They studied chemical constitution (polarity of fiber surface) and swelling behavior of the fiber in

water. As the water gets adsorbed on the fiber, the zeta potential starts to decrease. The adsorption of water also depend on the crystallinity and cellulose content of the fiber. The higher is the cellulose content and crystallinity, the lower is the amount of water adsorbed. A lower equilibrium value of zeta potential correspond to a higher adsorption capacity of the fiber. The acid base properties of the fiber surface can also be investigated by the electro-kinetic measurements [19, 20].

Recently, atomic force microscopy has become a powerful technique for measuring the surface energy of various polymeric and pharmaceutical materials [21, 22]. This method also proved successful for the characterization of cellulosic fibers [23, 24]. Pietak et al. investigated the surface properties of hemp fibers through atomic force microscopy. They treated the hemp fibers in four different ways: steam, alkaline, combination of steam-alkaline, and enzymatic treatments. Next they determined the variation of surface free energies among these four types of fibers. They also measured the contact angle formed by different liquids with these fibers, and predicted the relationship among the water contact angle, adhesion force, and surface free energy.

4.2. Theoretical background

Wetting refers to the displacement of air from a liquid or solid surface by water or an aqueous solution. Wetting process involves surfaces and interfaces and the degree of wetting is determined by the change of free energy of these surfaces and interfaces.There are mainly three types of wetting:

1. Spreading wetting
2. Adhesional wetting
3. Immersional wetting

4.2.1. Spreading wetting

In spreading wetting, a liquid in contact with a substrate spreads over the substrate and displaces another fluid, such as air, from the surface. For the spreading to occur spontaneously, the surface free energy of the system must decrease during the spreading process. When the area of an interface increases, the surface free energy at that interface increases and vice versa.
In the Figure 4.1, the liquid spreads from point C to point B, covering an area A. In this case, three distinct phenomena occurs:

a) There is a decrease in substrate-air interface. So, the decrease in surface energy associated with this area reduction is $. \gamma_{SA}$, where $\gamma_{SA} =$ interfacial free energy per unit area of the substrate in equilibrium with the liquid-saturated air above it.
b) There is an increase in liquid-substrate interfacial area and associated increase in the surface free energy of the system is $A . \gamma_{SL}$ ($\gamma_{SL} =$ interfacial free energy per unit area at the liquid substrate interface)
c) There is an increase in liquid-air interfacial area. So, the associated increase in the surface free energy of the system is $A . \gamma_{LA}$ Where $\gamma_{LA} =$ surface tension of the liquid

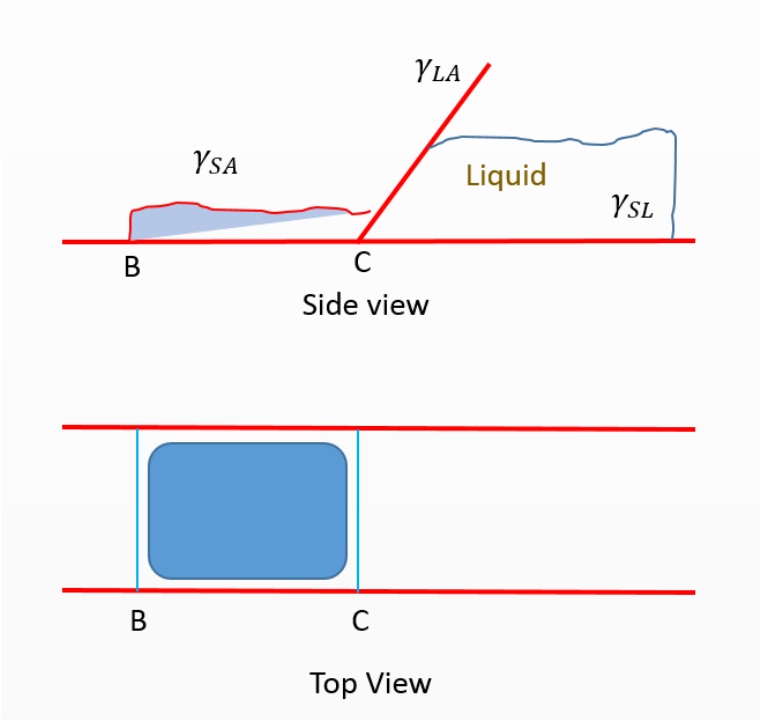

Figure 4.1: Schematic diagram of spreading wetting

As a result, the total change in surface energy of the system $S = \gamma_{SA} - (\gamma_{SL} + \gamma_{LA})$. If the quantity S is positive, the total energy of the system is decreased and the process can occur spontaneously. The quantity S is also called the spreading coefficient of the system. It can be observed that the spreading coefficient involves only the surface tensions of the solid and liquid being involved and the interfacial tension between them. As a result, if it is possible to determine the interfacial tension between the solid and liquid from their respective surface tension, it is possible to calculate the spreading co-efficient without additional experimental data, and predict whether the spreading will occur spontaneously. According to Good and Girifalco [6, 25],

$$\gamma_{SL} = \gamma_{LA} + \gamma_{SA} - 2\varphi\sqrt{\gamma_{SA}\gamma_{LA}} \tag{4.1}$$

where φ is an empirical factor measuring the degree of interaction between the solid and liquid involved in the process.

$$S = \gamma_{SA} - (\gamma_{LA} + \gamma_{SA} - 2\varphi\sqrt{\gamma_{SA}\gamma_{LA}} + \gamma_{LA})$$

$$S = 2(\varphi\sqrt{\gamma_{SA}\gamma_{LA}} - \gamma_{LA})$$

$$S = 2\gamma_{LA}\left(\varphi\sqrt{\frac{\gamma_{SA}}{\gamma_{LA}}} - 1\right) \tag{4.2}$$

In systems, where there is no strong interaction between solid and liquid, φ is less than 1. Thus, γ_{SA} must be greater than γ_{LA} for spreading coefficient S to be positive and spontaneous spreading to occur. Here comes the concept of critical surface tension. Zisman and coworkers [26, 27] have shown that, at least for low energy substrates, the surface energy of the wetting liquid must not exceed a certain critical value in order to wet the substrate.

Usually metals are considered as high surface free energy solids ranging from several hundred to several thousands $\mathrm{mJ/m^2(ergs/cm^2)}$. Low melting solids, such as organic polymers and covalent compounds have surface free energies ranging from 25-100 $\mathrm{mJ/m^2(ergs/cm^2)}$. With the exception of liquid metals, the surface energies of liquid are less than 75 $\mathrm{mJ/m^2(ergs/cm^2)}$. As a result, liquids readily spread on metals but may not spread on low melting solids such as polymers.

The contact angle θ that the liquid makes when it is at equilibrium with the other phases in contact with it, is related to the interfacial free energies per unit area of those phases. It is possible to write, from Figure 4.2,

$$\Delta G_w = -\gamma_{SA}\Delta A + \gamma_{SL}\Delta A + \gamma_{LA}\Delta A\cos\theta$$

As $\Delta A \to 0$, $\Delta G_w \to 0$

$$-\gamma_{SA}da + \gamma_{SL}da + \gamma_{LA}da\cos\theta = 0$$

Therefore,

$$\gamma_{LA}\cos\theta = \gamma_{SA} - \gamma_{SL} \tag{4.3}$$

Which is known as the Young's equation.

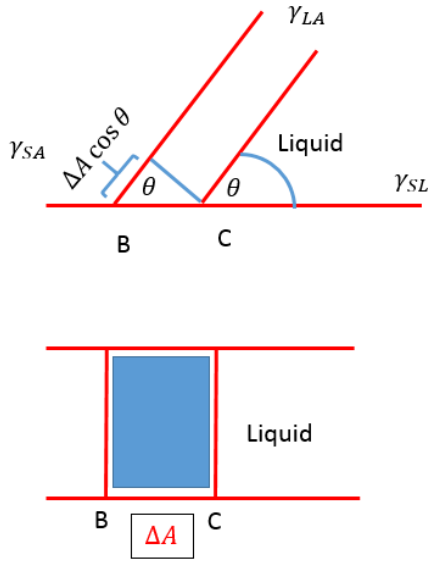

Figure 4.2: Schematic diagram of a contact angle and associated energy

4.2.2 Adhesional wetting

Unlike spreading wetting, a drop of liquid not in contact with the substrate is placed carefully on the substrate and the drop adheres to it. This phenomena is shown in Figure 4.3.

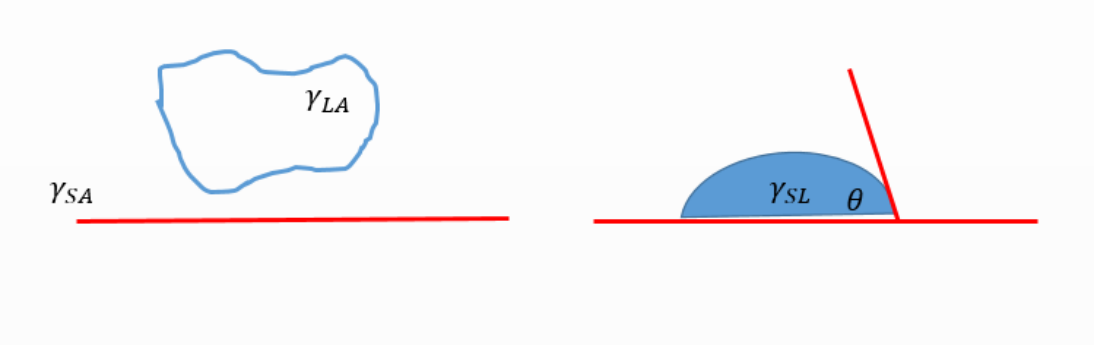

Figure 4.3: Adhesional wetting and contact angle

The change in surface free energy is,

$$W_a = \gamma_{SA} + \gamma_{LA} - \gamma_{SL} \tag{4.4}$$

This quantity is known as the work of adhesion. This equation is from Dupre. By combining Young's equation with Dupre equation, we get

$$W_a = \gamma_{LA} + \gamma_{LA}\cos\theta = \gamma_{LA}(1 + \cos\theta) \tag{4.5}$$

The work of self-adhesion of a liquid is known as the work of cohesion,

$$W_c = 2\gamma_{LA} \tag{4.6}$$

It is the work required to produce two unit areas of interface from an original unbroken column of the liquid. The difference between the work of adhesion and work of cohesion equals the spreading co-efficient.

$$W_a - W_c = \gamma_{SA} + \gamma_{LA} - \gamma_{SL} - 2\gamma_{LA}$$

$$= \gamma_{SA} - (\gamma_{SL} + \gamma_{LA})$$

$$W_a - W_c = S \tag{4.7}$$

If $W_a > W_c,\ S > 0, \theta = 0$, The liquid spreads spontaneously over the substrate to form a thin film. If $W_a < W_c,\ S < 0, \theta > 0$, The liquid does not spread over the substrate but forms droplets or lenses with a finite contact angle.

4.2.3 Immersional wetting

In immersional wetting, a substrate not previously in contact with a liquid, is immersed completely by the liquid. The surface energy change per unit area is,

$$S = \gamma_{SA} - \gamma_{SL} \tag{4.8}$$

4.2.4. Fowkes theory

Fowkes [28] proposed that surface energy term γ can be separated into different components.

$$\gamma = \gamma^d + \gamma^p + \gamma^{ind} + \gamma^H \tag{4.9}$$

Where, d, P, ind, H refers to the London dispersion, Keesom dipole-dipole, Debye induction, and hydrogen bond forces, respectively. Eventually, Fowkes et. al [29] settled on two dominant terms:

$$\gamma = \gamma^d + \gamma^{AB} \tag{4.10}$$

where,

$$\gamma^{AB} = \gamma^p + \gamma^{ind} + \gamma^H + \cdots \tag{4.11}$$

AB refers to acid base interaction. γ^p is very small if acid base interactions are present. On the other hand, Lifshitz proposed a surface energy component that takes into account all the interactions from oscillating temporary dipoles (γ^d), permanent dipoles (γ^p) or induced dipoles (γ^{ind}). According to this theory,

$$\gamma = \gamma^{LW} + \gamma^{AB} \tag{4.12}$$

where,

$$\gamma^{LW} = \gamma^p + \gamma^{ind} + \gamma^d \tag{4.13}$$

LW stands for Lifshitz- Vander Waals

4.3. Materials and methods

4.3.1. Materials

Flax fiber used in this study were Prairie Grande Flax, a medium early maturing oilseed flax (Linum usitatissimum L.), grown in Melita, Manitoba, Canada. The seeds were sown on May 22, 2015 and harvested on August 13, 2015. At harvest, the average height of the plants were 60 cm, and observed to be dry or fully mature.

Enzyme retting was performed for extracting the fiber from the cuticularized epidermis and the woody core cells. Bioprep 3000L was used as the enzyme which is an alkaline pectate lyase. Flax stems were fully immersed in a 5% Bioprep3000L plus Sodium Tetraborate Decahydrate (buffer) for 30 minutes. Next the stems were taken out and allowed to dry in oven at 55° centigrade for two hours.

After that the stems were again immersed in Ethylenediamine tetraacetic acid (EDTA) plus buffer for sometime. Then the stems were taken out and dried in the oven for 22 hours at 55 degree centigrade. The stems were then rinsed with water for 5 minutes and dried overnight in the fumehood.

The single fibers were carefully hand separated from the bundle with the help of a magnifying glass and a sharp twitzers. Next, they were carefully laid down on a glass slide and both sides were fixed with scotch tape. Care was taken so that the fiber make intimate contact with the glass slide. As a result, during the measurement of the force distance curve, the fibers were rigidly supported by the glass slide.

4.3.2. Adhesion force measurement

Adhesion force was measured using an AFM (Veeco 3100) equipped with a nanoscope. Measurements were performed at 23° celcius and 40% relative humidity. The AFM based

adhesion measurement was performed under the non-contact mode. The entire test bench was pneumatically cushioned to reduce the effect of vibration in the measurement. The AFM cantilever used in the experiment was from μmasch with the model NSC15 and made from silicon. The cantilever had a resonance frequency of 320 KHz and a quality factor of 657. To convert the AFM cantilever deflection into its corresponding force component, the spring constant of the cantilever is required by the formula $F=K.\Delta x$. Several method is available in the literature for calculating the spring constant such as the thermal fluctuation measurement method, the kinetostatic method, the heterodyne interferometry method and the extended added micro-drop method [30, 31]. The Sader method [32] was used here for determining the spring constant and calculated to be 37.5 N/m. The cantilever had a length and width of 125 μm and 30 μm, respectively. The tip of the cantilever was characterized by Field Emission Scanning Electron Microscopy (FESEM). Assuming a circular profile of the probe tip, a radius of 25 nm was determined. The indentation was performed at 10 different locations of the single flax fiber. The neighboring indentation distances were at least 500 nm apart to avoid the effect of adjacent deformations on flax fiber. The corresponding reaction force versus z-piezo displacement curve (F-DISP) curve was recorded. The z-piezo displacement curve after the tip-sample contact was a combination of the sample deflection and the cantilever deflection. Because flax fibers are soft materials. To separate the two deformations, indentations were also performed on glass slide, which resulted in only the deformations of the cantilever. Figure 4.4 schematically shows the adhesion measurement by AFM.

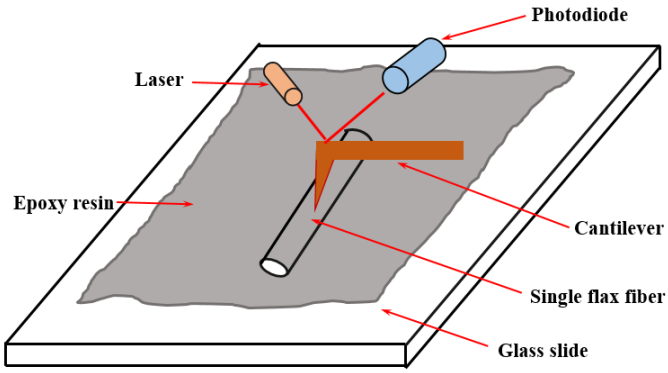

Figure 4.4: Schematic diagram of the experimental setup of the adhesion measurement by AFM

4.3.3 Results and discussion

Prior to performing AFM adhesion force measurement, an SEM micrographs was taken to observe the surface roughness of the sample specimen. Figure 4.5 reveals relatively smoother surface except a few localized inclusions on the surface. In ideal case, a perfectly smooth surface would be preferred for measuring the surface energy. However, flax fiber, being a natural fiber, offers limited opportunity for the manual surface finish and we would like to measure the surface energy of a single flax fiber in its natural state. During the measurement of adhesion force, it is possible to avoid the localized inclusion on the fiber surface and select a smoother region with the help of a polarized light microscope attached to the AFM. The surface roughness of the single flax fiber was determined to be 25 nm within a $1.5 \times 1.5\ \mu m$ area which is pretty high compared to the surface roughness of synthetic fibers.This value represents the root mean square value of the surface roughness. The surface topography of the single fiber was also analyzed by taking AFM images of the single fiber.

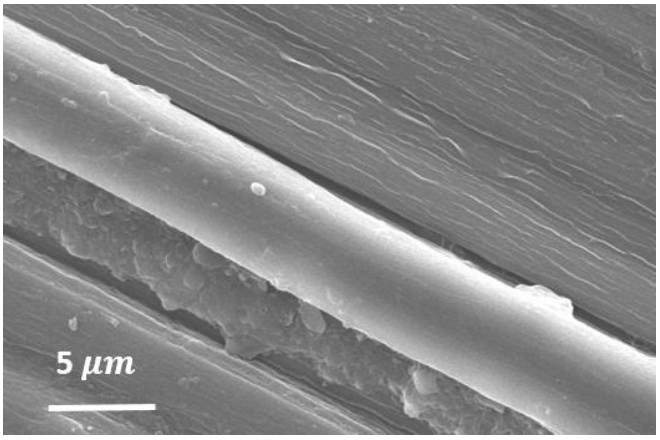

Figure 4.5: SEM image of a single fiber

Though the SEM micrograph of Figure 4.5 does not reveal the smaller component of a single fiber, the AFM image of Figure 4.6 reveals some of the intricate details of a single flax fiber. Though the mesofibrils in the S2 layer is covered by Primary layer and S1 layer, by using the tapping mode feature of AFM, it is possible to probe those meso-fibrils. In Figure 4.6 the individual meso-fibrils are visible. The dimensions of these meso-fibrils may very from 0.5-1.5 μm .There exists tiny grooves in between the regions from one meso-fibrils to another. These grooves may contribute to the higher surface roughness of a single flax fibers.

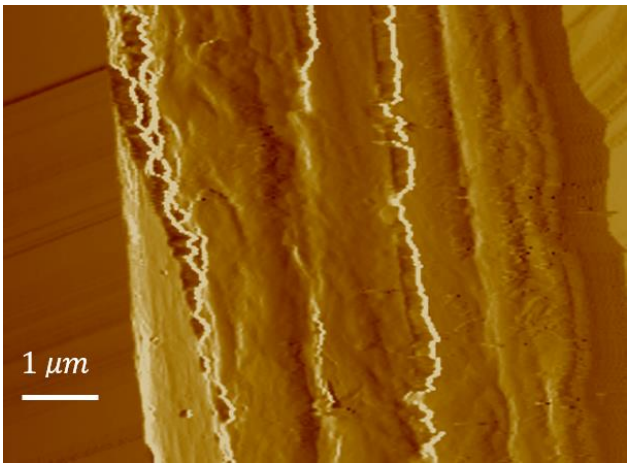

Figure 4.6: Localized surface topography

Figure 4.7 reveals the meso-fibril angle of a single flax fiber to be approximately 11°. Instead of a small angle X-ray scattering approach [33], this angle was determined by atomic force microscopy. A lower meso-fibril angle is responsible for higher strength and modulus but lower strain [34].

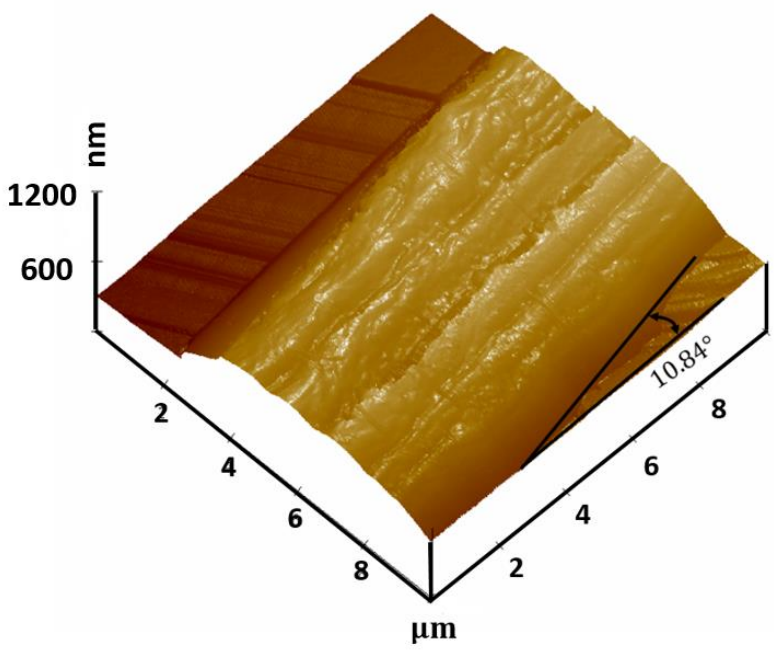

Figure 4.7: Arrangement of cellulose meso-fibrils in a single flax fiber determined by AFM.

The tip of the AFM was characterized by taking FESEM image of the AFM tip. Figure 4.8 (a) shows the side view of a used silicon AFM tip. In Figure 4.8(b), a magnified view of the tip shows that the tip diameter is 50 nm. The evidence of wear of the tip is present in the image.

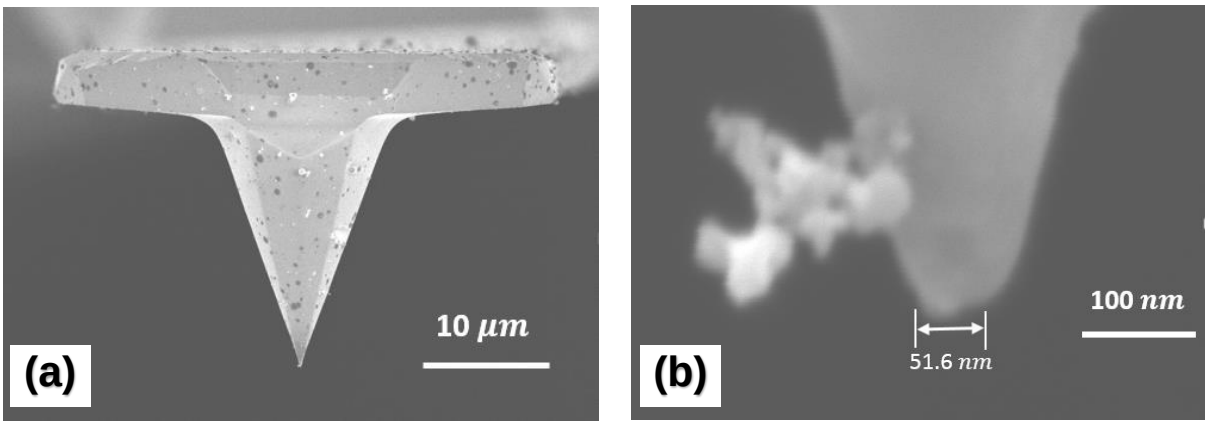

Figure 4.8: (a) FESEM image of the AFM tip, (b) magnified view of the tip shows the diameter

Figure 4.9 schematically shows the tip-surface interaction during the measurement of adhesion force. When the tip is far from the surface there is no interaction between the fiber and the tip. As the tip approaches closer and closer to the fiber surface, short range Van Der Waals force starts to operate and the tip is bent downwards to the surface. As the tip comes closer to the atomic radius of the fiber surface molecules, the repulsive force becomes activated and the tip is bent upward as shown in Figure 4.9.

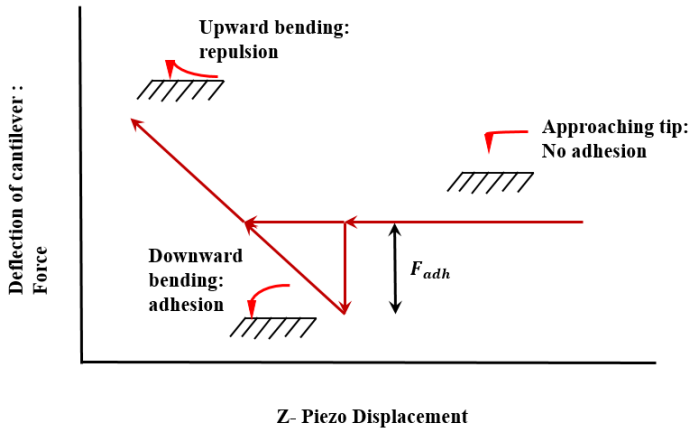

Figure 4.9: Schematic diagram of the cantilever deflection as it approaches the surface and moves away.

Figure 4.10 represents the force displacement curve of a single flax fiber. The blue curve represents the extend data or approach data and the magenta curve represents the retract data. The maximum load applied in pushing the probe tip to be in contact with the single fiber surface was approximately 180 nN. The region of the curve below the zero line represents the magnitude of pull off force. As the probe tip approaches from right to left along the curve, the distance between the probe tip and the sample surface decreases gradually. When the distance between the sample surface and the AFM tip is less than 20 nm, the short range Vander-waals force become activated and the probe tip is suddenly pulled towards the sample surface. This sudden pull can be seen as a downward or negative force in the curve. The negative sign of the force means no external force is required to pull the probe tip towards the fiber surface. The short range Vander Waals force acts as a driving force in this case. As the extend curve and the retract curve nearly overlaps to each other, it implies the AFM tip is operating within the elastic region.

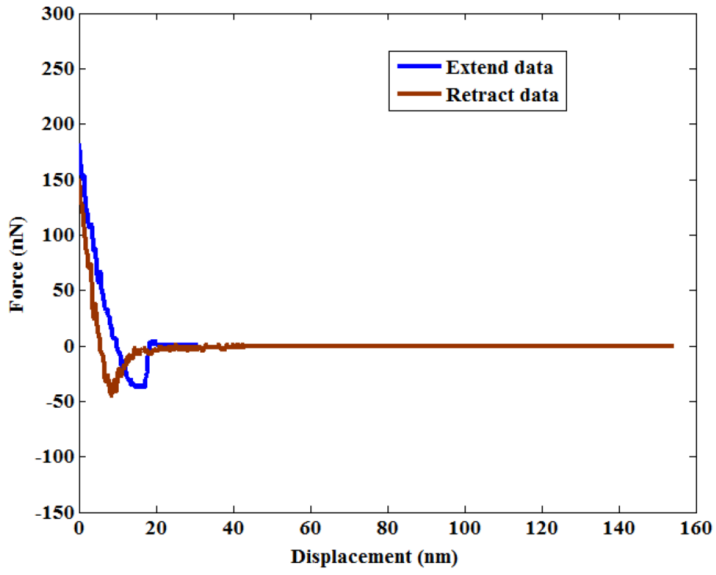

Figure 4.10: Force displacement curve of the single flax fiber showing the pull off force arising from the adhesion between the fiber surface and probe tip.

Again from the figure it can be observed that the value of the pull-off force in retract curve is slightly higher than the extend curve. Ideally, the value of the pull-off force from this two curve should be equal and it is true for linear elastic materials. However, most polymers are viscoelastic in nature and their load-deformation curve is strain-rate sensitive. Moerover, they show adhesion hysteresis that is more work is required to separate the contacting surfaces than the adhesion force required to bring them in contact. A detailed analysis of the viscoelastic nature of polymeric materials was presented in Wahl et.al [35]. They showed that the discrepancy between the experimental stiffness and the theoretical stiffness predicted by the JKR model can be accounted for by employing a model which incorporates this viscoelastic effect at the periphery of the contact zone.

For the measurement of the surface energy from the pull-off or adhesion force, equations from the contact mechanics are usually employed. There are several models which correlate the adhesion force to that of the surface free energy of the contacting materials. Among them the Johnson-Kendall-Roberts (JKR) model [36] and the Derjaguin-Muller-Toporov (DMT) model [37] are the most prominent. By performing numerical simulations of Lennard-Jones potential, Muller et. al [38, 39] showed that the JKR and DMT are two extreme limits of the adhesion force.

As a result, for the measurement of the surface free energy of a single flax fiber, it is necessary to identify which model to use. JKR model is more appropriate when the radius of the AFM tip is larger and the material being probed is more compliant. This model takes into account only the strong adhesion force under the probe tip in contact with the object. On the other hand, DMT model is appropriate when the probe tip radius is small and the material being probed is stiff. This model also takes into account the long range weak adhesion force present

between the periphery of the probe near the surface in addition to the strong adhesion force present under the probe tip in contact with the surface of the object.

Usually, two non-dimensional physical parameters are used to quantify the transition between the JKR and DMT model. One is known as the Tabor's parameter μ [40] and the another is known as the Maugis parameter λ [41, 42]. These two parameter's are related by the equation $\lambda = 1.1570\mu$ Where,

$$\mu = \left(\frac{16\, R\gamma^2}{9\, K^2 {z_0}^3}\right)^{1/3} \tag{4.14}$$

$$\lambda = 2\sigma_0 \left(\frac{R}{\pi\, K^2 \gamma}\right)^{1/3} \tag{4.15}$$

where, z_0 is the equilibrium separation of surfaces, R is the tip curvature radius, γ is the interfacial energy per unit area or work of adhesion, K is the combined elastic modulus of tip and sample, given by $K = \frac{4}{3}((1-{\upsilon_1}^2)/E_1 + (1-{\upsilon_2}^2)/E_2)^{-1}$ Where E_1 and E_2 are the tip and sample Young's modulus and υ_1 and υ_2 are the tip and sample Poisson ratio, σ_0 is the constant adhesive stress acting over a range δ_0 in Dugdale square well potential model. If $\lambda > 5$ then JKR model is more appropriate and if $\lambda < 0.1$, DMT model applies.

In the present experiment, the elastic modulus of the probe tip $E_1 = 165.1\ GPa$, $E_2 = 50\ GPa$, $\upsilon_1 = 0.223$, $\upsilon_2 = 0.1$. and $\gamma = 178\ nJ/m^2$ [43]. Thus $\lambda = 18.577 > 5$. As a result, JKR model is more appropriate here for the calculation of surface energy.

For the calculation of surface free energy, the pull-off force from the extend data was used and found to be $47.79 \pm 12.5\ nN$. Because the retract data shows higher values than the actual force due to the effect of viscoelasticity of the flax fiber substrate.

$$F_{(pull-off)} = -\frac{3}{2}\pi R\gamma \tag{4.16}$$

$$\gamma = 2\sqrt{s_1 s_2} \tag{4.17}$$

where s_1 and s_2 are the dispersive component of the surface energy of the probe tip and the sample respectively. The surface energy of the silicon was used as $1250\ \mathrm{mJ/m^2}$ [44]. Thus, the dispersive component of the surface energy of a single flax fiber was found to be $32.9 \pm 2.1\ \mathrm{mJ/m^2}$

The obtained value of the dispersive component of the surface free energy of a single flax fiber agrees well with other published literature. However, care should be taken while comparing among different literature values. Because, the methodology used to determine the surface free energy of single flax fiber and the theoretical approach to determine the equations for calculating surface free energy may potentially be different. As for example, Inverse Gas Chromatography (IGC) requires the flax fiber to be grounded in powder form and has been reported to exhibit higher surface energy values as it has a tendency to selectively probe higher energy regions [45]. Heng et. al [46] reported the dispersive component of surface energy of flax fiber by IGC method to be $43.1\ mJ/m^2$. Gassan et. al[47] studied the surface energy of untreated and silane treated jute fibers. They employed capillary rise method and IGC for measuring the surface energy and made comparison between these two results. They found the dispersive component of surface energy by IGC to be 41 mJ/m^2 while the capillary rise method generated 23 mJ/m^2. This result is consistent with other findings that IGC method tend to provide higher end value of surface free energy. The total surface energy of crystalline cellulosic fibers was reported to be $60 - 69\ mJ/m^2$. Askargorta et.al [48] investigated the surface energy of flax fiber by washburn or capillary rise techniques to be $29.2\ mJ/m^2$. Hazendonk et. al [49] measured the dispersive component of surface free energy to be $27.5 - 50\ mJ/m^2$ by a simple experimental method.

Thus the measurement of surface energy of single flax fiber is subjected to the method of separation of fibers, surface treatment applied on the fibers, degree of retting, and the method of measurement used.

During the measurement of adhesion force by AFM, the relative humidity and temperature of the laboratory was controlled at 40% RH and $23° \ C$. With the presence of humidity, the adhesion force between the probe tip and the sample surface is mainly governed by the short range vander walls force and the capillary force [50]. The situation may be more complicated due to the presence of electrostatic force and the formation of chemical bonding [51]. Due to the presence of humidity, the sample surface is generally covered by a thin water film. This thin film may form a capillary bridge between the probe tip and the sample surface which will contribute a capillary force and this force would be superimposed with other interactions such as vander walls force [52, 53]. However, the effect of this capillary force is subjected to the wettability of water to the sample surface and probe tip. A hydrophic sample surface would result in a very small capillary force. Binggeli et. al [54] studied the condensation of water around an AFM probe in contact with a flat surface. They found that a relative humidity of less than 75% has little effect on the capillary force. However, as the surrounding environment approaches to the point of saturation, significant capillary condensation occurs which affects nano-scale properties. A hydrophilic surface may expedite this process. Again, when the radius of curvature of the probe tip is large enough, the effect of capillary condensation is negligible [55].

As the relative humidity of the laboratory was maintained at around 40% RH and the radius of the probe tip (25 nm) was large enough, it is expected that the effect of capillary condensation is small enough, and thus negligible. To minimize the effect of electrostatic force

during adhesion force measurement, the experimental setup was periodically discharged and earth connected to prevent the buildup of excess charge. As a result, the effect of electrostatic force was also negligible. The single flax fibers were dry enough to prevent the formation of chemical bonding such as hydrogen or hydrophilic bonding between the tip and fiber surface. Hence, the adhesion force measured by AFM is expected to be arising from mainly due to the Vander Waals interactions between the probe tip and fiber surface.

4.4. Contact angle approach for measuring surface free energy

Owens and Wendt[56] developed a semi-empirical equation from Fowkes theory[57] which is especially applicable for the measurement of surface energies of polymeric materials. The proposed equation was in the following form:

$$\gamma_{SL} = \gamma_L + \gamma_S + 2\sqrt{\gamma_s^d \gamma_l^d} + 2\sqrt{\gamma_s^p \gamma_l^p} \tag{4.18}$$

Combining this equation with Young's equation, the following equation is achieved:

$$\gamma_L(1 + \cos(\theta)) = 2\sqrt{\gamma_s^d \gamma_l^d} + 2\sqrt{\gamma_s^p \gamma_l^p} \tag{4.19}$$

This equation can be rearranged to yield a straight line form $y = mx + c$ by the following equation:

$$\frac{\gamma_L(1 + \cos(\theta))}{2\sqrt{\gamma_l^d}} = \sqrt{\gamma_s^p}\sqrt{\frac{\gamma_l^p}{\gamma_l^d}} + \sqrt{\gamma_s^d} \tag{4.20}$$

where,

$$y = \frac{\gamma_L(1 + \cos(\theta))}{2\sqrt{\gamma_l^d}}$$

$$x = \sqrt{\frac{\gamma_l^p}{\gamma_l^d}}$$

$$m = \sqrt{\gamma_s^p}$$

$$c = \sqrt{\gamma_s^d}$$

From these equations, it is possible to measure the surface energy of different polymeric materials by measuring the contact angle of a series of well-characterized polar and non-polar liquids. However, it should be remembered that the assumptions involved are homogeneous surface, equilibrium of the sessile drop and hemispherical shape, reproducibility of the contact angle, no absorption and swelling of the surface when in contact with the test liquids. These assumptions are rarely achieved in reality for natural fiber surfaces.

In this study, flax fibers were carefully separated from the bundle with a diameter range of 80-130 μm. The fibers were placed on the microscope (Zeiss Axiovert 40 MAT) in such a way that only two ends of the fiber were fixed and the middle portion where the droplet would be put was free and taut. Then with the help of a micro-syringe, one micro-litre drop of liquid was placed on the fiber. As soon as the liquid droplet was stable, a light beam was thrown on the droplet from underneath, focused on the water droplet appropriately and the image formed was captured by a camera attached to it.

Four types of liquid was used: water, ethanol, toluene, and acetone. The contact angle was measured at three different locations on each fiber and averaged. In this way six separate fibers were used for each type of liquid. The dispersive and polar component of surface energy of these liquids are shown in Table 4.1. Figure 4.11a shows the advancing contact angle formed

by a water droplet on a technical flax fiber of 80 μm diameter. It is symmetrical about the circumference of the fiber. Figure 4.11b shows the edge of the droplet and the measured angle. The edge of the droplet is not precisely sharp rather they tend to be blunt. This is due to the formation of hydrogen bond between the water droplet and the hydroxyl molecules present on the fiber surface. As the water droplet rests on the fiber for 30-40 seconds, it starts to get absorbed and the contact angle is reduced which is shown in Figure 4.12.

Table 4.1: Properties of characterization liquids[58]

Liquid	**Dispersive component (γ_l^d) (mJ/m^2)**	**Polar component (γ_l^p)(mJ/m^2)**	**Surface energy (γ_L)(mJ/m^2)**	**Contact angle (θ)**
Water	21.8	1.4[59]	72.8	46°
Etanol	17	5	22	54°
Toluene	28.5	0	28.5	53°
Acetone	18	4.5	22.5	44°

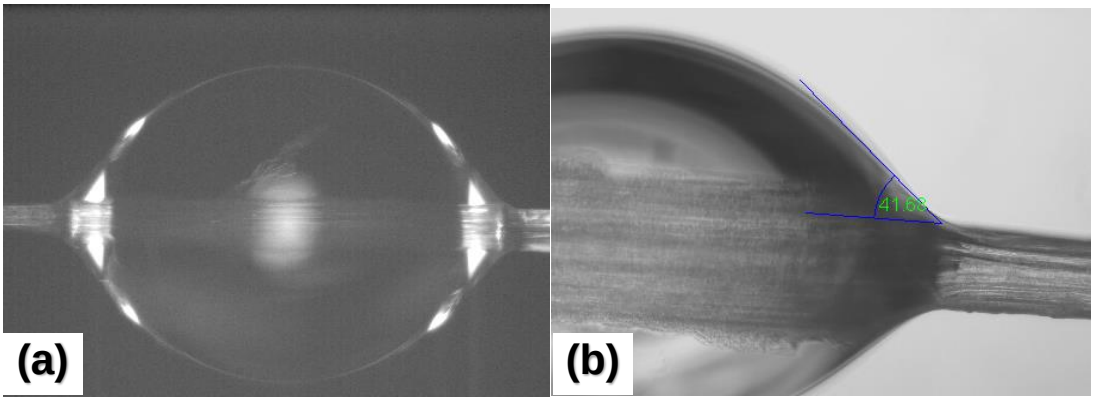

Figure 4.11: Image of an advancing water droplet captured by the optical microscope

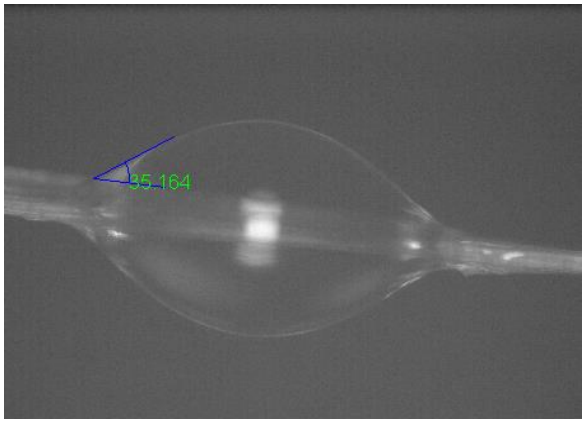

Figure 4.12**:** A receding water droplet

Figure 4.13 a-b shows the contact angle formed by acetone and toluene. They have a higher degree of interaction with the fiber. Therefore, there edge or contact angle is more blunter than the water. Their rate of absorption is also much faster than the water.

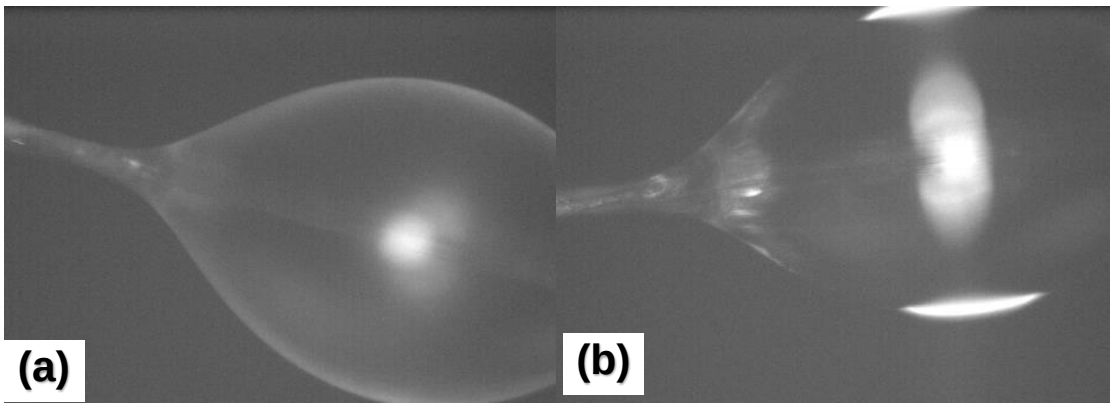

Figure 4.13: Contact angle of (a) acetone and (b) toluene

Using the properties of table 4.1, x and y coordinates of different liquids were determined and a best fit straight line was plotted. This is shown in Figure 4.14. The slope of this straight line is found to be 2.71. As a result, the polar component of the surface energy (γ_s^p) is determined to be 7.3 $\mathrm{mJ/m^2}$. On the other hand, $y-$axis intercept of the straight light is found to

be 7.39. As a result, the dispersive component of the surface energy (γ_s^d) is determined to be 54.61 $\mathrm{mJ/m^2}$. By combining these two components of surface energy (dispersive and polar), total surface energy of the flax fiber can be determined and it is found to be 62 $\mathrm{mJ/m^2}$.

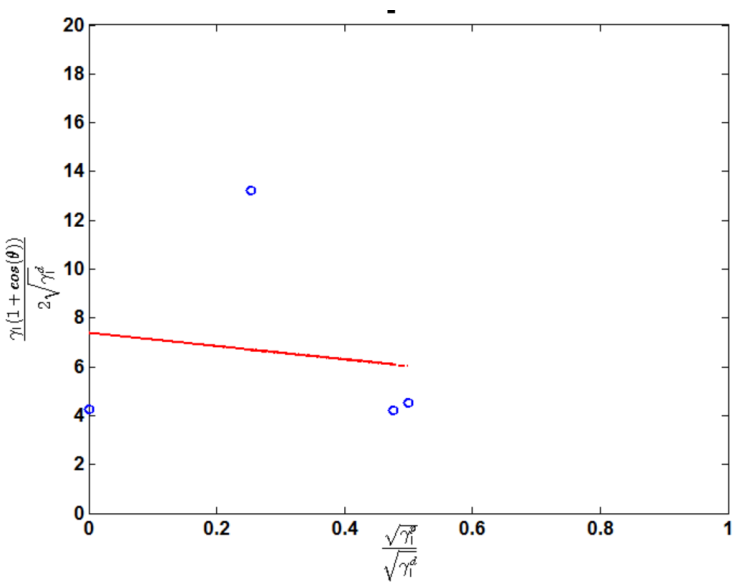

Figure 4.14: Plot of Owens and Wendt equation.

4.5. Summary

In this work, the dispersive component of surface free energy of a single flax fiber was determined by atomic force microscopy through the direct measurement of fiber-tip adhesion force. The value of $\gamma_d$was evaluated to be 32.9 ± 2.1 $\mathrm{mJ/m^2}$ which agrees well with other published literature values for natural fibers. The precise measurement of the contact angle of liquid on a single flax fiber is difficult due to its smaller dimension, higher roughness, formation of hydrogen bond with water and extreme wicking properties. On the other hand, Inverse Gas Chromatography (IGC), requires the fiber to be grounded up in the powder form. Hence, the atomic force microscopy shows promise in measuring the surface free energy by by-passing all these difficulties. No additional surface preparation is required and flax fibers are in its natural

state which is essential for proper understanding of its surface characteristics for manufacturing bio-composite materials. The measurement of adhesion force may also predict the surface wettability of single flax fibers. Thus, the method shown in this paper may serve as a useful tool for investigating the fiber-matrix adhesion properties of natural fiber reinforced composite materials.

4.6. References

1. Zafeiropoulos, N.E., et al., *Engineering and characterisation of the interface in flax fibre/polypropylene composite materials. Part I. Development and investigation of surface treatments.* Composites Part A: Applied Science and Manufacturing, 2002. **33**(8): p. 1083-1093.
2. Zafeiropoulos, N.E., C.A. Baillie, and J.M. Hodgkinson, *Engineering and characterisation of the interface in flax fibre/polypropylene composite materials. Part II. The effect of surface treatments on the interface.* Composites Part A: Applied Science and Manufacturing, 2002. **33**(9): p. 1185-1190.
3. Bismarck, A., et al., *Surface characterization of natural fibers; surface properties and the water up-take behavior of modified sisal and coir fibers.* Green Chemistry, 2001. **3**(2): p. 100-107.
4. Pease, D.C., *The significance of the contact angle in relation to the solid surface.* The Journal of Physical Chemistry, 1945. **49**(2): p. 107-110.
5. Banerji, B.K., *Physical significance of contact angles.* Colloid and Polymer Science, 1981. **259**(3): p. 391-394.

6. Girifalco, L. and R. Good, *A theory for the estimation of surface and interfacial energies. I. Derivation and application to interfacial tension.* The Journal of Physical Chemistry, 1957. **61**(7): p. 904-909.

7. Schellbach, S.L., S.N. Monteiro, and J.W. Drelich, *A novel method for contact angle measurements on natural fibers.* Materials Letters, 2016. **164**: p. 599-604.

8. Sauer, B.B. and T.E. Carney, *Dynamic contact angle measurements on glass fibers: influence of fiber diameter on hysteresis and contact line pinning.* Langmuir, 1990. **6**(5): p. 1002-1007.

9. Yampolskii, Y. and N. Belov, *Investigation of polymers by inverse gas chromatography.* Macromolecules, 2015. **48**(19): p. 6751-6767.

10. Conder, J.R. and C.L. Young, *Physicochemical measurement by gas chromatography*. 1979: John Wiley & Sons.

11. Newell, H.E., et al., *The use of inverse phase gas chromatography to measure the surface energy of crystalline, amorphous, and recently milled lactose.* Pharmaceutical research, 2001. **18**(5): p. 662-666.

12. Ahfat, N.M., et al., *An exploration of inter-relationships between contact angle, inverse phase gas chromatography and triboelectric charging data.* European journal of pharmaceutical sciences, 2000. **9**(3): p. 271-276.

13. Stokes, R.J. and D.F. Evans, *Fundamentals of interfacial engineering*. 1997: John Wiley & Sons.

14. Onabe, F., *Studies on interfacial properties of polyelectrolyte-cellulose systems. I. Formation and structure of adsorbed layers of cationic polyelectrolyte-(poly-DMDAAC) on cellulose fibers.* Journal of Applied Polymer Science, 1978. **22**(12): p. 3495-3510.

15. Madan, G. and S. Shrivastava, *Electrokinetic studies of cotton. Part IV.: Role of water in influencing surface charge density of cotton in electrolyte solution.* Colloid & Polymer Science, 1977. **255**(3): p. 269-275.

16. Jacobasch, H.-J., G. Bauböck, and J. Schurz, *Problems and results of zeta-potential measurements on fibers.* Colloid & Polymer Science, 1985. **263**(1): p. 3-24.

17. Bismarck, A., et al., *Surface characterization of flax, hemp and cellulose fibers; surface properties and the water uptake behavior.* Polymer composites, 2002. **23**(5): p. 872-894.

18. Bellmann, C., et al., *Electrokinetic properties of natural fibres.* Colloids and Surfaces A: Physicochemical and Engineering Aspects, 2005. **267**(1): p. 19-23.

19. Pothan, L.A., et al., *Determination of polarity parameters of chemically modified cellulose fibers by means of the solvatochromic technique.* Journal of Polymer Science Part B: Polymer Physics, 2000. **38**(19): p. 2546-2553.

20. Gutmann, V., *donor-acceptor approach to molecular interactions*. 1978: Plenum Press.

21. Louey, M.D., P. Mulvaney, and P.J. Stewart, *Characterisation of adhesional properties of lactose carriers using atomic force microscopy.* Journal of Pharmaceutical and Biomedical analysis, 2001. **25**(3): p. 559-567.

22. Roberts, C.J., *What can we learn from atomic force microscopy adhesion measurements with single drug particles?* European Journal of Pharmaceutical Sciences, 2005. **24**(2): p. 153-157.

23. Magonov, S.N. and D.H. Reneker, *Characterization of polymer surfaces with atomic force microscopy.* Annual Review of Materials Science, 1997. **27**(1): p. 175-222.

24. Bastidas, J.C., et al., *Chemical force microscopy of cellulosic fibers.* Carbohydrate Polymers, 2005. **62**(4): p. 369-378.

25. Good, R.J., L.A. Girifalco, and G. Kraus, *A theory for estimation of interfacial energies. II. Application to surface thermodynamics of teflon and graphite.* The Journal of Physical Chemistry, 1958. **62**(11): p. 1418-1421.

26. Zisman, W.A., *Relation of the equilibrium contact angle to liquid and solid constitution*. 1964, ACS Publications.

27. Fox, H. and W. Zisman, *The spreading of liquids on low energy surfaces. I. polytetrafluoroethylene.* Journal of Colloid Science, 1950. **5**(6): p. 514-531.

28. Fowkes, F.M., *Attractive forces at interfaces.* Industrial & Engineering Chemistry, 1964. **56**(12): p. 40-52.

29. Fowkes, F.M. and M.A. Mostafa, *Acid-base interactions in polymer adsorption.* Industrial & Engineering Chemistry Product Research and Development, 1978. **17**(1): p. 3-7.

30. Tseytlin, Y.M., *Atomic force microscope cantilever spring constant evaluation for higher mode oscillations: A kinetostatic method.* Review of Scientific Instruments, 2008. **79**(2): p. 025102.

31. Torii, A., et al., *A method for determining the spring constant of cantilevers for atomic force microscopy.* Measurement science and Technology, 1996. **7**(2): p. 179.

32. Sader, J.E., et al., *Method for the calibration of atomic force microscope cantilevers.* Review of Scientific Instruments, 1995. **66**(7): p. 3789-3798.

33. Müller, M., et al., *Direct observation of microfibril arrangement in a single native cellulose fiber by microbeam small-angle X-ray scattering.* Macromolecules, 1998. **31**(12): p. 3953-3957.

34. Baley, C., et al., *Influence of drying on the mechanical behaviour of flax fibres and their unidirectional composites.* Composites Part A: Applied Science and Manufacturing, 2012. **43**(8): p. 1226-1233.

35. Wahl, K., et al., *Oscillating adhesive contacts between micron-scale tips and compliant polymers.* Journal of colloid and interface science, 2006. **296**(1): p. 178-188.

36. Johnson, K., K. Kendall, and A. Roberts. *Surface energy and the contact of elastic solids*. in *Proceedings of the Royal Society of London A: Mathematical, Physical and Engineering Sciences*. 1971. The Royal Society.

37. Derjaguin, B.V., V.M. Muller, and Y.P. Toporov, *Effect of contact deformations on the adhesion of particles.* Journal of Colloid and interface science, 1975. **53**(2): p. 314-326.

38. Muller, V., V. Yushchenko, and B. Derjaguin, *On the influence of molecular forces on the deformation of an elastic sphere and its sticking to a rigid plane.* Journal of Colloid and Interface Science, 1980. **77**(1): p. 91-101.

39. Muller, V.M., V.S. Yushchenko, and B.V. Derjaguin, *General theoretical consideration of the influence of surface forces on contact deformations and the reciprocal adhesion of elastic spherical particles.* Journal of Colloid and Interface Science, 1983. **92**(1): p. 92-101.

40. Tabor, D. and R. Winterton. *The direct measurement of normal and retarded van der Waals forces*. in *Proceedings of the Royal Society of London A: Mathematical, Physical and Engineering Sciences*. 1969. The Royal Society.

41. Maugis, D., *Adhesion of spheres: the JKR-DMT transition using a Dugdale model.* Journal of colloid and interface science, 1992. **150**(1): p. 243-269.

42. Carpick, R.W., D.F. Ogletree, and M. Salmeron, *A general equation for fitting contact area and friction vs load measurements.* Journal of Colloid and Interface Science, 1999. **211**(2): p. 395-400.

43. Hurley, D. and J.A. Turner, *Measurement of Poisson's ratio with contact-resonance atomic force microscopy.* Journal of Applied Physics, 2007. **102**(3): p. 033509.

44. Jaccodine, R., *Surface energy of germanium and silicon.* Journal of The Electrochemical Society, 1963. **110**(6): p. 524-527.

45. Zhang, J., et al., *Determination of the surface free energy of crystalline and amorphous lactose by atomic force microscopy adhesion measurement.* Pharmaceutical research, 2006. **23**(2): p. 401-407.

46. Heng, J.Y., et al., *Methods to determine surface energies of natural fibres: a review.* Composite Interfaces, 2007. **14**(7-9): p. 581-604.

47. Gassan, J., V.S. Gutowski, and A.K. Bledzki, *About the surface characteristics of natural fibres.* Macromolecular materials and engineering, 2000. **283**(1): p. 132-139.

48. Aranberri-Askargorta, I., T. Lampke, and A. Bismarck, *Wetting behavior of flax fibers as reinforcement for polypropylene.* Journal of colloid and interface science, 2003. **263**(2): p. 580-589.

49. Van Hazendonk, J., et al., *A simple experimental method for the measurement of the surface tension of cellulosic fibres and its relation with chemical composition.* Colloids and Surfaces A: Physicochemical and Engineering Aspects, 1993. **81**: p. 251-261.

50. Van Honschoten, J., N. Tas, and M. Elwenspoek, *The profile of a capillary liquid bridge between solid surfaces.* American Journal of Physics, 2010. **78**(3): p. 277-286.

51. Sedin, D.L. and K.L. Rowlen, *Adhesion forces measured by atomic force microscopy in humid air.* Analytical Chemistry, 2000. **72**(10): p. 2183-2189.

52. Eastman, T. and D.-M. Zhu, *Adhesion forces between surface-modified AFM tips and a mica surface.* Langmuir, 1996. **12**(11): p. 2859-2862.

53. Moon, S.-h. and M.D. Foster, *Influence of humidity on surface behavior of pressure sensitive adhesives studied using scanning probe microscopy.* Langmuir, 2002. **18**(21): p. 8108-8115.

54. Binggeli, M. and C. Mate, *Influence of capillary condensation of water on nanotribology studied by force microscopy.* Applied physics letters, 1994. **65**(4): p. 415-417.

55. Sugawara, Y., et al., *Effects of humidity and tip radius on the adhesive force measured with atomic force microscopy.* Wear, 1993. **168**(1-2): p. 13-16.

56. Owens, D.K. and R. Wendt, *Estimation of the surface free energy of polymers.* Journal of applied polymer science, 1969. **13**(8): p. 1741-1747.

57. Fowkes, F.M., *Dispersion force contributions to surface and interfacial tensions, contact angles, and heats of immersion*. 1964, ACS Publications.

58. Koenhen, D. and C. Smolders, *The determination of solubility parameters of solvents and polymers by means of correlations with other physical quantities.* Journal of Applied Polymer Science, 1975. **19**(4): p. 1163-1179.

59. Good, R.J. and M.K. Chaudhury, *Theory of adhesive forces across interfaces. 1. The Lifshitz-van der Waals component of interaction and adhesion.* Fundamentals of Adhesion, 1991: p. 137-151.

CHAPTER 5. CONCLUSIONS AND RECOMMENDATIONS

5.1. Conclusions

In this study, different aspects of flax fibers such as statistical analysis of different mechanical parameters (ultimate strength, ultimate strain, and elastic modulus), failure analysis of both technical and single flax fibers, and measurement of surface energy was performed. For the purpose of statistical analysis, experiments were carried out on six different samples in two different facilities to confirm and compare the results. At least 50 fiber specimens were considered for each sample. In one facility, the diameter of the diameter of the fiber was measured by optical microscope and in other facility, rotating laser was employed to measure the same parameter. The differences that arose from these two measurements were quantified and the implications of diameter measurements in terms of strength and modulus were discussed. Hypothesis testing and ANOVA analysis were performed to verify the difference between the mean of two samples: one from large stalk diameter and other from small stalk diameter. Thus, it was confirmed that the effect of stalk diameter on strength and elastic modulus of technical flax fiber were statistically significant which is consistent with the study performed by Lefeuvre et.al [1] for single flax fibers. The applicability of weakest link theory was investigated in terms of the strength of technical flax fibers for two different gauge lengths. It was found that the probability model for single flax fibers can also be applied to technical flax fibers considering appropriate load sharing rules. This finding is in agreement with the study performed by S.L Phoenix [2-5] in a series of technical papers.

To investigate the appropriate probability distribution model for the strength of technical flax fibers, a number of probability distribution model was employed. It was found that a 3-parameter Weibull distribution model possess the highest degree of fit for the strength

distribution of technical flax fibers. In literature, a two parameter Weibull model and a modified two parameter Weibull model was reported for simulating the strength distribution [6, 7]. However, a three parameter Weibull distribution for technical flax fibers was not considered before this study. Next, the effect of strain rate on technical flax fibers was investigated. Three different displacement rates were applied for this investigation. The mean strength did not vary significantly with different displacement rate. This was attributed to the lower displacement rate applied to the fibers. For polymeric fibers, there is a threshold point of displacement rate below which the fibers do not show enough sensitivity to different displacement rate [8]. No study is yet available in literature for flax fibers or natural fibers considering the effect of strain rate for comparison purposes.

Usually, the higher strength and modulus of single and technical flax fibers are not fully realized in their corresponding composite materials. To investigate this phenomena, a dynamic failure analysis of technical flax fiber was performed with the help of SEM. The tensile test bench was integrated with the SEM and the process of fiber failure was captured and analyzed by SEM movie. Next, fractographic analysis of the fracture surface of single flax fibers and meso-fibrils were performed. The internal structure of flax fibers such as nano-fibrils (micro-fibrils) were made visible and their failure mechanism was explained. It was found that in addition to the meso-fibril pull out from the hemicellulose matrix, the hierarchical fibril pull out and crack-bridging phenomena contribute to the high energy absorption capacity of flax fibers which has not been considered in existing literature yet.

Surface free energy of the fiber and the matrix determine the interfacial bond strength of composite materials. This bond strength govern the failure mechanism of composite materials. Therefore, it is necessary to investigate the surface properties and surface energies of flax fiber to

be able to study interfacial bond strength in order to use them in composite materials for load bearing applications. In this study, surface energy of flax fibers were determined by two different approaches and compared. Contact angle approach for measuring the surface energy of natural fibers is rather erroneous as natural fibers possess a rough surface and fiber-liquid interactions are present. For contact angle approach, a perfectly smooth, defect free, solid-liquid interaction free surface is required which in practice is difficult to achieve. Due to the hydrophilic nature of natural fibers, a hydrogen bond is formed between the fiber surface and probe liquid which tend to render the line of contact blunt. This complicates the exact measurement of contact angle. In addition, a strong wicking property makes the measurement time sensitive. On the other hand, atomic force microscopy approach is capable of avoiding these difficulties as it relies on the precise measurement of fiber-tip interaction or adhesion force. Pietak et.al [9] investigated the wetting properties of hemp fibers by atomic force microscopy for the first time. However, correlating adhesion force with surface energy for flax fibers or natural fibers through contact mechanics models was not shown in literature before this study.

From an application point of view, the investigation on the failure mechanism of flax fiber is important as it would provide insight into manufacturing of bio-mimetic and bio-mimicking novel composite materials [10]. Flax fibers are essentially polymer-polymer composite materials. The understanding and knowledge gained from this study regarding the energy absorbing mechanism of flax fibers may inspire the improvement of design principles for technical composite materials. Because flax fibers are stiff and tough at the same time. A few recent works [11-13] suggest that to achieve these two contradicting properties in composite materials, a tight interface between the stiff fiber and soft matrix is required. In flax fiber, the hemicellulose molecules acts as this interface polymers. Because the chemical nature of

hemicellulose is similar to cellulose and as a result, they can form a strong non-covalent bond. On the other hand, the hemicellulose being extremely hydrophilic can form a gel-like hydrated network with pectin which is necessary for imparting toughness. As explained previously, this gel-like matrix is able to flow plastically without fracturing beyond their yield stress [14]. The interface of technical composite materials can be improved by taking lesson from these natural composite materials, such as wood fiber [15] and flax fiber. By selecting appropriate amphiphilic molecules or surfactants, it is possible to achieve a strong bond between an aqueous and a hydrophobic phase, thus improving the interfacial strength of composite materials.

5.2. Recommendations

Based on the findings of the present work, the following points are recommended for further study:

1. Though it was mentioned that the stalk diameter has influence on the ultimate strength of flax fibers, however, the exact reason for this influence was not properly understood. A study could be conducted to analyze if the chemical constituents of the fibers and the arrangement of micro-fibrils are different in large diameter and small diameter fibers.
2. For the strain rate testing, the strain rate used were below 0.2 mm/min. However, 0.2 mm/min is the threshold strain rate above which polymeric fibers starts to show strain rate sensitivity. For further study, strain rate greater than 0.2 mm/min could be applied and the resulting effect could be investigated.
3. In literature, there is a debate about the dimensions of micro-fibrils and meso-fibrils of flax fibers. The dimensions of the micro-fibrils of wood cells are frequently referred to as the same for flax fibers. In this study, the smallest dimension that was detected was 40

nm. Further study is required to confirm if this 40 nm fibrils are made up of bundles of smaller dimension fibrils.

4. Flax fiber surface could be modified by different chemical treatments and their surface free energy could be measured by atomic force microscopy. The surface free energy of different bio-based matrix could also be measured with this method. After the manufacture of composite materials with different fiber treatment, the interfacial bond strength could be quantitatively measured and analyzed.

5.3. References

1. Lefeuvre, A., et al., *Elementary flax fibre tensile properties: correlation between stress–strain behaviour and fibre composition.* Industrial Crops and Products, 2014. **52**: p. 762-769.
2. Hearle, J.W., *Mechanics of flexible fibre assemblies*. 1980: Kluwer Academic Publishers.
3. Phoenix, S.L., *Statistical theory for the strength of twisted fiber bundles with applications to yarns and cables.* Textile Research Journal, 1979. **49**(7): p. 407-423.
4. Phoenix, S.L. and H.M. Taylor, *The asymptotic strength distribution of a general fiber bundle.* Advances in Applied Probability, 1973. **5**(02): p. 200-216.
5. Phoenix, S.L., *Probabilistic strength analysis of fibre bundle structures.* Fibre Science and Technology, 1974. **7**(1): p. 15-31.
6. Andersons, J., E. Poriķe, and E. Spārniņš, *The effect of mechanical defects on the strength distribution of elementary flax fibres.* Composites Science and Technology, 2009. **69**(13): p. 2152-2157.
7. Andersons, J., et al., *Strength distribution of elementary flax fibres.* Composites science and technology, 2005. **65**(3): p. 693-702.

8. Schwartz, P., A. Netravali, and S. Sembach, *Effects of strain rate and gauge length on the failure of ultra-high strength polyethylene fibers.* Textile Research Journal, 1986. **56**(8): p. 502-508.

9. Pietak, A., et al., *Atomic force microscopy characterization of the surface wettability of natural fibres.* Applied surface science, 2007. **253**(7): p. 3627-3635.

10. Fratzl, P., *Biomimetic materials research: what can we really learn from nature9s structural materials?* Journal of the Royal Society Interface, 2007. **4**(15): p. 637-642.

11. Gao, H., et al., *Materials become insensitive to flaws at nanoscale: lessons from nature.* Proceedings of the national Academy of Sciences, 2003. **100**(10): p. 5597-5600.

12. Jäger, I. and P. Fratzl, *Mineralized collagen fibrils: a mechanical model with a staggered arrangement of mineral particles.* Biophysical journal, 2000. **79**(4): p. 1737-1746.

13. Fratzl, P., I. Burgert, and H.S. Gupta, *On the role of interface polymers for the mechanics of natural polymeric composites.* Physical Chemistry Chemical Physics, 2004. **6**(24): p. 5575-5579.

14. Burgert, I. and J.W. Dunlop, *Micromechanics of cell walls*, in *Mechanical integration of plant cells and plants*. 2011, Springer. p. 27-52.

15. Navi, P., et al., *Micromechanics of wood subjected to axial tension.* Wood Science and Technology, 1995. **29**(6): p. 411-429.

APPENDIX A. ADDITIONAL FIGURES

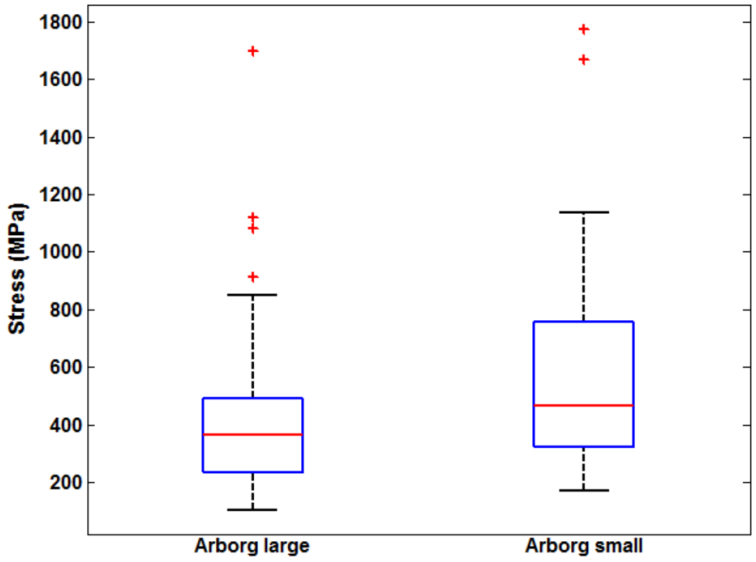

Figure A1: Distribution of failure strength for Arborg Large and Arborg Small sample.

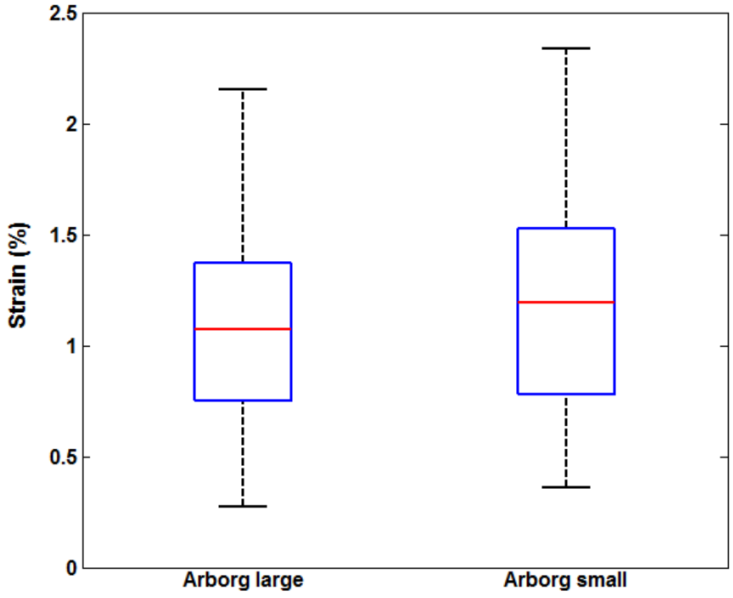

Figure A2: Distribution of failure strain for Arborg Large and Arborg Small sample

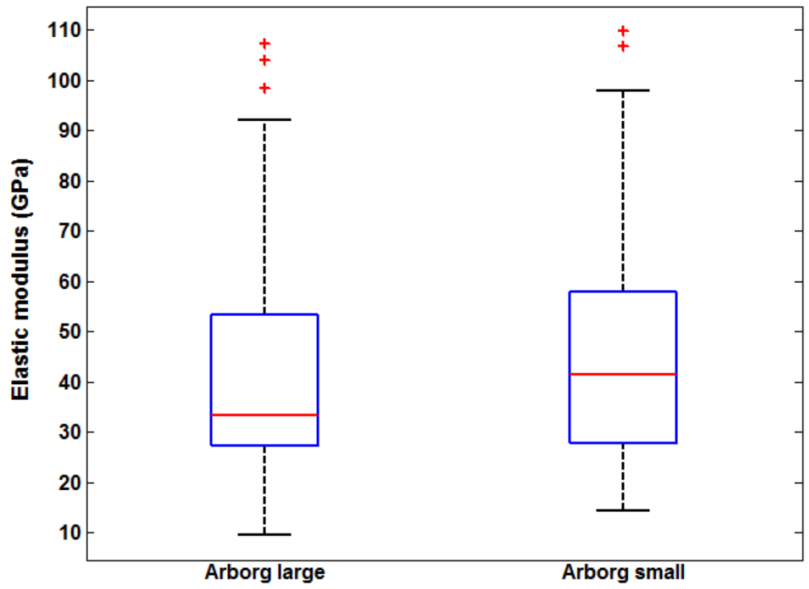

Figure A3: Distribution of Young's modulus for Arborg Large and Arborg Small sample

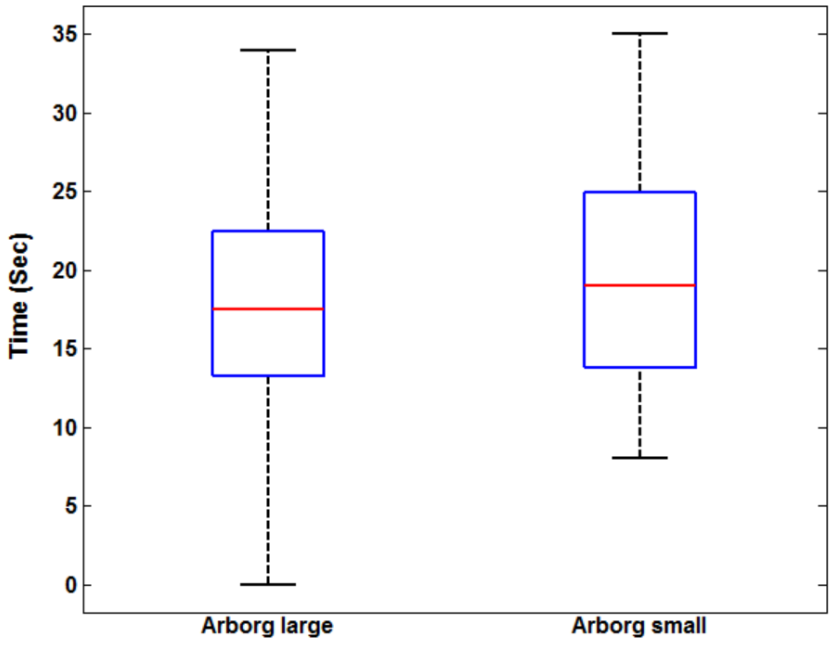

Figure A4: Distribution of failure time for Arborg Large and Arborg Small sample

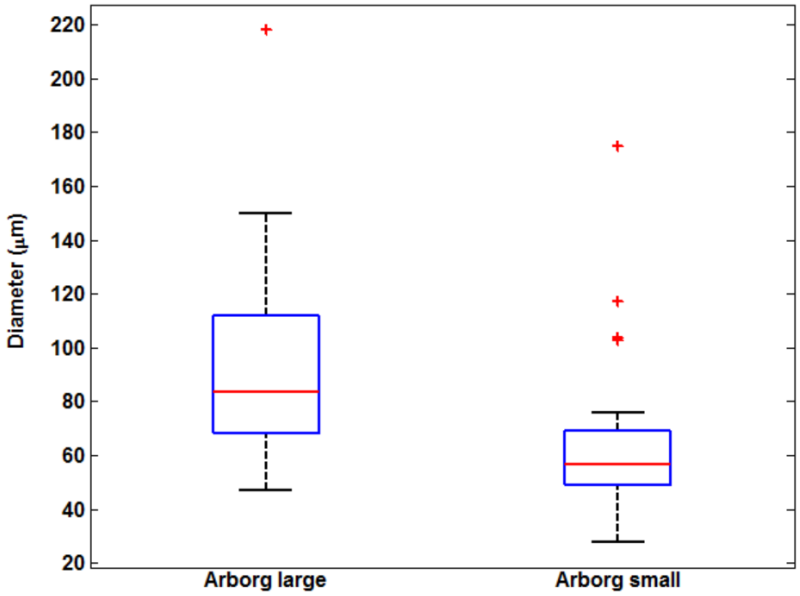

Figure A5: Distribution of diameter for Arborg Large and Arborg Small sample

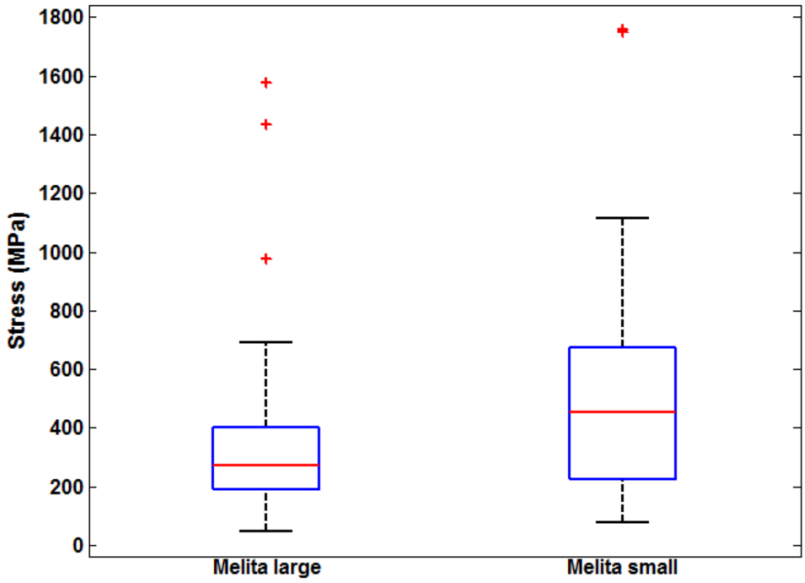

Figure A6: Distribution of failure strength for Melita Large and Melita Small sample.

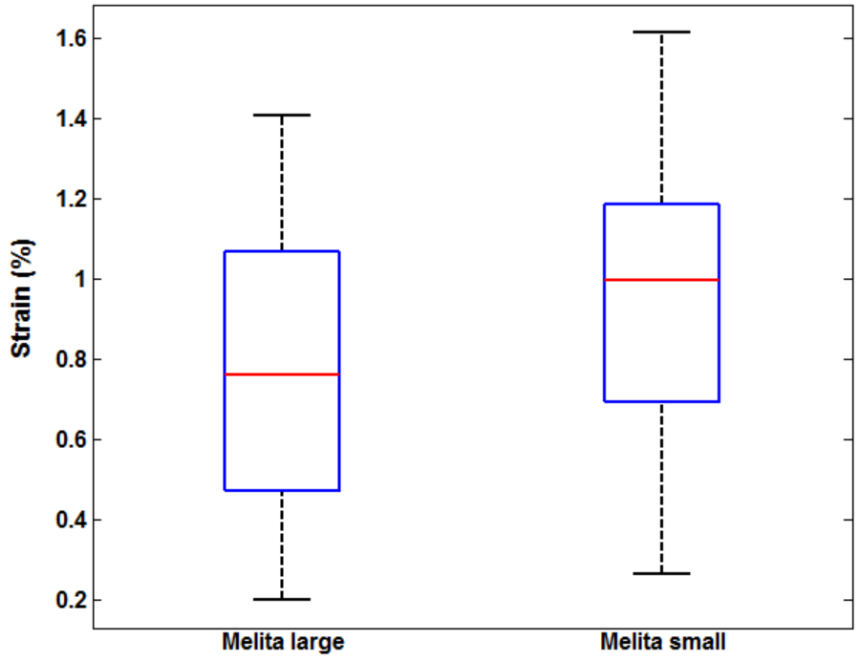

Figure A7: Distribution of failure strain for Melita Large and Melita Small sample

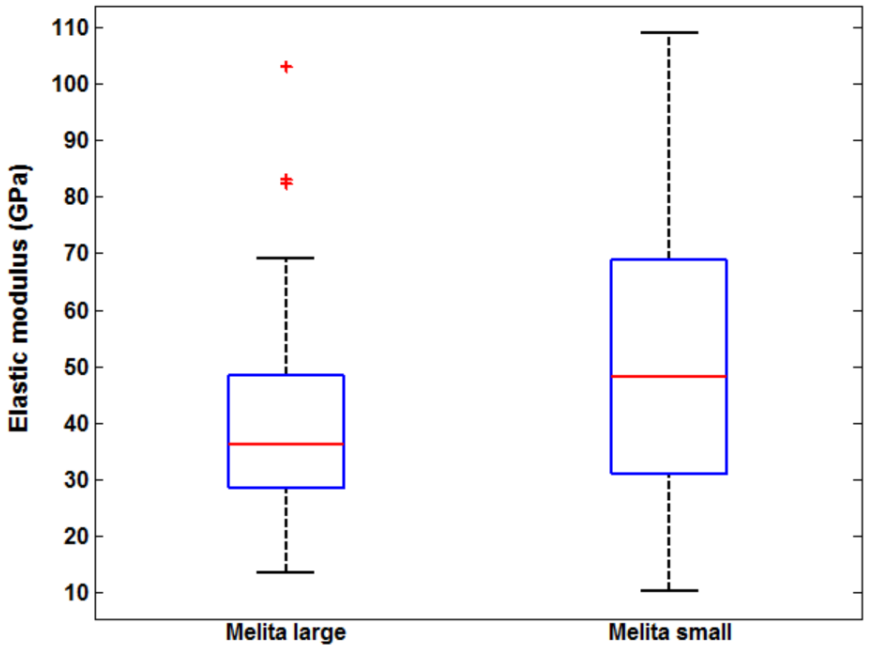

Figure A8: Distribution of Young's modulus for Melita Large and Melita Small sample

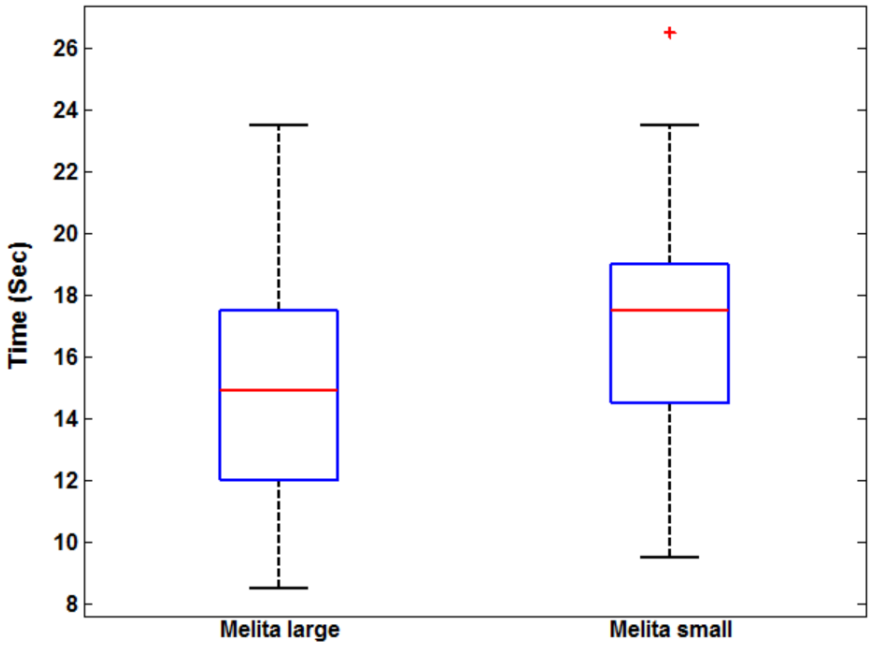

Figure A9: Distribution of failure time for Melita Large and Melita Small sample

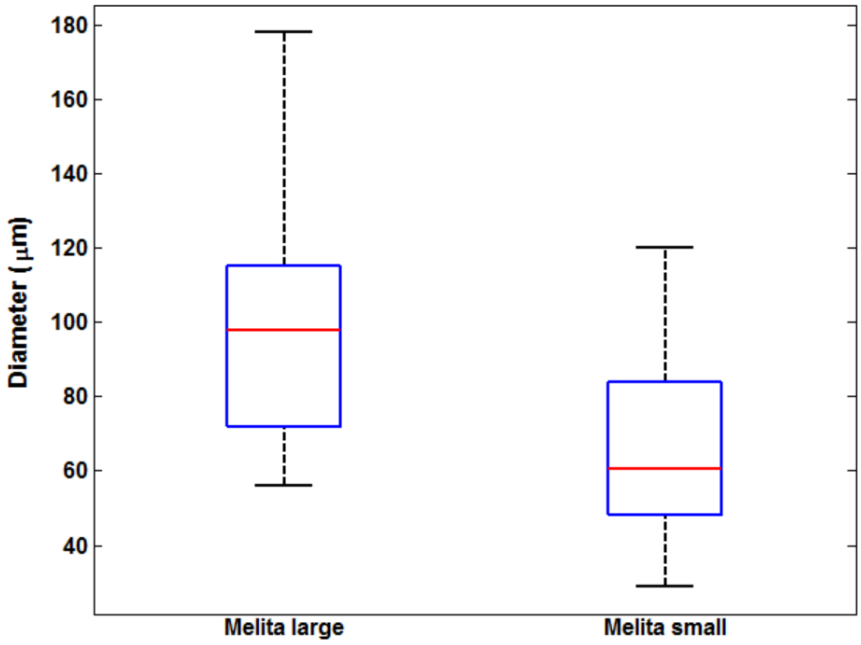

Figure A10: Distribution of diameter for Melita Large and Melita Small sample